

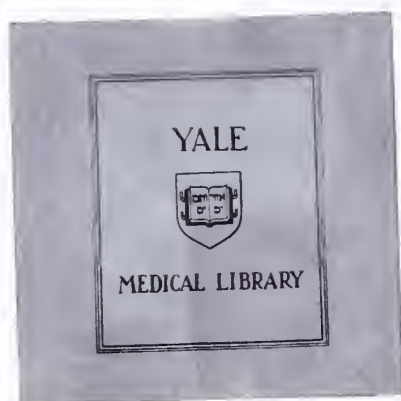
YALE MEDICAL LIBRARY



3 9002 08627 9248

LATERAL MOBILITY OF  
BAND 3 IN THE HUMAN  
ERYTHROCYTE  
GHOST MEMBRANE

DAVID ERIC GOLAN  
DECEMBER, 1979





Digitized by the Internet Archive  
in 2017 with funding from  
Arcadia Fund

<https://archive.org/details/lateralmobilityo00gola>







LATERAL MOBILITY OF BAND 3 IN THE HUMAN ERYTHROCYTE  
GHOST MEMBRANE

A Thesis Submitted to the Yale University School of Medicine  
in Partial Fulfillment of the Requirements for  
the Degree of Doctor of Medicine

by

David E. Golan

December, 1979



## ABSTRACT

Band 3 is the major intrinsic protein of the human erythrocyte membrane as well as the putative site for anion permeation through the membrane. It can be specifically labeled in intact erythrocytes with the covalent fluorescent probe eosin-isothiocyanate. The lateral mobility of labeled band 3 in the plane of the membrane under various conditions of ionic strength and temperature was examined using the fluorescence photobleaching recovery technique. Low temperature and high ionic strength favored immobilization of band 3 (10% mobile at 21°C) as well as slow diffusion of the mobile fraction (diffusion coefficient ( $D$ ) =  $4 \times 10^{-11}$  cm<sup>2</sup>/sec at 21°C). Increasing temperature and decreasing ionic strength led to an increase in the fraction of mobile band 3 (>90% mobile at 37°C) and a reversible increase in the diffusion rate of the mobile fraction ( $D = 2 \times 10^{-9}$  cm<sup>2</sup>/sec at 37°C). These two effects were markedly dissociated by their ionic strength and temperature dependencies, however, in that the fraction of mobile band 3 always increased before (i.e. at higher ionic strength and lower temperature than) the increase in diffusion rate. This dissociation was manifested kinetically on prolonged incubation of ghosts at constant ionic strength and temperature: the diffusion rate of the mobile fraction increased very slowly for the first hour and much more rapidly over the following two hours, whereas the fraction of mobile band 3 increased to >90% within the first hour and remained maximal for the duration



of the experiment. Further, changes in diffusion rate with temperature were promptly and totally reversible whereas increases in the mobile fraction were only slowly and partially reversible. These effects were shown not to be due to complete dissociation of spectrin, the major protein of the erythrocyte cytoskeleton, from the membrane. To be consistent with these observations, any model for erythrocyte membrane structure must include at least two separate processes capable of restricting the lateral mobility of band 3. The process which determines the rate at which the mobile fraction of band 3 diffuses must be a completely reversible one; this may involve a metastable state of cytoskeleton structure intermediate between tight binding to and complete dissociation from the membrane.



Dedicated to my parents,  
without whose emotional,  
educational, and financial  
support this work would  
have been impossible.



## ACKNOWLEDGMENTS

I thank above all my thesis advisor, Dr. William Veatch, for his untiring support and encouragement. He provided countless hours of teaching mixed with a genuine and warm friendship. I am grateful to Dr. Gerald Fischbach for his unselfish loans of various pieces of equipment (fluorescence microscope, air stream stage incubator) and instruction in their use. Dr. Samuel Latt kindly provided the oil immersion objective used in this work. I especially thank Drs. Jon Morrow and Vincent Marchesi for discussions which led to various hypotheses upon which this thesis is based. I am grateful to the Department of Molecular Biophysics and Biochemistry and the Medical Scientist Training Program at Yale University for their support, and especially to Drs. Frederic Richards and James Jamieson for allowing me to pursue the paths of scientific inquiry wherever they led. I also thank the members of the Department of Pharmacology at Harvard Medical School for welcoming me into their community. I thank Ms. Jane Gharibian for excellent technical assistance. Finally, I want to thank Laura for her companionship and love when the need was greatest.

I gratefully acknowledge a National Institutes of Health - Medical Scientist Training Program traineeship for the entire period in which this work was conducted.



# CONTENTS

	<u>page</u>
Introduction . . . . .	1
Chapter 1. Literature Review . . . . .	7
A. The Erythrocyte Membrane . . . . .	7
1. General Review of Structure . . . . .	7
a. The Lipid Bilayer . . . . .	7
b. The Proteins. . . . .	8
2. Band 3 . . . . .	12
a. Physical and Chemical Properties . . . . .	12
b. Conformation in the Membrane . . . . .	14
c. Associations with Other Membrane Proteins . . . . .	19
d. Functions . . . . .	20
3. Cytoskeleton . . . . .	24
a. Definitions and Components . . . . .	24
b. Spectrin: Structure in Solution . . . . .	26
c. Spectrin: Polymerization with Actin and Band 4.1 . . . . .	27
d. Spectrin: Binding to the Membrane . . . . .	28
4. Band 3 - Cytoskeleton Interactions . . . . .	31
a. Band 3 - Ankyrin . . . . .	31
b. Band 3 - Spectrin . . . . .	32
B. Measurements of Lateral Diffusion . . . . .	36
1. Protein Diffusion . . . . .	36
a. Cell Fusion . . . . .	37
b. Photobleaching Recovery . . . . .	41
2. Lipid Diffusion . . . . .	42
Chapter 2. Fluorescence Photobleaching Recovery System . . . . .	45
A. Theory. . . . .	45
1. Design of the Experiment . . . . .	45
2. Photobleaching . . . . .	47
3. Fluorescence Recovery Curves . . . . .	48
B. Methods . . . . .	53
1. Optics and Electronics . . . . .	53
2. Experimental Data Analysis . . . . .	61
3. Calibration of Beam Size and Profile . . . . .	62
C. Results: Beam Calibration . . . . .	65
D. Discussion . . . . .	67
Chapter 3. Eosin-Isothiocyanate Labeling of Band 3 . . . . .	68
A. Materials and Methods . . . . .	68
1. Labeling of Human Erythrocytes with Eosin-Isothiocyanate . . . . .	68
2. Identification of Labeled Membrane Components . . . . .	70
a. SDS-Polyacrylamide Gel Electrophoresis . . . . .	70



	<u>page</u>
b. Selective Extraction Procedures . . . . .	71
1. Low Ionic Strength Extraction . . . . .	71
2. Triton Extraction . . . . .	71
3. Chloroform/Methanol Extraction . . . . .	71
B. Results . . . . .	72
1. Eosin Labeling . . . . .	72
2. SDS-Polyacrylamide Gel Electrophoresis . . . . .	72
3. Selective Extraction Procedures . . . . .	74
C. Discussion . . . . .	76
Chapter 4. Fluorescence Photobleaching Recovery on Eosin-Labeled Ghosts. . . . .	78
A. Methods . . . . .	79
1. Fluorescence Photobleaching Recovery System . . . . .	79
2. Preparation of the Sample. . . . .	79
3. Fluorescence Photobleaching Recovery Experiment . . . . .	82
B. Results . . . . .	85
1. Effect of Ionic Strength . . . . .	85
2. Effect of Temperature . . . . .	95
3. Effect of Time . . . . .	100
4. Rebleaching Experiments . . . . .	103
C. Discussion. . . . .	105
Chapter 5. Ionic Strength-Dependent Dissociation of Spectrin from Ghost Membranes. . . . .	110
A. Methods . . . . .	110
B. Results and Discussion . . . . .	112
Chapter 6. Discussion . . . . .	117
A. Comparisons with Measurements of Translation and Rotational Diffusion . . . . .	118
B. Models of Erythrocyte Membrane Structure . . . . .	127
C. Concluding Remarks. . . . .	137
References . . . . .	139



TABLES

	<u>page</u>
1. The Major Erythrocyte Membrane Proteins and Glycoproteins. . . . .	10
2. Lateral Mobility of Membrane Proteins. . . . .	39
3. Lateral Mobility of Membrane Lipids and Lipid Analogues. . . . .	44
4. Selective Extraction Experiments on Eosin-Labeled Ghost Membranes.	75
5. Summary of FPR Experiments on Eosin-Labeled Ghost Membranes. . . .	86
6. Rebleaching Experiments on Eosin-Labeled Ghost Membranes . . . . .	104
7. Estimates of Membrane Viscosity. . . . .	123



## FIGURES

page

1. Models for Membrane Structure . . . . .	2
2. SDS-Polyacrylamide Gel Electrophorogram of Erythrocyte Membrane Proteins Stained with Coomassie Blue. . . . .	9
3. Structure of Band 3 . . . . .	17
4. Structure of the Erythrocyte Cytoskeleton . . . . .	25
5. Parameters Involved in a Typical Fluorescence Photobleaching Recovery Experiment . . . . .	46
6. Fluorophore Concentration Profiles Immediately After Bleaching . .	49
7. Ratio of Fluorescence Immediately After Bleaching to Fluorescence Before Bleaching <u>vs.</u> Bleaching Parameter. . . . .	50
8. Fluorescence Recovery $F(t)$ <u>vs.</u> $t/\tau_D$ for Diffusion, with Gaussian Laser Beam, for Various Values of $K$ . . . . .	51
9. Fractional Fluorescence Recovery $f(t)$ <u>vs.</u> $t/\tau_D$ for Diffusion, with Gaussian Laser Beam, for Various Values of $K$ . . . . .	51
10. Fractional Fluorescence Recovery $f(t)$ <u>vs.</u> $t/\tau_F$ for Flow, with Gaussian Laser Beam, for Various Values of $K$ . . . . .	51
11. a. Schematic Optical and Electronic System for Fluorescence Photobleaching Recovery. . . . .	54
b. Detailed Optical System for Fluorescence Photobleaching Recovery	55
12. Scheme for Rapid Removal and Replacement of Neutral Density Filter.	58
13. Factor $\gamma$ , ( $\gamma_D$ or $\gamma_F$ ), <u>vs.</u> $K$ for a Gaussian Beam . . . . .	63
14. Flow Recovery Curve on Immobile Fluorophore Used for Beam Calibration . . . . .	66
15. SDS-Polyacrylamide Gel Electrophoresis of Eosin-Labeled Ghost Membranes . . . . .	73
16. Experimental FPR Curves Under Extreme Conditions of $[\text{NaPO}_4]$ and Temperature . . . . .	87
17. Diffusion Coefficients and Fractional Recoveries of Fluorescence Under Various Conditions of Ionic Strength and Temperature . . . .	90



	<u>page</u>
18. Smoothed Experimental Fluorescence Recovery Curves at 21°C. . . . .	91
19. Smoothed Experimental Fluorescence Recovery Curves at 37°C. . . . .	93
20. Diffusion Coefficients and Fractional Recoveries of Fluorescence <u>vs.</u> Temperature at Various Ionic Strengths. . . . .	96
21. Reversibility of Diffusion Coefficients and Fractional Recoveries of Fluorescence . . . . .	98
22. Diffusion Coefficients and Fractional Recoveries of Fluorescence <u>vs.</u> Incubation Time at 37°C, 13 mM NaPO <sub>4</sub> . . . . .	101
23. Ionic Strength Dependent Dissociation of Spectrin . . . . .	113



## INTRODUCTION

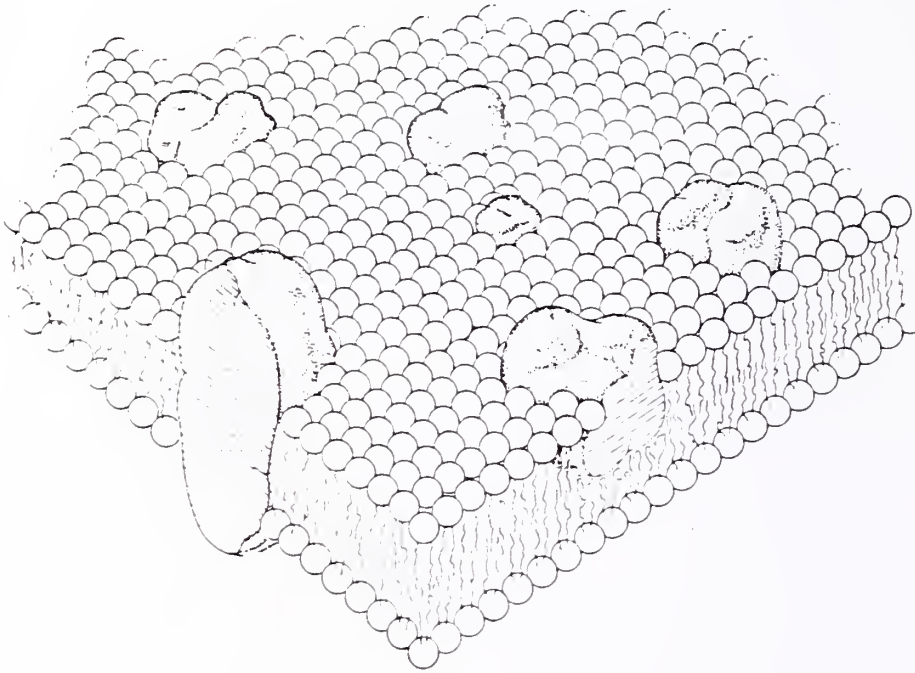
Cell membranes exist in a dynamic state. The observed lateral mobility of various membrane components has been instrumental in the formulation of a series of models for membrane structure and function introduced over the past decade. The fluid-mosaic model of Singer and Nicolson (ref. 1, fig. 1a) proposes that the major structural feature of cell membranes is a fluid lipid bilayer in which a population of proteins heterogeneous in size, shape, orientation, and function is embedded. Such a mosaic has no long-range order, and integral proteins are free to undergo translational diffusion within the membrane at rates determined both by lipid viscosity and by specific interactions (unspecified) with other intramembranous or extramembranous components. Functional roles for unrestricted translational diffusion are hypothesized in the enhancement of reaction rates on the membrane and in the rapid communication of signals across the plane of the membrane (1,2). Evidence in support of the fluid-mosaic model has been reviewed (1-3); much of the evidence will be presented in this thesis as part of the literature review.

The concept of controls or restrictions on the lateral mobility of membrane elements has proven to be an even more interesting avenue of investigation than the notion of lateral mobility itself. The fact that ligand binding by a cell surface receptor protein, for example, can lead to restriction of the lateral mobility of membrane

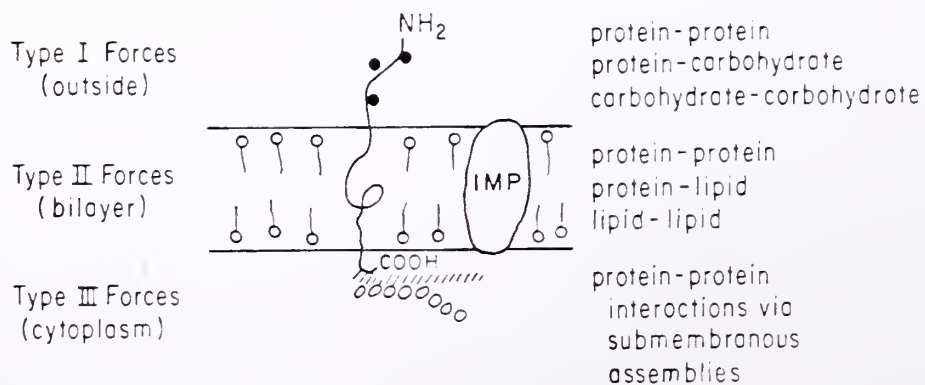




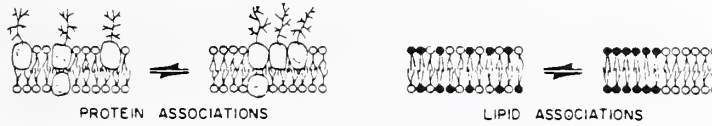
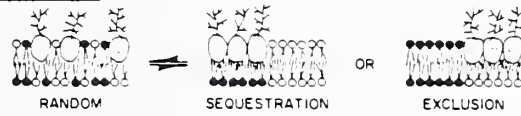
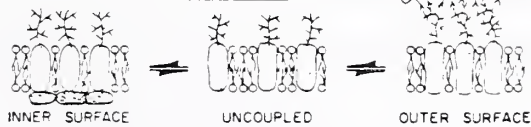
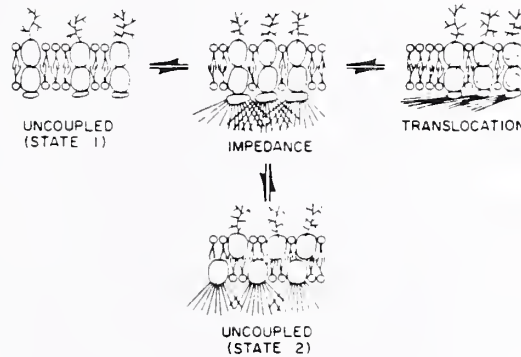
Figure 1. Models for Membrane Structure



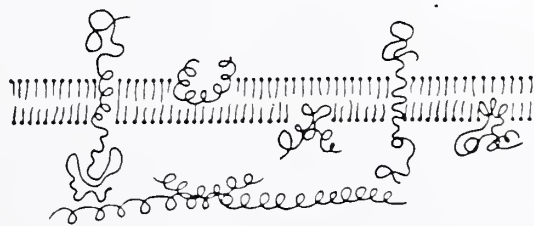
a. Fluid-Mosaic Model (ref. 1)



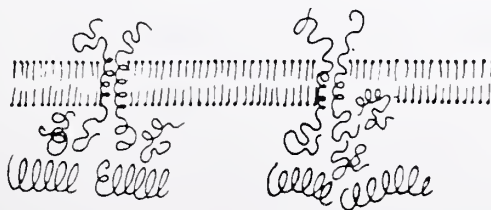
b. Forces Acting on Transmembrane Glycoproteins (ref. 5)

PLANAR AGGREGATION OR ASSOCIATIONDOMAIN FORMATIONPERIPHERAL MEMBRANE COMPONENTSMEMBRANE-ASSOCIATED (CYTOSKELETAL) COMPONENTS

## c. Restraint Mechanisms on Lateral Mobility of Membrane Glycoproteins (ref. 4)



FLUID-MOSAIC



FIXED-MATRIX

## d. Fixed Protein Matrix Model (ref. 6)



components and thereby influence cell behavior has been shown in several systems (reviewed in 2,4,5). In order to account for such observations, Edelman (ref. 5, fig. 1b) and Nicolson (ref. 4, fig. 1c) have stressed the importance of intramembraneous (and especially transmembranous) forces in the modulation of lateral mobility. Unlike the earlier fluid-mosaic model, in which the dominant factor affecting protein mobility is assumed to be the fluidity of the lipids, the later models consider protein-protein interactions both within the lipid bilayer and at the inner surface of the membrane to be the controlling features of many systems. Evidence for the importance of such interactions has come mainly from studies of antibody-induced patching and capping on lymphoid cells, cross-linking of surface glycoproteins by lectins leading to inhibition of patching and capping on lymphoid cells (anchorage modulation), and ligand-induced redistribution and capping on fibroblast cells (reviewed in 4,5).

With specific reference to the erythrocyte membrane, Marchesi (6) has proposed a fixed protein matrix model as an alternative to the fluid mosaic model (fig. 1d). In this formulation, protein-protein interactions are clearly of primary importance. The major peripheral protein, spectrin, is visualized as being along the inner membrane surface in a shell or matrix of closely-packed units, which may interact with integral, transmembrane proteins. This matrix could then support the overlying lipid bilayer. Translational diffusion of membrane elements is not precluded by such a model, though one would expect



mobility to be much more restricted in a membrane organized on a framework of fixed protein than in one governed by a fluid lipid bilayer. For example, in order for an integral transmembrane protein which is complexed to the fixed (inner surface) protein matrix to undergo lateral diffusion, either the transmembrane protein - peripheral protein complex would have to be dissociated, or the peripheral protein matrix itself would have to be disrupted.

This thesis addresses the question of restrictions on the lateral mobility of a well-characterized transmembrane protein, band 3, in a well-characterized mammalian cell membrane, that of the human erythrocyte. Although the erythrocyte does not possess the microtubule and microfilament systems important in control of lateral mobility in other mammalian cells, similar interactions between transmembrane proteins and peripheral (cytoskeletal) proteins might be expected to apply. The advantage of studying the lateral mobility of the major protein of the erythrocyte membrane is that, if mobility is restricted by membrane-associated forces, it should eventually be possible to dissect out those forces in detail since all the major protein and lipid components of this membrane are known and fairly well characterized. Furthermore, there already exists indirect evidence for restricted lateral mobility of band 3 (ref. 7,8). In this thesis, then, I present a systematic and direct study of the restriction on lateral mobility of band 3 in the human erythrocyte membrane. I demonstrate reversible conditions under which the restrictions on mobility are progressively lifted, and propose a model involving



at least two separate processes capable of restricting the lateral mobility of band 3. It is hoped that this research will lead to specific correlations between changes in lateral mobility of band 3 and both membrane structure and membrane function.

This paper begins with a critical summary of the published literature on the erythrocyte membrane, with particular reference to band 3 and evidence for its associations with other membrane components. Various techniques for the measurement of lateral diffusion on membranes are also described, concentrating on the technique of fluorescence photobleaching recovery. Chapters 2-5 comprise the experimental sections of this report. Finally, chapter 6 includes a discussion of my data in the light of previous work in this field as well as several models for the interactions of band 3 with the erythrocyte membrane which could account for my observations.



## CHAPTER 1. LITERATURE REVIEW

### A. THE ERYTHROCYTE MEMBRANE

#### 1. General Review of Structure

a. The Lipid Bilayer. The lipids of the erythrocyte membrane are believed to be organized as a fluid bilayer extending completely around the surface of the cell (reviewed in 2,9). This picture is drawn largely from extrapolations of lipid behavior in other membrane systems, both natural and artificial, as the erythrocyte membrane has proved refractory to study by the usual techniques for demonstrating the existence of a fluid bilayer (9). One piece of circumstantial evidence, as well as an extremely interesting observation in its own right, is the asymmetric distribution of the various phospholipid classes in specific halves of the bilayer (reviewed in 3,9). Through comparison of phospholipid degradation due to the action of purified phospholipases on intact erythrocytes versus that on permeable ghost membranes, it was shown that approximately 70% of the membrane phosphatidylcholine and 80-90% of the total sphingomyelin (both choline-containing phospholipids) are located in the outer half of the bilayer. Study of phospholipid labeling on intact erythrocytes by permeable versus impermeable amino group reagents further revealed that 80-90% of the membrane phosphatidylethanolamine and all of the phosphatidylserine (both amino-containing phospholipids) are located in the inner half of



the membrane. Although erythrocyte membranes have a high cholesterol content (approximately equimolar with phospholipid), the distribution of this neutral lipid between the two halves of the bilayer has not been determined with any degree of certainty.

b. The Proteins. The literature concerning the polypeptides of the erythrocyte membrane has been extensively reviewed in the past decade (3,6,9-13). Denaturation and separation of the various polypeptides from the membrane lipid and from each other can be achieved by dissolution of erythrocyte membranes in sodium dodecyl sulfate (SDS). Polyacrylamide gel electrophoresis of SDS-treated membranes reveals eight major protein bands when stained with Coomassie blue and four additional glycoprotein bands when stained with PAS-Schiff reagent (14); these bands are named according to their relative mobilities on the gel (fig. 2; table 1). Singer and Nicolson (1) have categorized the polypeptides according to the ease with which they can be extracted from the membrane. Those proteins extractable by simple manipulation of the ionic strength or pH of the medium (bands 1,2,4,5,6) are considered peripheral or extrinsic to the membrane, and are presumably membrane-bound through electrostatic interactions alone. Those polypeptides extractable only with detergents or other chaotropic agents (bands 3,7,PAS-1,2,3,4) are considered integral or intrinsic membrane proteins; they are presumably anchored in the membrane through hydrophobic interactions with membrane lipid.



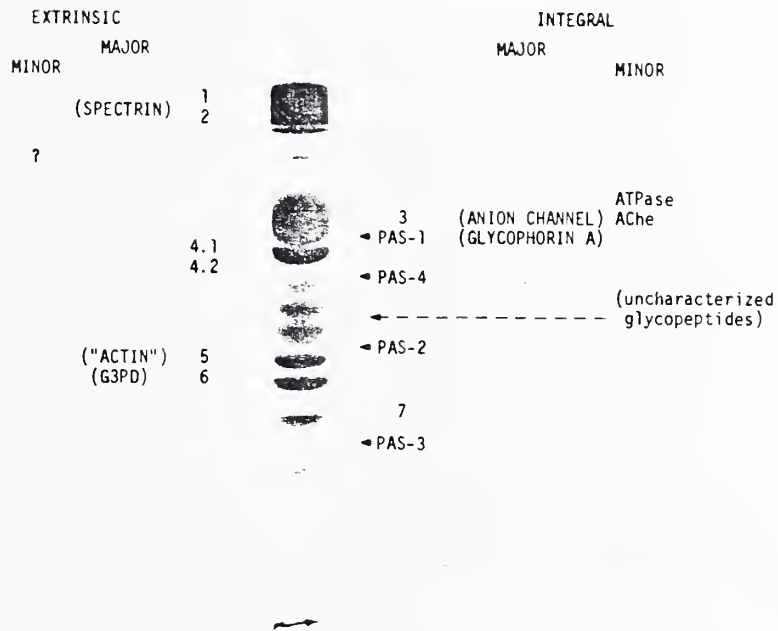


Figure 2. SDS-polyacrylamide gel electrophorogram of erythrocyte membrane proteins stained with Coomassie blue. See text for details. (taken from ref. 9)



TABLE 1. THE MAJOR ERYTHROCYTE MEMBRANE PROTEINS  
AND GLYCOPROTEINS<sup>a</sup>

<u>Component</u>	<u>molecular wt.</u> <u>(daltons)</u>	<u>% of total</u> <u>protein</u>	<u>copies/cell</u>	<u>% carbohydrate</u>
1	240,000	15	216,000	
2	215,000	15	235,000	
2.1 <sup>b</sup>	200,000	6	100,000	
3	88,000	24	940,000	4-9
4.1	78,000	4.2	180,000	
4.2	72,000	5.0	238,000	
5	43,000	4.5	359,000	
6	35,000	5.5	540,000	
7	29,000	3.4	403,000	
PAS-1 <sup>c</sup>	62,000	6.7 (2.8) <sup>d</sup>	500,000	60
PAS-2	31,000			60

<sup>a</sup> All values from ref. 13 unless otherwise indicated.

<sup>b</sup> Values from ref. 15.

<sup>c</sup> Values from refs. 13, 209.

<sup>d</sup> 6.7% by total weight: 2.8% by weight of protein portion.



More recently, Marchesi (6) has classified the various membrane proteins according to function. Those polypeptides exposed to the extracellular environment are termed contact or receptor proteins; they include glycophorins A and B and band 3 as well as several minor, poorly characterized components. All of these proteins are glycoproteins oriented such that their carbohydrate is accessible at the outer membrane surface. It is interesting that the major contact proteins are also exposed to the intracellular surface (3,9); as we shall see, this may be important in their mode of attachment to various membrane elements. Transmembrane proteins involved in the transport of ions or metabolites, as well as various glycolytic enzymes which are located on the inner membrane surface, are grouped together as catalytic proteins. Bands 3 (anion permeation site) and 4.5 (glucose permeation site) are examples of transport proteins; band 6 (glyceraldehyde-3-phosphate dehydrogenase) and aldolase are two membrane-bound enzymes involved in glycolysis. The third major class of polypeptides consists of peripheral membrane proteins which are found exclusively at the inner membrane surface and are involved in stabilizing the membrane structure. These proteins are named support proteins, and include spectrin (bands 1,2), ankyrin (band 2.1), actin (band 5), and bands 4.1 and 4.2 (refs. 9,15,16). The remainder of this review of the erythrocyte membrane will focus on band 3 and its possible interactions with other membrane proteins, including glycophorin and the various cytoskeletal or support proteins.



## 2. Band 3

a. Physical and Chemical Properties. Band 3 is defined as a heavily stained, diffuse band of protein of about 90,000 daltons on SDS-polyacrylamide gel electrophoresis of human erythrocyte membranes (14; reviewed in 1,9-13,17,18). It is the major protein component of the erythrocyte membrane, comprising approximately 25% of the total membrane protein and approximately 80% of the intrinsic membrane protein (13,14,19). An approximate calculation (13,14) estimates the number of band 3 monomers per cell at about  $1 \times 10^6$ . The apparent molecular weight of band 3 covers the range 85,000 - 110,000 daltons; this band spread is usually attributed to extreme heterogeneity of carbohydrate (13,20,21), although polypeptide heterogeneity cannot be absolutely ruled out without primary sequence data. Heterogeneity of carbohydrate has also been demonstrated by the binding of lectins to band 3, in that concanavalin A binds fairly specifically to band 3 (ref. 22) but only a fraction of band 3 interacts (23,24).

Band 3 has been isolated and purified in a number of laboratories (22,24-27). Its carbohydrate content is estimated at 4-9% (refs. 13, 22,25,28), with mannose, galactose, and N-acetylglucosamine present in approximately 1:2:2 molar ratio, but with little sialic acid (21,22). This composition suggests the presence on band 3 of complex-type oligosaccharides attached to asparagine residues by N-glycosidic bonds (9). Indeed, it has recently been shown (21) that there is a single primary site of glycosylation in the COOH-terminal part of the molecule, in



a region with composition  $Asx_1Ser_2$ . The amino acid composition of band 3 is marked by its high proportion (about 40%) of nonpolar residues (10,22,26,28). This observation is consistent with the solubility characteristics of band 3. It is a highly hydrophobic protein that is soluble only in ionic or nonionic detergents (12-14, 25,29). Solubilization by Triton X-100 is accompanied by the binding of 0.77 grams of detergent per gram of protein (30).

Several functions have been ascribed to polypeptides in the band 3 region. These include anion transport (28,31-38), NaK ATPase activity (39,40), water permeation (41), and acetylcholinesterase activity (42), and each is presumably mediated by a different protein. It is likely that some of these functions involve very small amounts of protein relative to the total amount in band 3. For example, the total content of NaK ATPase per cell is estimated at three hundred copies (43). It is also possible that some of these functions may not be present in band 3 at all, residing instead in minor proteins which do not comigrate with band 3 on polyacrylamide gel electrophoresis but which are contaminated with band 3 protein in various other purification procedures. It is pertinent in this regard that recent reconstitution experiments have demonstrated that glucose transport across the membrane, originally thought to be mediated by band 3 (refs. 44-47), is in actuality performed by band 4.5 protein (48,49).

Chemical heterogeneity of protein in the band 3 region has been shown in several ways. Treatment of intact erythrocytes with pronase results in cleavage of most of the protein in the band 3 region,



but at least three pronase-resistant polypeptides always remain at the location of native band 3 in SDS-polyacrylamide gels (18). Two-dimensional electrophoresis (50,51) and isoelectric focusing (18) separate band 3 into one major and four or five minor components. It is likely, however, that an overwhelming proportion of band 3 polypeptide is homogeneous, since well over 90% of the protein behaves uniformly in various labeling and cleavage studies (52), and peptide maps of protein taken from all parts of the band 3 region on SDS gels appear identical (53). In addition, only a single COOH-terminal amino acid is found (52), as well as a uniformly blocked NH<sub>2</sub>-terminus (22,25,26,28,54).

b. Conformation in the Membrane. The disposition of band 3 in the membrane has been extensively studied and recently reviewed (17,18). Portions of band 3 are exposed to both the extracellular and intracellular surfaces of the membrane, proving its transmembrane orientation. This conclusion is based on a series of experiments using membrane-impermeable reagents to label either the extracellular surface of intact erythrocytes, the intracellular surface of either resealed ghost membranes or inside-out vesicles (55), or both surfaces of leaky ghost membranes. These probes include: 1) chemical agents such as FMMP<sup>1</sup> (3,56,57), TNBS (58), IBSA (28), DIDS (31-33,38), NAP-aurine (59),

---

<sup>1</sup>Abbreviations used in this section include: formylmethionylmethylphosphate, FMMP; 2,4,6-trinitrobenzenesulfonic acid, TNBS; 1-isothiocyano-4-benzenesulfonic acid, IBSA; 4,4'-diisothiocyano-2,2'-stilbenedisulfonic acid, DIDS; N-(4-azido-2-nitrophenyl)-2-aminoethylsulfonic acid, NAP-aurine.



and others (19,60-63); 2) proteolytic enzymes (11,13,33,37,55-57,64-68); and 3) iodination catalyzed by the enzyme lactoperoxidase (69-75). For example, one study demonstrated that the same band 3 fragment produced by proteolytic cleavage from the outside was iodinated from the inside (70), while another study showed that band 3 fragments labeled from the inside were different from those labeled from the outside (71). The latter experiment, as well as many others cited above, further implies that the arrangement of band 3 in the membrane is both asymmetric with respect to the two membrane surfaces and permanent on the time scale of the labeling. It has been demonstrated recently that the linear band 3 sequence must cross the membrane at least twice, as the membrane-impermeable (76) sulfhydryl reagent N-ethylmaleimide is found to label intracellular cysteine residues on both sides of an extracellular proteolytic cleavage point (77).

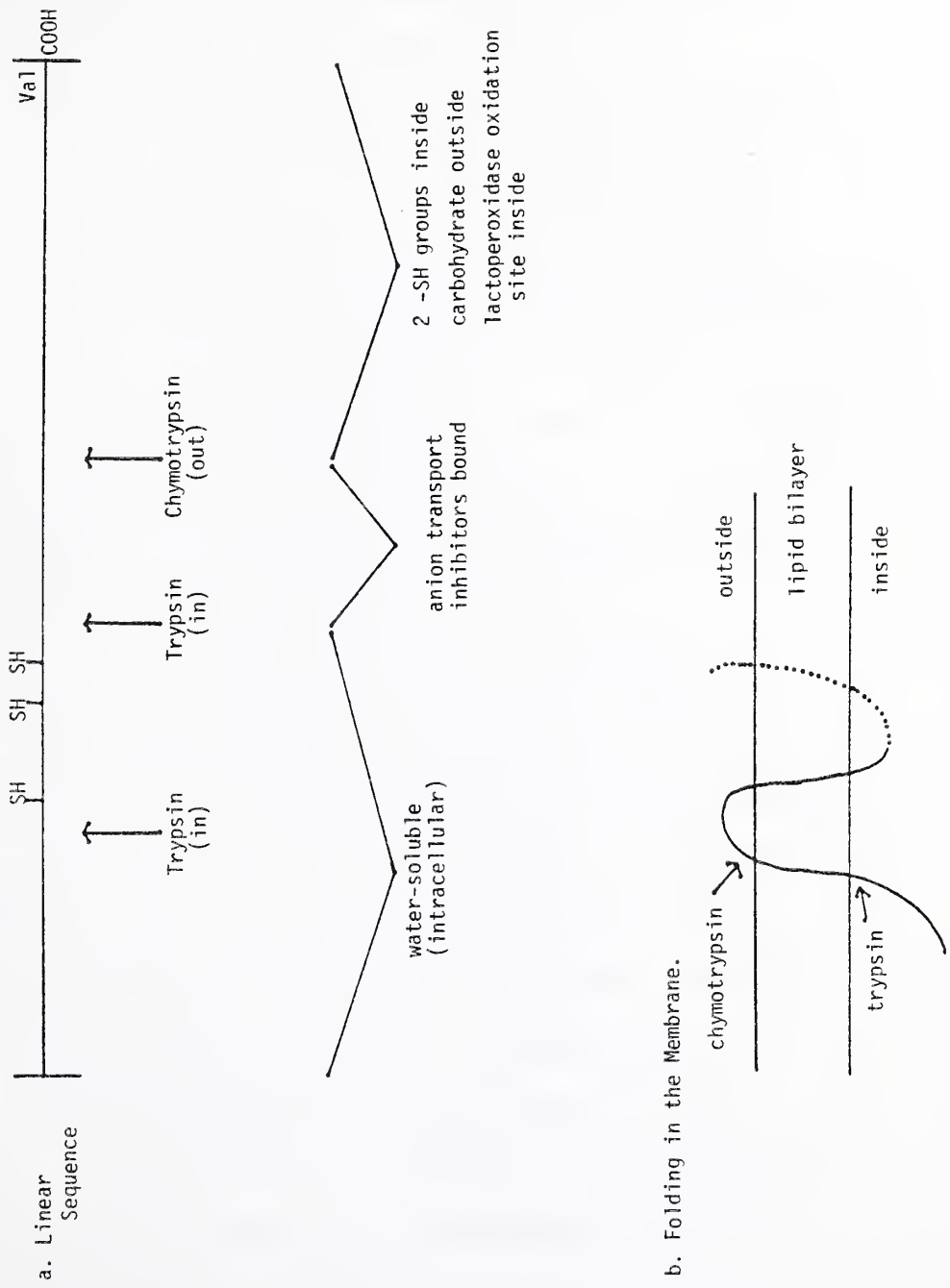
Studies completed over the past three years have greatly advanced our knowledge of the detailed folding of band 3 in the membrane. Chymotrypsin treatment of intact cells generates a pair of membrane-bound fragments of approximate molecular weights 55,000 and 35,000 from band 3, while extracellular trypsin has no effect on band 3 at physiological ionic strength (52,65,67,78). At low ionic strength, however, cleavage by trypsin from the outside can occur (78), implying changes in band 3 conformation with ionic strength. The blocked  $\text{NH}_2$ -terminus of the protein is located in the 55,000 dalton fragment, while the  $\text{COOH}$ -terminus is associated with the 35,000 dalton piece (21,52,78). Intracellular trypsin treatment produces a membrane-bound fragment reported as around 50,000 daltons and



staining with a diffuse pattern on SDS gels (37,54,65,67,78); this fragment contains the COOH-terminus. In addition, water-soluble fragments of approximate molecular weights 40,000, 18,000, and 22,000 are produced by intracellular trypsin treatment, where the latter two peptides are fragments generated from the former by proteolysis at a second cleavage site (67,79,80). Fukuda et al. (81) used S-cyanylation of the 55,000 dalton chymotryptic fragment of band 3 combined with lactoperoxidase-catalyzed iodination and antibodies directed against the cytoplasmic region of band 3 to show that the 40,000 dalton tryptic fragment bearing the NH<sub>2</sub>-terminus is in an intracellular location. Finally, when cells are treated with chymotrypsin on the outer surface followed by trypsin on the inner surface, an approximately 17,000 dalton membrane-bound segment is obtained (67,82); this peptide is labeled by various anion transport inhibitors (52,67,82,83). These and other features of band 3 structure have been incorporated into a linear map of various cleavage sites, together with the minimum model for folding of band 3 in the membrane consistent with experimental evidence (fig. 3a,b).

Several lines of experimentation suggest that band 3 exists as a dimer in the membrane. Solubilization of erythrocyte membranes in Triton X-100 results in 180,000 dalton protein which can be quantitatively converted to 90,000 dalton band 3 monomer in denaturing detergents (30,84). Treatment of intact erythrocytes with noncleavable disulfide cross-linking reagent (85,86), cleavable bifunctional cross-linking reagent (86,87), or cleavable bifunctional photoactivatable



Figure 3. Structure of Band 3.



cross-linking reagent (88) all lead to production of dimer as the major (85-87) or only (88) cross-linked band 3 species. Most recently, native and cross-linked band 3 in the intact ghost membrane have been reported to have identical rotational correlation times, implying similar cross-sectional areas in the plane of the membrane before and after cross-linking and hence similar states of aggregation in the membrane (89). The site of cross-linking between band 3 monomers appears to reside in the  $\text{NH}_2$ -terminal, intracellular portion of the molecule (67), specifically in the cysteine-rich 16-20,000 dalton fragment produced by intracellular trypsin cleavage at both of its major sites of proteolysis (79,90) (see fig. 3a).

Freeze-fracture electron microscopy (91-93) of erythrocyte membranes reveals the presence of 80-85A intramembranous particles (IMP) in the cleavage plane, which are presumed to be protein embedded in the center of the lipid bilayer (94). Early studies of the particles, including experiments correlating the distribution of ferritin-conjugated lectins with the distribution of the particles, suggested their connection with glycophorin (92,94-97). Arguments were soon advanced against glycophorin being the sole constituent of the particles, however, because of its small hydrophobic (intramembrane) portion relative to the large mass of the intramembranous particle (3,10,13). More recent evidence, including correlation between the distribution of ferritin-conjugated DIDS and the particles, has implicated band 3 protein as the major component of the particles in the intact membrane (22,36,98). Eighty Angstrom particles have



been seen both in Triton-extracted vesicles containing predominantly (90%) band 3 along with erythrocyte membrane lipids (99) and in membranes reconstituted from purified band 3 and egg phosphatidylcholine (100), as well as in membranes prepared from En(a-) erythrocytes which lack glycophorin A (101). The total number of particles in the intact cell is about  $5 \times 10^5$  (ref. 97), which is the same as the number of band 3 dimers (13). As the number of glycophorin monomers is also about  $5 \times 10^5$ , some have suggested that the contents of one intramembranous particle might be one band 3 dimer combined with one glycophorin monomer (4,98). It has yet to be demonstrated, however, that there is one particle which contains both molecules. Whereas band 3 alone appears to yield particles of similar size in reconstituted membranes to those in intact cells (100), reconstituted glycophorin particles are smaller and more aggregated than those in intact cells (102). This suggests that glycophorin does not form particles of its own in intact cells, while band 3 may. Rather, glycophorin may either be included in band 3 particles as postulated above or exist free of band 3 in the membrane, becoming artificially included between the particles when they are aggregated (see below).

c. Associations with Other Membrane Proteins. As noted in the previous section, association between glycophorin monomer and band 3 dimer in the intramembranous particles has been postulated. The observations that trypsin degradation of glycophorin in intact cells exposes additional sites on band 3 for interaction with DIDS (33) and lactoperoxidase (103) further imply that at least part of band 3 may be shielded from the outside by glycophorin. On the other hand,



extraction of erythrocyte membranes by Triton X-100 readily separates glycophorin from band 3 (refs. 26,84), and cross-linking between glycophorin and band 3 has never been demonstrated chemically (104). The latter piece of negative evidence must be tempered, however, by the knowledge that glycophorin itself is very resistant to the action of cross-linking reagents, perhaps because of its extensive glycosylation. Unlike glycophorin, bands 4.2 and 6 remain associated with band 3 after extraction with nonionic detergent. Dissociating agents such as p-chloromercuribenzoate must be introduced in order to separate band 4.2 from band 3 (refs. 26,84), while high ionic strength is sufficient to dissociate the band 3 - band 6 complex (26,84). The stoichiometry of band 6 binding is one-to-one with band 3, and the site is located in the cytoplasmic NH<sub>2</sub>-terminal portion of band 3 which is susceptible to trypsin cleavage (84,105). Specific binding of the enzyme aldolase to the cytoplasmic domain of band 3 has also been demonstrated, in the ratio of one aldolase tetramer per band 3 monomer (106,107). Associations such as these have led some to suggest that the cytoplasmic region of band 3 may be the site of organization of a number of glycolytic enzymes into functional enzyme complexes (108).

Evidence implicating band 3 in direct interactions with various cytoskeletal elements has been accumulating. These data will be presented in a separate section of this literature review, after the organization of the cytoskeleton has been discussed.

d. Functions. Proteins in the band 3 region have been implicated



in anion transport, NaK transport, water permeation, and acetylcholinesterase activity (see above). The amount of protein involved in the latter three activities is likely to be very small compared to the quantity concerned with anion transport (18). This summary, therefore, will focus on evidence identifying band 3 as the anion transport protein, in the expectation that the various structural properties attributed to the bulk of band 3 will also apply to this functional system.

The importance of anion transport in erythrocytes has long been recognized. Rapid exchange of chloride for bicarbonate across the erythrocyte membrane greatly increases the CO<sub>2</sub> carrying capacity of the blood (43,109). The evidence that band 3 is involved in anion permeation is of three kinds: 1) covalent labeling of band 3 by irreversible inhibitors of anion transport; 2) retention of the anion transport system in erythrocyte membrane-derived vesicles containing band 3 as their major component; and 3) reconstitution of anion transport activity in phospholipid vesicles using partially purified band 3 preparations (17,36).

The most potent and site-specific covalent binding inhibitors of anion transport are the isothiocyano derivatives of stilbene-disulfonic acid such as [<sup>3</sup>H]-DIDS, [<sup>3</sup>H]-H<sub>2</sub>-DIDS, and [<sup>125</sup>I]-I<sub>2</sub>-DIDS. These compounds irreversibly inhibit anion exchange upon binding, complete inhibition corresponding to 0.9-1.1 x 10<sup>6</sup> molecules bound per cell (31-33,38,110,111). This is also the number of band 3 monomers per cell, providing circumstantial evidence at least for the role



of band 3 in anion permeation. There is further a linear relationship between the inhibition of transport activity and the binding of inhibitor. At maximal inhibitory concentrations, more than 90% of the label is found in the band 3 region on SDS-polyacrylamide gels. The remaining 7-10% is associated mainly with glycophorin. Since anion exchange across the membrane is so rapid, it is argued that the major protein labeled by covalent anion transport inhibitors must, in fact, be the protein involved in anion permeation. Unreasonably high turnover numbers would have to be invoked for the exchange process if a minor labeled component, rather than band 3, were responsible for this activity (32,33).

Eosin derivatives (isothiocyanate, iodoacetamide, maleimide) inhibit anion exchange by 50% when approximately  $5 \times 10^5$  molecules are bound per cell (112). These compounds are irreversibly bound and occupy common binding sites with  $H_2$ -DIDS, although other sites on band 3 are labeled as well (112). It is curious that a maleimide derivative, which should react specifically with -SH groups, is reported to be an irreversible ligand for band 3, which has no external -SH groups (77). This question is not addressed by the authors.

There exist substrates of the anion transport system which are also capable of covalent reactions. Thus reduction of pyridoxal-5-phosphate with  $NaBH_4$  (ref. 63) or photoactivation of NAP-aurine (113) leads to inactivation of anion exchange and preferential (DIDS-inhibitable) labeling of band 3. When inhibitor-treated (DIDS,



pyridoxal phosphate, or NAP-aurine) intact cells are reacted with proteolytic enzymes under conditions which do not affect anion transport in native erythrocytes (33), nearly all of the nonspecific membrane label, as well as the glycophorin-associated label, is removed from the membrane without affecting band 3-associated label (33,63,113). Taken together, covalent labeling studies provide very strong evidence that inhibition of anion transport is associated with modification of band 3.

Anion permeability is retained in erythrocyte membranes from which almost all the major proteins have been removed except band 3. Changes in ionic strength and pH can be used to remove extrinsic membrane proteins and low concentrations of Triton X-100 to extract the sialoglycoproteins. The remaining vesicles contain essentially all the original lipid of the erythrocyte plus band 3. They retain nearly all the permeability parameters of the anion transport system, although some kinetic features cannot be entirely reproduced (99). DIDS-inhibitable anion fluxes can be reconstituted into artificial lipid vesicles using crude Triton X-100 extracts of erythrocyte ghosts (containing band 3 and glycophorin) (34). Purified band 3 protein reconstituted in vesicles containing lecithin, erythrocyte lipids, and exogenous glycophorin mediates anion exchange which is 60% inhibited by pyridoxal phosphate -  $\text{NaBH}_4$  (27), although it is not at all certain whether this preparation could transport ions in the absence of glycophorin. Reconstitution studies are clearly the only direct and definitive method for



proving the relationship between band 3 and anion transport in the erythrocyte membrane, and the reconstitution results to date must be considered highly preliminary. Nonetheless, an overwhelming body of indirect data implicates better than 90% of band 3 protein in the activity of anion transport.

### 3. Cytoskeleton

a. Definition and Components. The erythrocyte membrane cytoskeleton can be operationally defined as the insoluble material remaining after extraction of intact erythrocytes or ghosts with the nonionic detergent Triton X-100 (29,114; see 6,115,116 for review). This material contains approximately 60% of the original membrane protein, including all of the spectrin (bands 1 and 2), actin (band 5), ankyrin (bands 2.1,2.2,2.3,2.6) and band 4.1 as well as portions of bands 3, 4.2,4.9, and 7 (refs. 29,114,117; fig. 4a). The core of the cytoskeleton apparently comprises bands 1, 2, 5, 4.1, and 4.9, since the shape and structure of the skeleton are retained when the other elements are eluted with hypertonic KCl (118) but destroyed if either spectrin or actin is removed (119). Spectrin can be localized to the inner membrane surface through the use of ferritin-conjugated antibodies (120); this is the orientation of the cytoskeleton as well. Electron micrographs of the cytoskeleton reveal a continuous web-like reticulum consisting of twisted, randomly orientated microfilaments (5-40 nm diameter) irregularly coated with nodular protrusions (30-100 nm diameter) (121). The network appears to cover approximately



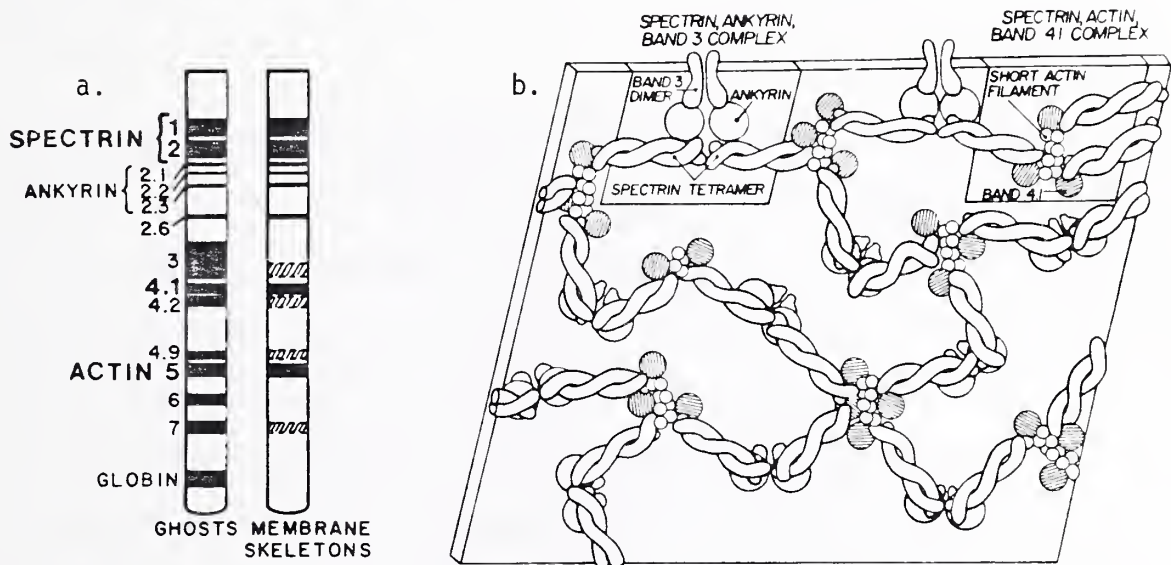


Figure 4. Structure of the Erythrocyte Cytoskeleton

- a. Schematized SDS-polyacrylamide gel electrophorogram of erythrocyte ghost proteins and cytoskeletal proteins, as revealed on staining with Coomassie blue.
  - b. Postulated organization of the cytoskeleton (not to scale).
- (taken from ref. 116)



30-35% of the inner membrane surface (115). This assembly provides support and stability to the erythrocyte membrane, endowing the erythrocyte with both its characteristic shape and its unusual flexibility.

b. Spectrin: Structure in Solution. The major protein of the cytoskeleton, spectrin, is composed of two high molecular weight polypeptides, bands 1 and 2 (molecular weight 240,000 and 220,000 daltons, respectively) (see 6,115,116,122,123 for review). These subunits are similar in structure but not identical (6,124). They associate in solution to form heterodimers (1+2) and heterotetramers (1+2)<sub>2</sub>, but only traces of higher aggregates (125-129). Spectrin dimers and tetramers are linked in a simple equilibrium which is readily reversible at 29°C but kinetically trapped at 4°C. The tetramer seems to be the physiological species on the intact membrane (88,130), although appreciable amounts of dimer are also found in low ionic strength medium (130). When examined by electron microscopy after low-angle shadowing, purified spectrin heterodimers appear as long (90-105 nm), slender (5 nm), flexible molecules in which two distinct strands lie partially separated or variably coiled in a loose double helix (131). Associations between the strands appear to be weak except at the ends of the molecule, where sites of tight binding exist. The electron microscopic finding that spectrin dimers exist as long, thin rods in solution is consistent with the results of some (125), but not all (127,129), hydrodynamic studies.



Spectrin dimers join end-to-end to form tetramers of length 180-210 nm, but higher aggregates are not seen. The latter observation indicates a head-to-head binding of the dimers, since head-to-tail binding would be expected to produce higher order oligomers as well (131).

c. Spectrin: Polymerization with Actin and Band 4.1. The inability of purified spectrin to polymerize beyond the tetramer in solution suggests that at least one other membrane element may be necessary in order to form the anastomosing cytoskeletal reticulum. Stripping of ghost membranes down to spectrin, actin, and bands 4.1 and 4.9 alone with hypertonic KCl leaves an intact cytoskeletal network (118), implicating at least one of the latter three proteins in the role of cross-linking spectrin. A mixture containing purified spectrin tetramer, filamentous (polymerized) actin (F-actin), and band 4.1 at physiological ionic strength forms a high molecular weight complex consisting of all three elements (132). Electron microscopy of the ternary complex shows actin filaments linked by spectrin bridges, suggesting that the actin-binding regions of the tetramer are at the tail ends of the molecule. Spectrin dimer is univalent in that it binds to but does not crosslink the actin filaments. Globular (unpolymerized) actin (G-actin) also fails to form extended complexes, as do mixtures of any two of the three purified proteins (132).

Other findings consistent with these observations are the following:

1) "purified" spectrin tetramer (contamination with band 4.1 was not



rigorously excluded) is found to cross-link F-actin (but not G-actin) into a highly viscous gel, while spectrin dimer binds to but does not cross-link F-actin (133); 2) oligomeric complexes of spectrin, actin, and band 4.1 cause exogenous actin to gel whereas purified spectrin dimers or tetramers lack this ability (134); and 3) at low but not at physiological ionic strength, binary complexes between spectrin and band 4.1, as well as between spectrin and actin, can form (cited in 116). Electron microscopy of spectrin-band 4.1 complexes indicates that the binding site for band 4.1 (a 60Å sphere) is at the same end of the spectrin molecule as the actin site (135).

Taken together, these studies provide strong evidence for a basic cytoskeletal network composed mainly of long, flexible, bivalent spectrin tetramers cross-linked at each end by actin and band 4.1 (ref. 116; see fig. 4b). The actin is probably present in the form of short oligomers, since the ratio of spectrin monomer to actin monomer in the membrane is roughly one to one (132,136). Some nonpolymerized or G-actin may also be present (137), as well as some spectrin tetramers which are unassociated with either actin or band 4.1 (ref. 115).

d. Spectrin: Binding to the Membrane. Several modes of interaction between the spectrin-actin-band 4.1 complex and the overlying lipid bilayer have been demonstrated. Purified spectrin binds specifically to a population (about 100,000 per cell) of high-affinity ( $K_D \approx 10^{-7}M$ ) sites on the inner surface of ghost membranes (138). The binding is



ionic strength-dependent, saturable, and reversible under conditions which favor extraction of spectrin from red cell membranes. Band 2 appears to contain the site on spectrin which is involved in binding, since isolated band 2 both binds to the inner surface of erythrocyte membranes and inhibits the binding of native spectrin, while isolated band 1 is inactive in both respects (6). Chymotryptic digestion of spectrin-depleted, inside-out membrane vesicles releases a 72,000 dalton polypeptide which retains spectrin-binding activity in solution and competitively inhibits ( $K_I \approx 10^{-7}M$ ) the binding of spectrin to vesicles which have not been treated with chymotrypsin (139). Antibody to purified 72,000 dalton proteolytic fragment cross-reacts only with band 2.1 among the membrane proteins; this reaction is blocked in the presence of the 72,000 dalton fragment (15). The extrinsic membrane protein band 2.1 is thus identified as the primary attachment site for spectrin in the membrane, and is named ankyrin (15). Electron microscopy shows the ankyrin binding site on spectrin to be 200Å distal to the end of spectrin involved in the dimer-tetramer interaction (135). The stoichiometry of binding is not clear, although ratios of spectrin to ankyrin (2 moles spectrin dimer per mole ankyrin) and spectrin to high-affinity binding sites (2 moles spectrin dimer per mole of binding sites) on the intact membrane might imply that each spectrin heterotetramer is bound to a single high-affinity membrane attachment site containing band 2.1 (refs. 15,140; but see below). Peptide maps of bands 2.1, 2.2, 2.3, and 2.6 are all homologous with the 72,000 dalton fragment (140,141), suggesting either that



a family of closely related spectrin-binding proteins exists on the membrane, or that the lower molecular weight bands are artifactual proteolysis products of the parent band 2.1.

In addition to the 72,000 dalton water-soluble fragment which interacts with spectrin, ankyrin contains a 100,000 dalton domain which does not bind spectrin (15). The larger domain is membrane-bound but not transmembrane, since it cannot be labeled from the extracellular surface of the membrane in intact cells (13) and since it can be eluted from the membrane in dilute acid without detergent (15). Interactions between band 3 and ankyrin, probably involving this 100,000 dalton domain, are discussed below.

It is important to note that the binding studies summarized above are performed under conditions such that associations between spectrin and the membrane with  $K_D > 10^{-6}M$  would not be detectable (15). Spectrin may therefore interact in a meaningful way, although with lower affinity, with proteins other than ankyrin or with membrane lipids. Evidence for spectrin-lipid interactions includes the following: 1) spectrin extracts stabilize artificial phospholipid vesicles and prevent calcium-induced vesicle fusion (142); 2) spectrin stabilizes membrane phospholipid asymmetry in that oxidative cross-linking of spectrin allows 30-50% of the inner membrane phospholipids (phosphatidylserine and phosphatidylethanolamine) to become accessible at the outer membrane surface (143); and 3) spectrin is easily crosslinked to inner membrane phospholipids in the intact red cell (144). In addition to spectrin, actin may play a role in attaching the cytoskeleton to the membrane, since F-actin but not G-actin can bind



directly to a trypsin-sensitive site on spectrin-depleted inside-out vesicles (145).

One model for the organization of the principal proteins of the cytoskeleton which is consistent with the data available is given by Lux (ref. 116; see fig. 4b).

#### 4. Band 3 - Cytoskeleton Interactions

a. Band 3 - Ankyrin. Triton X-100 extracts of spectrin-depleted erythrocyte membranes contain ankyrin tightly linked to band 3 in one-to-one molar ratio (146). This complex, which may also include some band 4.2, involves 10-15% of the total band 3 in the membrane. The ankyrin - band 3 bond is so strong that nondenaturing conditions under which the two proteins are separated have not been found. The ankyrin-linked band 3 has a transmembrane orientation and appears to be nearly identical to the remaining band 3 by peptide mapping and immunologic cross-reactivity. Solubilized ankyrin-linked band 3 binds purified spectrin, while free band 3 does not. Finally, detergent-extracted cytoskeleton preparations are always found to contain a certain amount of firmly bound band 3. Taken together, these data implicate 10-15% of the total band 3 as the ultimate membrane attachment site for spectrin, ankyrin serving as a link between band 3 and spectrin (146).

The stoichiometry of this linkage is as yet unresolved. If ankyrin-linked band 3 has the same tendency as the major portion of band 3 to dimerize in situ (26,85,89,100), then one would expect the ankyrin-linked band 3 oligomer to be arranged with two moles each of band 3 and ankyrin. Such a stoichiometry is supported by the finding that band 2.1, like band 3, is cross-linked in dimeric form (85).



On the other hand, ratios of total spectrin to total ankyrin in the membrane suggest the binding of one spectrin tetramer by one band 2.1 monomer, if all the spectrin is linked to ankyrin. Since cross-linking and solubilization studies have consistently failed to demonstrate the presence of spectrin hexamer or octomer on the membrane, it seems unlikely that two spectrin tetramers would be organized in close proximity by (band 3-ankyrin)<sub>2</sub> oligomers. Assuming that the spectrin tetramer is symmetric (131), with one ankyrin binding site per dimer (135), such an arrangement would also leave one end of each spectrin tetramer unattached to ankyrin. One possible resolution to this dilemma stems from the observation that, at physiological ionic strength, approximately 45% of the total spectrin is present as dimers and tetramers which are unassociated with actin or band 4.1 in both ghost extracts (147) and membrane cytoskeletons prepared directly from intact erythrocytes (114,148). If, at any one time, approximately 50% of the spectrin in the intact membrane is also unassociated with ankyrin (perhaps bound to the membrane through interactions with lipid), complexes involving one spectrin tetramer and one ankyrin-linked band 3 dimer would be consistent with all the available data (see fig. 4b).

b. Band 3 - Spectrin. Information regarding direct band 3 - spectrin interactions on the intact erythrocyte membrane has been gathered using four general techniques: copurification of detergent-extracted band 3 with other membrane components; inhibition of spectrin binding



to spectrin-depleted inside-out vesicles; perturbation of membrane composition leading to aggregation of intramembranous particles on freeze-fracture electron microscopy; and cross-linking of membrane components in situ under various conditions. No direct associations between band 3 and spectrin or actin are observed in Triton X-100 extracts of ghost membranes, as judged by the ready separation of these proteins on ion exchange chromatography and rate zonal sedimentation (26,84). If such associations are especially sensitive to dissolution by nonionic detergents, however, they would not be seen in this system. Close proximity between the cytoplasmic segment of band 3 and the membrane binding site(s) for spectrin is demonstrated by experiments showing that antibodies directed against the cytoplasmic segment of band 3 inhibit the binding of spectrin to inside-out vesicles (6).

Evidence has been presented linking band 3 to the intramembranous particles seen on freeze-fracture electron microscopy. In the native erythrocyte membrane, these particles assume a random, dispersed distribution which cannot be perturbed by agents such as multivalent ligands, proteolytic enzymes, or low pH treatments (149,150). When the inner membrane surface is made accessible by hypotonic lysis of erythrocytes, however, low pH (<5.8) (refs. 149-151) or trypsin treatment (96,151,152) causes the particles to become clustered. Incubation of ghost membranes with bivalent but not monovalent antispectrin antibody at the inner membrane surface also causes aggregation of colloidal iron hydroxide-labeled sites (glycophorin) at the outer



surface (153). All conditions which favor precipitation of solubilized spectrin-actin extracts (low pH,  $\text{Ca}^{++}$ ,  $\text{Mg}^{++}$ , polylysine, basic proteins) also induce intramembranous particle aggregation in partially spectrin-depleted ghost membranes (150,154). The same spectrin-aggregating conditions also cause release from fresh ghosts of small lipid vesicles which are free of both spectrin and integral membrane proteins (154). Low pH-induced clustering of particles reconstituted in egg phosphatidylcholine vesicles is dependent on prior binding of solubilized spectrin-actin extracts (100). Spectrin (visualized by ferritin-conjugated antispectrin) is clustered on the inner membrane surface in patches directly underlying intramembranous particle aggregates (155). Branton and coworkers have synthesized these data into a model in which spectrin and intramembranous particles are involved in strong, specific interactions. The particles are thought to be immobilized by spectrin in the intact membrane. They are therefore incapable of aggregation, a process which must involve lateral movement in the membrane. The particles are mobilized only on partial depletion of spectrin from the membrane, although the presence of some residual spectrin seems to be necessary for particle aggregation. It is the precipitation of this residual spectrin into small patches on the inner membrane surface which is thought to cause the clustering of the particles (100,150,154,155).

Chemical evidence of in situ interactions between band 3 and spectrin is seen in the results of various cross-linking studies (see 104 for review). Bands 1 and 2 are more readily cross-linked



by dimethylmalonimide in ghosts which have been pretreated with multivalent Ricinus communis lectin (156), which binds fairly specifically to band 3 on the outer surface of ghost membranes (23). Cross-linking of ghost membrane proteins induced by cleavable bifunctional reagents results in very high molecular weight ( $>3.5 \times 10^6$  dalton) complexes which contain spectrin, actin, ankyrin, and band 3 as well as bands 4.2 and 6 (refs. 86-88,157). Unfortunately it is not possible to determine which of these proteins is cross-linked directly to spectrin. Disulfide-linked complexes involving bands 1+3, bands 2+3, and bands 5+3, as well as heterogeneous aggregates containing bands 1+2+3+4.2+5, are created spontaneously in ghost membranes exposed at low ionic strength to acid pH (pH 4.0-5.5, temperature 0-4°C) or elevated temperature (37°C) (ref. 158). Aggregation at all temperatures is maximal near the isoelectric point of spectrin (159), which is also the precipitation point of spectrin (100,126,150). Furthermore, a complex of bands 1+3 (yield unspecified) results from catalytic oxidation of ghost membranes at pH 7.4 and physiological ionic strength (but not at low ionic strength) (123). These observations suggest to the authors that decreased electrostatic repulsion between adjacent proteins on the membrane may be responsible for changes in cross-linking with pH and ionic strength (123,158). An alternative explanation could involve more specific rearrangements of cytoskeleton structure with pH and ionic strength, such as conformational changes or polymerization of various membrane components.

The data presented in this section support the contention that



band 3 interacts rather intimately with spectrin in the erythrocyte membrane. Whether this interaction involves actual binding of band 3 by spectrin or simply entrapment of band 3 in the underlying cytoskeletal network is an unresolved question. High-affinity binding ( $K_D < 10^{-7}M$ ) has been ruled out by several experiments (15,138,139) but lower affinity binding is still a possibility, since the concentration of spectrin inside red cells may be as high as  $10^{-5}M$  (ref. 15). More long-range, but nonetheless specific, connections involving other membrane proteins (actin, band 4.1, band 4.2) or even membrane lipids are also conceivable.

## B. MEASUREMENTS OF LATERAL DIFFUSION

### 1. Protein Diffusion

Several methods have been devised for the measurement of protein diffusion in the plane of the membrane (reviewed in 2,160). All of the techniques involve labeling of proteins in some way so that their distribution in the membrane may be visualized. Changes in distribution with time imply lateral movement; under appropriate conditions this motion can be shown to be due to diffusion and can be quantified to permit calculation of diffusion coefficients. The overall scheme of these experiments consists of setting up, by some means, a non-uniform distribution of proteins (usually fluorescently labeled) in the membrane. The relaxation of this distribution to its equilibrium state is then observed with the aid of a (fluorescence) microscope. The most widely



used methods are cell fusion and, more recently, photobleaching recovery. These have both been applied to lateral diffusion in the erythrocyte membrane, and will be discussed in detail. Two other methods involve observation of the spreading of a patch of fluorescently-labeled anti-membrane protein antibody after application onto a membrane surface (161), and study of the kinetics of return to uniform distribution of fluorescently-labeled membrane receptors which have been electrophoretically aggregated at one end of a cell (162).

a. Cell Fusion. Frye and Edidin (163) provided the first evidence that rapid lateral diffusion of membrane proteins may occur. They used inactive Sendai virus to fuse human and mouse cells, and observed the intermixing of the human and mouse surface antigens with time by adding human- and mouse-specific antibodies labeled with different colored fluorescent dyes. Total mixing was seen in 90% of the heterokaryons after a forty minute incubation at 37°C (ref. 163). A coefficient of lateral diffusion ( $D$ ) of approximately  $2 \times 10^{-10} \text{ cm}^2/\text{sec}$  can be estimated from the intermixing rate (160,164). The intermixing process was insensitive to metabolic inhibitors but sensitive to changes in temperature. Further study showed a decrease in the diffusion coefficient with temperature in the range 37°C to 21°C and 15°C to 4°C, but a paradoxical increase with decreasing temperature from 21°C to 15°C (ref. 165). This behavior may be a consequence of lateral phase separations in the membrane lipid (166). A more detailed analysis of the intermixing kinetics revealed that



a small population of heterokaryons (10-15%) had cell surface antigens which diffused laterally more rapidly ( $D=1-4 \times 10^{-9} \text{ cm}^2/\text{sec}$ ) than the antigens of the majority of heterokaryons. This heterogeneity was taken as evidence that, in the majority of cells, integral membrane proteins may not be completely free to diffuse on the cell surface (164). Changes in membrane potential (produced by altering the potassium ion concentration of the medium or by adding drugs such as ouabain, gramicidin, and diphenylhydantoin) were reported to affect the lateral diffusion rates of surface antigens in those cells (80-85%) which restricted diffusion to some extent, but not the rates of the freely diffusing antigens (167).

Lateral mobility of fluorescein-isothiocyanate-labeled integral membrane proteins of human erythrocytes (>70% of label on band 3 and PAS-1) has also been examined by the cell fusion technique (8). A 50/50 mixture of labeled and unlabeled cells in 310 mOsm phosphate-buffered saline, pH 7.6, was treated with Sendai virus to fuse the cells, and redistribution of fluorescence from the labeled to the unlabeled cells was scored with time. A minimum diffusion coefficient of  $4 \times 10^{-11} \text{ cm}^2/\text{sec}$  at 37°C was calculated. Lateral diffusion was found to be highly temperature-dependent (see table 2) and to be two- to three-fold faster in fresh than in aged (ATP-depleted) cells (8). Incubation of virus-treated (hence "leaky") cells with the 72,000 dalton spectrin-binding fragment of ankyrin resulted in a two-fold increase in diffusion coefficient, although standard errors for the control and experimental values were not stated (168).





TABLE 2. LATERAL MOBILITY OF MEMBRANE PROTEINS

Membrane	$D \times 10^{11}{}^a$	$f(\infty)$	temp, °C	method	label	Ref.
mouse/human heterokaryon	10		15	cell fusion	fl. Ab <sup>b</sup>	165
	4		21	"	"	165
	20		37	"	"	163
rat myotube	<1		0	spread of fl. spot	fl. Ab	161
	100-300		21	"	"	161
Xenopus myoblast	510		22	electrophor. + diffusion	fl. conA	162
frog disc	200-500		20	APR <sup>c</sup>	retinal	169 177
erythrocyte ghost	<0.3		20	FPR <sup>d</sup>	FITC <sup>e</sup>	7
	0		0	cell fusion	FITC	8
	0.6		23	"	"	8
	3		30	"	"	8
	4		37	"	"	8
human embryo fibroblast	2-20	0.80	25	FPR	fl. WGA <sup>f</sup>	172
mouse fibroblast	14-33		23	FPR	FITC	174
	<0.1		23	FPR	fl. conA	178
mouse 3T3 cell	5-10			FPR	succ-conA <sup>g</sup>	179
	22 <sup>k</sup>	0.45		FPR	fl. conA-pl. <sup>j</sup>	189
	2 <sup>l</sup>	0.45		FPR	fl. conA-pl.	189
rat myotube	22	0.25		FPR	FITC	180
	3-4	0.67		FPR	fl. conA	180
	20	0.5		FPR	fl. Ab	181
diffuse patch	5	0.75	22	FPR	fl. Bgt <sup>h</sup>	176
	<0.1	0	22	"	"	176
diffuse patch	16	0.75	37	"	"	176
	<0.1	0	37	"	"	176
chick embryo fibroblast	0.9	0.15		FPR	fl. CSP <sup>i</sup>	186
mouse ova fertilized	5	0.18	25	FPR	fl. Ab	187
unfertilized	14.5	0.4	25	"	"	187
rat peritoneal mast cell	21	0.65		FPR	fl. IgE	188
mouse spleen lymphocytes	30	0.7		FPR	fl. Ab	190
glial cells	4			FPR	fl. conA	183
neuroblastoma cells	12			FPR	fl. conA	183
	6	0.35		FPR	fl. conA	182

TABLE 2. continued

- 
- a  $\text{cm}^2/\text{sec}$
  - b fluorescently labeled antibody
  - c absorbance photobleaching recovery (see text)
  - d fluorescence photobleaching recovery
  - e fluorescein-isothiocyanate
  - f wheat germ agglutinin
  - g succinyl-concanavalin A
  - h tetramethylrhodamine-conjugated  $\alpha$ -bungarotoxin
  - i fluorescently labeled cell surface protein
  - j concanavalin A-conjugated platelets
  - k platelets covering <3% of cell surface
  - l platelets covering >3% of cell surface



b. Photobleaching Recovery. Poo and Cone (169) used the natural chromophore present in rhodopsin to measure the lateral diffusion of this integral membrane protein in the disc membrane of rod outer segments. They partially bleached the rhodopsin molecules in one half of a single rod outer segment with a light flash, and monitored by absorbance the change in the rhodopsin distribution as the bleached and unbleached molecules diffused laterally in the membrane. A uniform distribution was approached exponentially with a half-time of approximately thirty seconds at 20°C, corresponding to a diffusion coefficient of  $4-5 \times 10^{-9} \text{ cm}^2/\text{sec}$ .

The first fluorescence photobleaching recovery experiment was performed on fluorescein-isothiocyanate-labeled erythrocyte membrane proteins (7). Single ghosts suspended in 7 mM sodium phosphate buffer, pH 8.0, were observed in a fluorescence microscope at room temperature (20-23°C) and fluorescein on one half of the ghost bleached with an intense light beam. No significant diffusion of fluorescent material into the bleached half of the ghost was detected in a measuring time of 20 minutes. This data apparently set an upper limit on the average lateral diffusion coefficient of the labeled membrane components of  $3 \times 10^{-12} \text{ cm}^2/\text{sec}$  at 20-23°C.

More sophisticated versions of the fluorescence photobleaching recovery (FPR) system have been recently developed (170-175). These methods involve observation, generally in a fluorescence microscope using a sharply focused laser beam for excitation, of a single cell membrane containing fluorescently labeled protein



or lipid. A small area of the membrane is exposed to a brief intense pulse of laser light, which causes irreversible photochemical bleaching of the fluorophore in that area. The rate and total amount of recovery of the fluorescence in the bleached region, which results from lateral diffusion of unbleached fluorophore into the bleached area, are monitored using a photomultiplier tube connected to the emission system of the microscope. Appropriate analysis of the fluorescence recovery curves allows estimation of: 1) the type of process which is leading to the recovery, i.e. diffusion vs. flow; 2) the relative amounts of mobile and immobile fluorophore; 3) the lateral diffusion coefficient of the mobile fraction; and 4) the presence or absence of protein or lipid domains in the membrane comparable in size to the bleaching laser beam. One example of the versatility of the FPR system is seen in an experiment involving the lateral motion of fluorescently labeled acetylcholine receptors in cultured rat myotube membranes (176). Two distinct coexisting classes of receptors are found: a mobile, uniformly distributed population of receptors and an immobile, dense, patchy population of receptors. Diffusion coefficients and fractional recoveries (corresponding to the fraction of fluorophore which is mobile) which have been measured for membrane proteins in these and other systems are given in table 2.

## 2. Lipid Diffusion

Electron spin resonance (ESR), nuclear magnetic resonance (NMR),



and, more recently, fluorescence photobleaching recovery (FPR) have all been used to measure lateral diffusion coefficients of lipids in natural and artificial membranes (see 2 for review). Since this thesis is not concerned with lipid diffusion per se, the ESR and NMR methodologies will not be reviewed. One caveat in interpreting FPR data on lipid diffusion involves the use of various fluorescent lipid analogs as probes of native lipid mobility. It is not clear that these analogs, which are exogenous compounds introduced into the natural membrane, are true models for endogenous membrane lipid. Diffusion coefficients which have been measured for lipids or lipid analogs in natural membranes are given in table 3, for comparison with the protein diffusion coefficients of table 2. In general, it may be noted that lipid diffusion is faster than protein diffusion and has higher fractional recoveries (fraction of mobile lipid) than protein diffusion. These comparisons are further evidence for restriction on the lateral mobility of membrane proteins in many systems.



TABLE 3. LATERAL MOBILITY OF MEMBRANE LIPIDS  
AND LIPID ANALOGUES

<u>Membrane</u>	<u>D x10<sup>11</sup><sup>a</sup></u>	<u>f(<math>\infty</math>)</u>	<u>temp, °C</u>	<u>method</u>	<u>label</u>	<u>Ref.</u>
<u>E. coli</u>	1800		31	NMR	<sup>31</sup> P	195
sciatic nerve	500		31	NMR	<sup>1</sup> H	197
sarcoplasmic	600		8	NMR	<sup>31</sup> P	197
reticulum	1800		25	NMR	"	195
	1000		50	NMR	"	197
	2500		25	ESR	SLL <sup>b</sup>	193
	6000		40	ESR	"	193
liver	9500		20	ESR	SLFA <sup>c</sup>	194
microsomes	11000		30	ESR	"	194
	13700		40	ESR	"	194
electroplax membrane	>100		33	NMR	<sup>1</sup> H	197
rat myotube	>100	1	23	FPR	diI	180
	900	1		FPR	diI	181
patch	120	0.7	37	FPR	diI	185
diffuse	150	0.6	37	FPR	diI	185
chick embryo	200	0.9	12	FPR	diI	184
myotube	600	0.9	30	FPR	diI	184
chick embryo fibroblast	45			FPR	fl. gan. <sup>d</sup>	186
mouse 3T3 cells	800			FPR	diI	186
mouse ova						
fertilized	200	0.05	25	FPR	diI	187
unfertilized	1900	0.28	25	FPR	diI	187
mouse spleen lymphocytes	1500	1		FPR	diI	190
DMPC <sup>e</sup>	<50		23	FPR	diO/NBD-PE	173
multilayers	6000		25	FPR	NBD-PE	192
	8500		35	FPR	NBD-PE	192
Egg PC	15000		25	FPR	diO	173
multilayers	4000		25	FPR	NBD-PE	173
erythrocyte ghost	2-fold ↑		0 to 40	FPR	diI	191

<sup>a</sup>cm<sup>2</sup>/sec

<sup>c</sup>spin-labeled fatty acid

<sup>e</sup>dimyristoyllecithin

<sup>b</sup>spin-labeled lecithin

<sup>d</sup>fluorescein ganglioside



## CHAPTER 2. FLUORESCENCE PHOTOBLEACHING RECOVERY SYSTEM

### A. THEORY

#### 1. Design of the Experiment

Quantitative measurement of lateral transport processes (diffusion and/or flow) by fluorescence photobleaching recovery (FPR) is simple in concept (170,172). A sharply focused, circularly symmetric, attenuated laser beam is used to excite fluorescence in a small region of a surface containing fluorescent molecules, e.g. a cell membrane which has been fluorescently labeled. After a measurement of the initial fluorescence ( $F(-)$ ) is made, the same laser beam is employed, now unattenuated, to deliver a brief, intense pulse of light to the same region of the surface. This pulse causes irreversible photochemical bleaching of the fluorophore in the region. At the end of the bleaching pulse, defined as time zero, periodic measuring pulses are delivered to the labeled surface, using the same laser beam attenuated to the same intensity as that used to measure  $F(-)$ . A record of the fluorescence excited by these measuring pulses with time (see fig. 5) can be characterized empirically by two parameters: the first is the fractional recovery of fluorescence

$$f(\infty) = (F(\infty) - F(0)) / (F(-) - F(0)), \quad (1)$$

where  $F(\infty)$  is the fluorescence value attained long after bleaching and  $F(0)$  the fluorescence at time zero; the second is the time,  $\tau_{1/2}$ , required to reach 50% of the final recovery of fluorescence, i.e.

$$F(\tau_{1/2}) = 1/2 (F(\infty) - F(0)) + F(0). \quad (2)$$



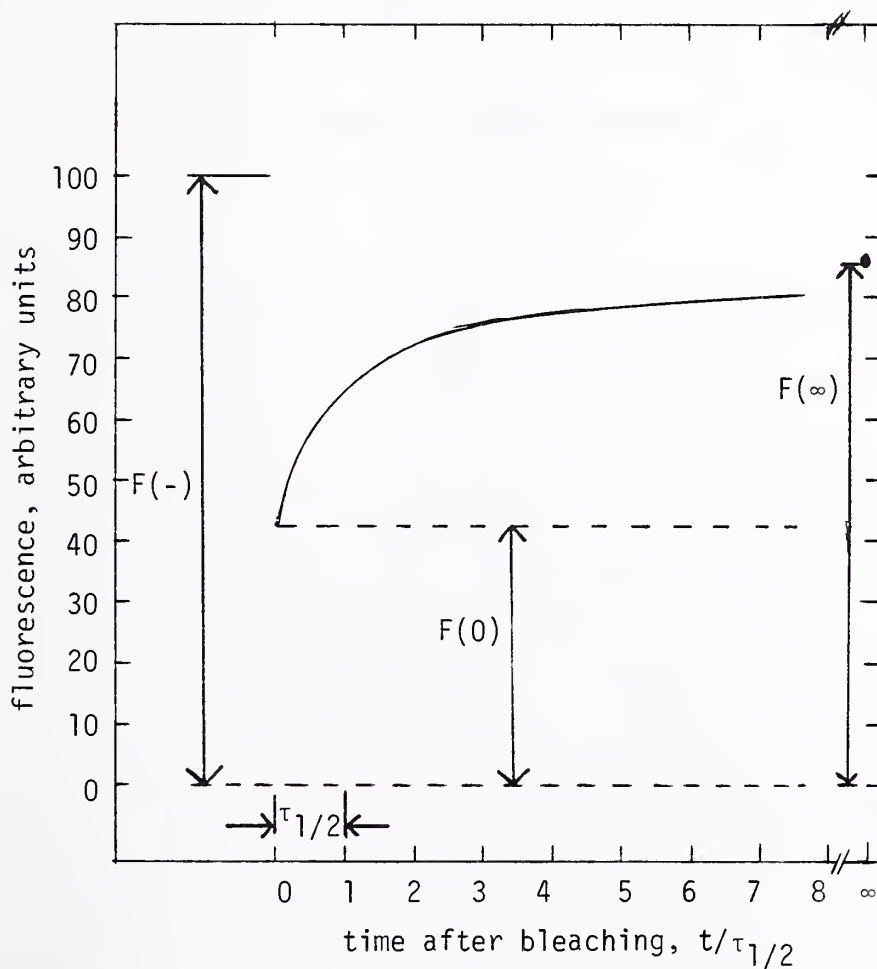


Figure 5. Parameters Involved in a Typical Fluorescence Photobleaching Recovery Experiment.  $F(-)$ , fluorescence before bleaching.  $F(0)$ , fluorescence immediately after bleaching.  $F(\infty)$ , fluorescence long after bleaching.  $\tau_{1/2}$ , half-time for recovery.



Assuming that photochemical recovery of previously bleached fluorophores does not occur and that the measuring pulses do not themselves induce bleaching, recovery of fluorescence in the region of the surface sampled by the laser beam must reflect movement of unbleached fluorophore into the previously bleached region. Such movement could occur either by lateral diffusion or lateral flow; these two cases are treated separately.

## 2. Photobleaching

The theory for photobleaching on a two-dimensional, uniform distribution of fluorophores used in this thesis is taken from Axelrod et al. (170). It is first assumed that the bleaching of fluorophore to a nonfluorescent compound is an irreversible, first-order reaction characterized by a rate constant  $\alpha I(r)$ , where  $\alpha$  is a proportionality constant and  $I(r)$  is the intensity of the bleaching laser beam at distance  $r$  from the center of the beam. The instantaneous concentration profile of unbleached fluorophore at distance  $r$  immediately after a bleaching pulse which is short compared with the characteristic times for diffusion and/or flow will then be:

$$C(r) = C_0 \exp(-\alpha T_B I(r)), \quad (3)$$

where  $C_0$  is the initial uniform fluorophore concentration and  $T_B$  is the duration of the bleaching pulse. The extent of photobleaching for any given pulse can be completely characterized by the bleaching parameter  $K$ :

$$K \equiv \alpha T_B I(0), \quad (4)$$



where  $I(0)$  is the intensity of the laser beam at its center.

Fluorophore concentration profiles immediately after bleaching for a Gaussian laser beam (i.e. operated in the  $TEM_{00}$  mode) at several different values of  $K$  are given in fig. 6. Experimentally,  $K$  can be determined from the values of the fluorescence immediately before and after the bleaching pulse, according to the relation:

$$F(0)/F(-) = K^{-1}(1 - e^{-K}). \quad (5)$$

In fig. 7 this relation is graphically displayed. It should be noted that this method for calculating the bleaching parameter is valid for both diffusion and flow recovery curves, since neither  $F(0)$  nor  $F(-)$  is dependent on the mode of fluorescence recovery.

### 3. Fluorescence Recovery Curves

Theoretical recovery curves for diffusion and flow on a two-dimensional surface can be generated from solutions to the differential equations of transport subject to the initial condition caused by photobleaching and characterized by  $K$  (derivations in ref. 170). Such curves have been calculated for a laser beam of Gaussian spatial intensity profile (170) and are reproduced in figs. 8-10. The characteristic time for diffusion is defined as

$$\tau_D \equiv w_0^2/4D, \quad (6)$$

where  $w_0$  is the  $1/e^2$  radius of the beam at the plane of the fluorescent surface and  $D$  is the diffusion coefficient. Similarly, the characteristic time for flow is defined as

$$\tau_F \equiv w_0/V_0, \quad (7)$$



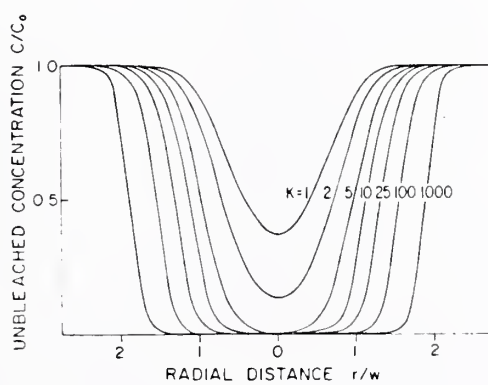


Figure 6. Fluorophore concentration profiles immediately after bleaching with a Gaussian laser beam of  $(1/e^2)$  radius  $w$ , for various values of bleaching parameter  $K$ .



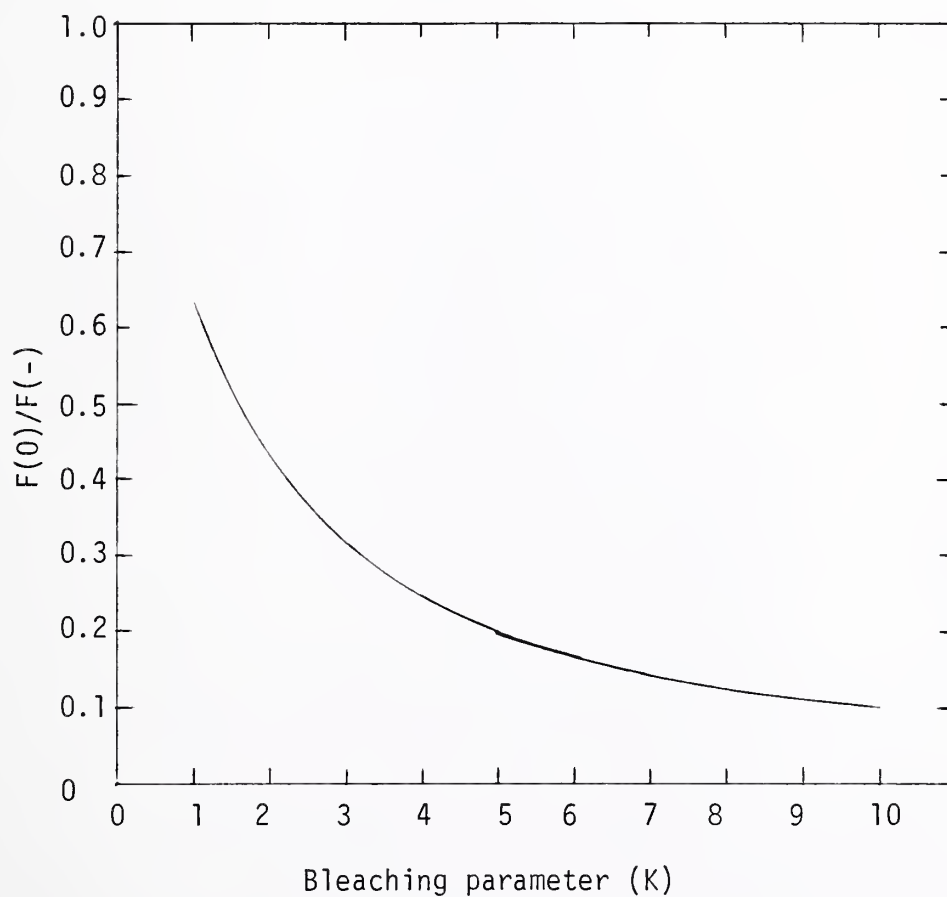


Figure 7. Ratio of fluorescence immediately after bleaching to fluorescence before bleaching vs. bleaching parameter.  $F(0)$ , fluorescence immediately after bleaching.  $F(-)$ , fluorescence before bleaching.





Figure 8. Fluorescence recovery  $F(t)$  vs.  $t/\tau_D$  for diffusion, with Gaussian laser beam, for various values of  $K$ . Fluorescence recovery is normalized to a prebleach value  $F(-)=1.0$ .  $\tau_D$ , characteristic time for diffusion (see text). (taken from ref. 170)

Figure 9. Fractional fluorescence recovery  $f(t)$  vs.  $t/\tau_D$  for diffusion, with Gaussian laser beam, for various values of  $K$ .  $f(t) \equiv [F(t)-F(0)]/[F(\infty)-F(0)]$ . (taken from ref. 170)

Figure 10. Fractional fluorescence recovery  $f(t)$  vs.  $t/\tau_F$  for flow, with Gaussian laser beam, for various values of  $K$ . (taken from ref. 170)

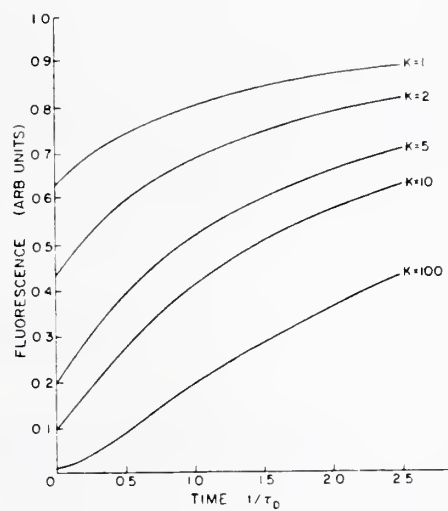


Figure 8.

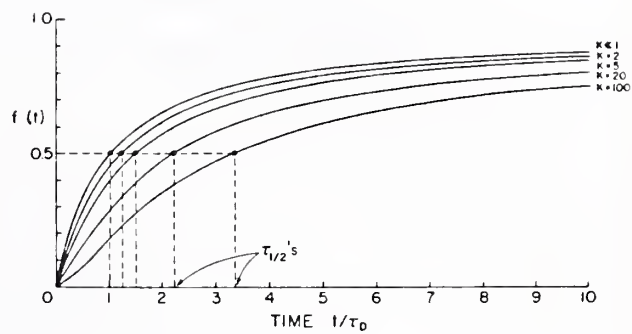


Figure 9.

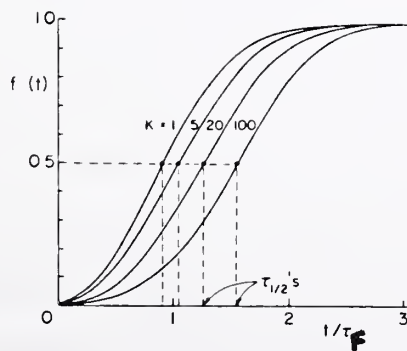


Figure 10.



where  $V_0$  is the velocity of uniform flow. It should be noted that figs. 9 and 10 are presented in the form of fractional fluorescence recovery  $f(t)$  vs. time, where

$$f(t) \equiv [F(t)-F(0)]/[F(\infty)-F(0)], \quad (8)$$

while fig. 8 is given as absolute fluorescence recovery vs. time.

The variation in initial fluorescence  $F(0)$  with bleaching parameter  $K$  can be seen clearly in fig. 8.

## B. METHODS

### 1. Optics and Electronics

The design of the optical system for FPR measurements was adapted from Jacobson et al. (172), and is shown in diagrammatic form in fig. 11. A 4W argon-ion laser (Spectra-Physics Model 164-08) tuned to 488 nm was used as the excitation source for a fluorescence microscope (Leitz Ortholux II) equipped for incident-light (Ploem) illumination. Operation of the laser in the  $TEM_{00}$  mode (Gaussian intensity profile) was checked by expansion of the beam onto a distant surface, where its circular symmetry could be easily appreciated (198), as well as by the form of flow recovery curves obtained on translating a spot bleached in a thin layer of immobile fluorophore through the beam (170). Excitation filters were not needed due to the sharpness of the laser line, so the excitation diaphragm and filter assembly of the conventional Ploem illuminator was removed. The laser output was controlled by an automatic current





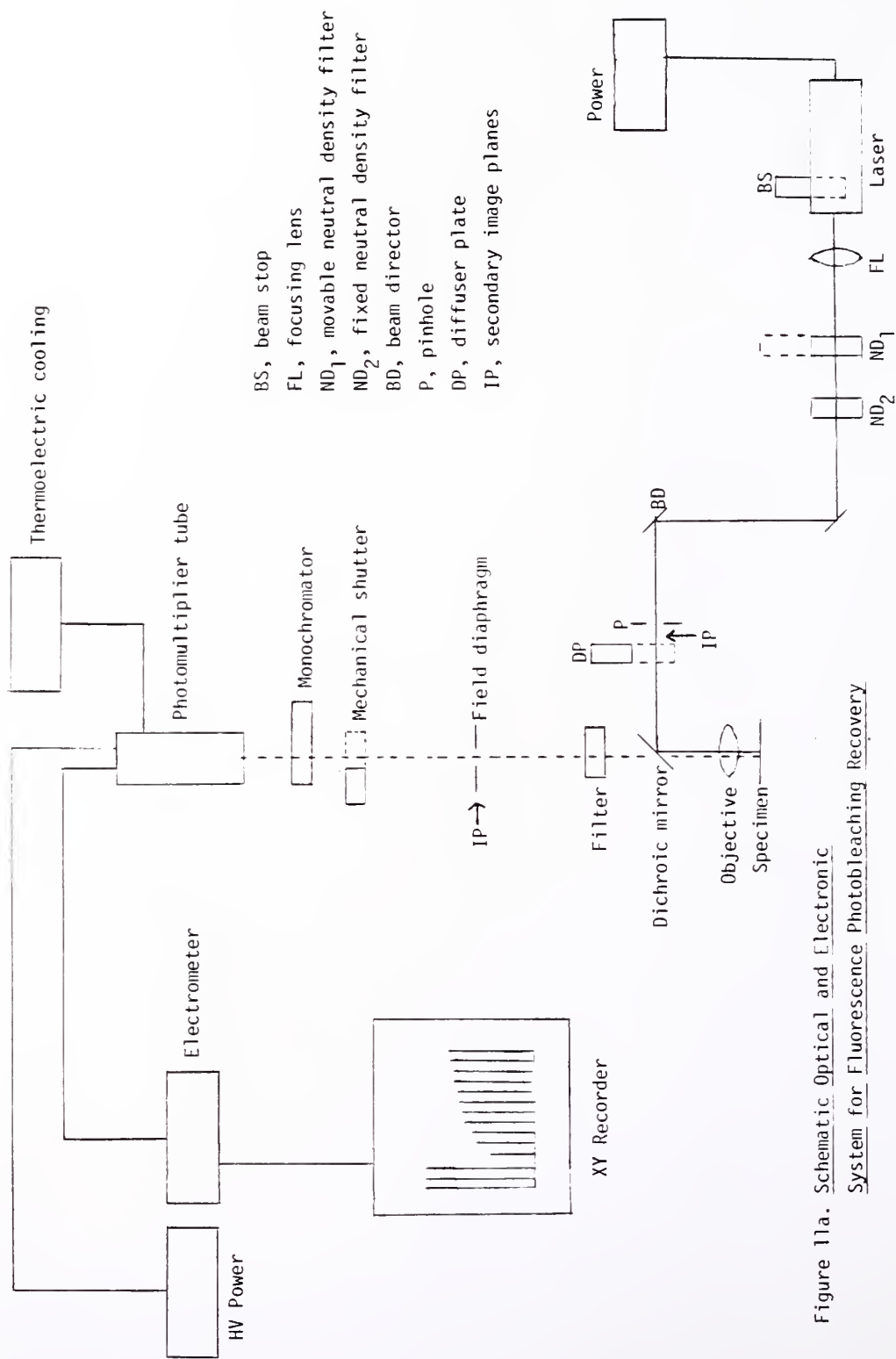


Figure 11a. Schematic Optical and Electronic System for Fluorescence Photobleaching Recovery

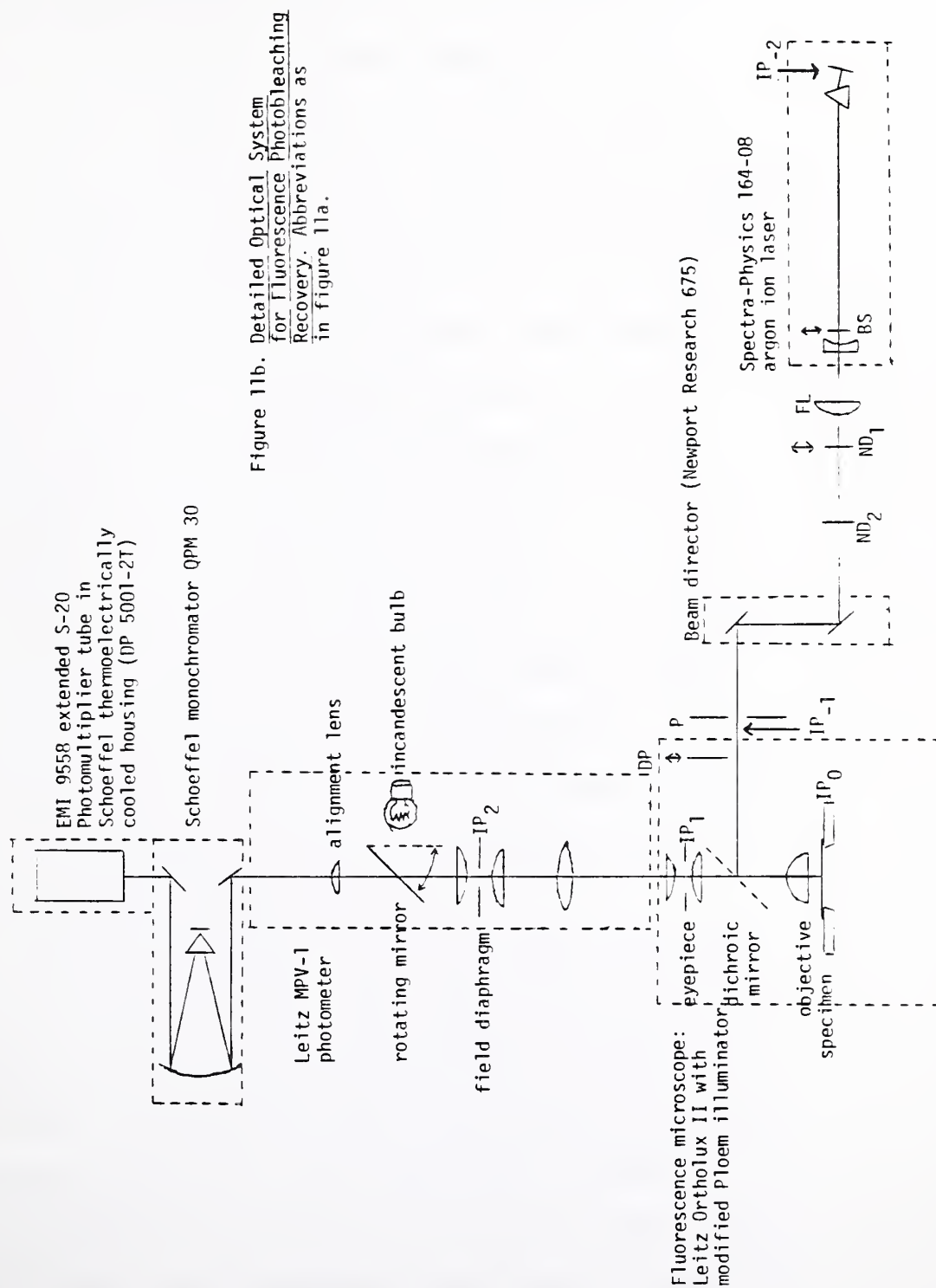


Figure 11b. Detailed Optical System for Fluorescence Photobleaching Recovery. Abbreviations as in figure 11a.



regulator which stabilized the intensity to  $\pm 1\%$ . The beam was focused to a waist ( $w_{-1}$ ) at the secondary image plane of the microscope ( $IP_{-1}$ ) by a weak planoconvex lens ( $f=500$  mm, quartz, Melles-Griot), and to another waist ( $w_0$ ) at the specimen plane ( $IP_0$ ) by the 100x oil immersion objective ( $f=1.9$  mm, Leitz Oel 100/1.30). A beam director (Newport Research Corp. Model 675) was used to change the height of the beam so that it entered the microscope along the direction used by conventional incident excitation sources. The focusing lens and beam director were mounted on an optical rail (Newport Research Corp. URL-18). A pinhole (0.51 mm diameter) drilled in a brass plate (0.020 inch drill bit, Dixon) and fastened to an XYZ manipulator (Narishige) for fine positioning was placed as close as possible to the secondary image plane of the objective ( $IP_{-1}$ ) in order to improve the Gaussian beam profile (see below). The illuminated field could be expanded by placement of a diffuser plate (Leitz) in the beam approximately 3 cm after the secondary image plane ( $IP_{-1}$ ).

Emitted light was collected by the objective and filtered by the dichroic mirror (Leitz TK510) and a suppression filter (Leitz K510) to eliminate most of the back-scattered and reflected excitation light. The emission was then passed through a series of alignment lenses (Leitz, MPV-1) and a monochromator (Schoeffel QPM 30) to an extended S-20 photomultiplier tube (EMI 9558) which was thermoelectrically cooled (Schoeffel Model DP5001-2T) and driven by a stabilized high voltage power supply (Schoeffel Model M600).



An adjustable (square) field diaphragm placed in the image plane ( $IP_2$ ) was used to discriminate against fluorescence from regions other than the sample plane of interest (171). The photocurrent was fed into an electrometer which formed a single unit with the high voltage power supply and the output read by an XY recorder operated in the time-base mode (Hewlett-Packard 7004B). A dark current of  $1 \times 10^{-9}$  amp at a power of 1100 V was obtained with thermoelectric cooling. The laser, optical rail, microscope, and photomultiplier tube were all mounted on a 22"x72"x4" 750 lb. granite slab (Colonial Marble) which was resting on four rubber inner tubes (Sears) in order to provide vibration isolation.

A mechanical beam stop within the laser was used to control when the specimen was illuminated for measuring and bleaching pulses. The intensity of illumination for the measuring pulses could be adjusted by changing the power output of the laser or the optical density of a neutral density filter (Fish-Schurman) which was fixed in position during the experiment. The bleaching pulse was delivered by mechanical removal of a neutral density filter (O.D. 3.0, Fish-Schurman) as depicted in fig. 12. Coincident with removal of the attenuating filter, the shutter to the photomultiplier tube was mechanically closed to protect the tube from the high level of fluorescence emitted during the bleaching pulse. The shutter was mechanically opened at the same time the attenuating filter was replaced in the beam, in order to obtain an initial fluorescence value as close as possible to the termination of the bleaching



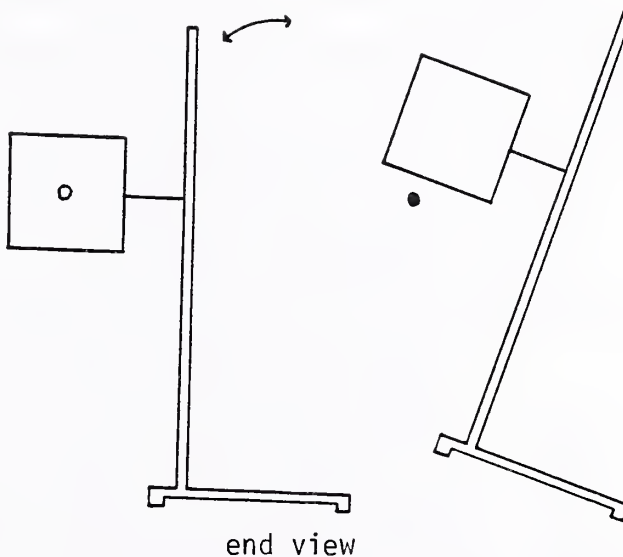


Figure 12. Scheme for Rapid Removal and Replacement of Neutral Density Filter. Neutral density filter (O.D. 3.0) is mounted on triangular-based ring stand which can be rapidly and reproducibly tilted to allow a brief, unattenuated laser pulse to photobleach the specimen.



pulse. Periodic measuring pulses were then delivered by mechanically removing and replacing the beam stop within the laser. This was done to avoid excessive bleaching of the sample by excitation light during the recovery period. The entire experiment was conducted in a light-tight room to reduce background noise.

The placement of the weak focusing lens along the optical axis was critical for obtaining the smallest possible beam at the specimen plane. The laser beam waist ( $w_{-2}$ ) is located at the rear, flat mirror of this laser (198). Here, the  $1/e^2$  radius of the (Gaussian) beam is 0.625 mm. The focusing lens produces another beam waist ( $w_{-1}$ ) at the secondary image plane of the microscope ( $IP_{-1}$ ) in accordance with the waist-waist transformation law:

$$(1/w_b^2) = (1/w_a^2)(1-d_1/f)^2 + (1/f^2)(\pi w_a/\lambda)^2, \quad (9)$$

where  $w_a$  is the  $1/e^2$  radius of the initial waist,  $w_b$  the  $1/e^2$  radius of the final waist,  $d_1$  the distance from the initial waist to the lens,  $f$  the focal length of the transforming lens, and  $\lambda$  the laser wavelength (199). For the present system,  $w_a=0.625$  mm,  $f=500$  mm,  $d_1=1050$  mm (including the length of the laser), and  $\lambda=4.88 \times 10^{-4}$  mm, resulting in a  $1/e^2$  radius of the beam of 0.121 mm at the secondary image plane. This value was used to calculate the appropriate diameter of pinhole P (see fig. 11), which should be at least twice the beam diameter in order to avoid truncation errors leading to unwanted diffraction (199). The distance between the secondary image plane ( $IP_{-1}$ ) and the focusing lens which is appropriate for production of a waist at the image plane was



determined by (199):

$$(d_1' - f) = (d_1 - f)f^2 / [(d_1 - f)^2 + (\pi w_a^2 / \lambda)^2], \quad (10)$$

where  $d_1'$  is the distance from the transforming lens to the final waist. Substitution yielded a value for  $d_1'$  of 521 mm. A second application of the waist-waist transformation for the microscope objective ( $d_1 = 250$  mm from the secondary image plane ( $IP_1$ ) to the objective,  $f = 1.9$  mm for 100x oil immersion objective) gave a  $1/e^2$  radius of the focused beam in the specimen plane ( $w_0$ ) of  $0.87\mu$ . This value was also checked experimentally by a completely different procedure (see below).

Alignment of the fluorescent spot in the specimen plane with the excitation and emission systems was accomplished as follows. One drop of a 0.5 mg/ml solution of eosin-5-isothiocyanate (Molecular Probes) in  $H_2O$  was placed on a glass slide and covered with a cover slip. An incandescent light bulb above the field diaphragm on the emission system was used to image the field diaphragm (which is also in image plane  $IP_2$ ) on the region of the specimen plane whose fluorescence was collected by the photomultiplier tube. The center of this region thus defined the axis of the emission system. Adjustments of the horizontal position of the Ploem illuminator housing and the angle of the focusing lens with respect to the optical axis of the excitation system were used to bring the fluorescent spot into the center of the emission axis. Fine adjustment of the position and angle of the upper mirror on the beam director was then employed to line up the fluorescent (green) spot from the eosin



with the reflected (blue) spot from the cover glass; perfect alignment indicated that the exciting and emitted light beams were both vertical with respect to the specimen plane. Finally, the pinhole was translated into the beam using the XYZ manipulator; its position with respect to the optical axis was monitored by the appearance or disappearance of the eosin fluorescence on the microscope slide.

## 2. Experimental Data Analysis

A three-point fit of the data contained in one FPR curve can be used to determine the diffusion coefficient,  $D$ , or flow rate,  $V_0$ , if the nature of the transport (diffusion vs. flow), the final fluorescence value ( $F(\infty)$ ), and the absolute beam diameter and profile (Gaussian vs. uniform circular disc) are known (170). In general, the nature of transport may be ascertained from the shape of the recovery curve (see figs. 8-10); flow curves are sigmoidal at all  $K$  values while diffusion curves are sigmoidal only at very high  $K$  values for a Gaussian beam. The shape of the experimental recovery curve can also be compared to the shape of theoretical curves for diffusion and flow at particular  $K$  values (figs. 8-10). The final fluorescence value ( $F(\infty)$ ) is simply the asymptote of the experimentally determined recovery curve (fig. 5). The absolute beam diameter in the specimen plane ( $w_0$ ) and profile can be experimentally determined (see below).

Once these parameters are known, the analysis for a Gaussian beam profile proceeds as follows:



(1) The time required to reach 50% of the final fluorescence recovery ( $\tau_{1/2}$ ) is determined (eqn. 2).

(2) The bleaching parameter  $K$  is calculated from the fluorescence values before bleaching ( $F(-)$ ) and immediately after bleaching ( $F(0)$ ) (eqn. 5, fig. 7).

(3) The mobility rates are calculated according to the formulas:

$$\text{Diffusion coefficient:} \quad D = (w_0^2/4\tau_{1/2})\gamma_D \quad (11)$$

$$\text{Flow rate:} \quad V_0 = (w_0/\tau_{1/2})\gamma_F, \quad (12)$$

where  $\gamma_D$  and  $\gamma_F$  are functions of beam shape and  $K$ . Fig. 13 gives  $\gamma_D$  and  $\gamma_F$  for diffusion and flow, respectively, with a Gaussian beam (170). The necessity for these correction factors can be seen qualitatively in fig. 6, where it is shown that larger  $K$  values lead to bleaching of a wider area on the fluorescent surface. It will thus take longer for the same amount of recovery to occur at higher  $K$ , and correction must be made for this in calculating mobility rates. Finally, eqn. 1 is used to determine the fractional recovery of fluorescence, which is a measure of the fraction of total fluorophore which is mobile.

### 3. Calibration of Beam Size and Profile

The FPR technique itself was used to characterize the profile of the focused laser beam in the plane of the specimen (170). The experiment involved scanning with known velocity  $V_0$  through a spot bleached in a thin layer of immobile fluorophore in order to generate a flow recovery curve which could be matched to a



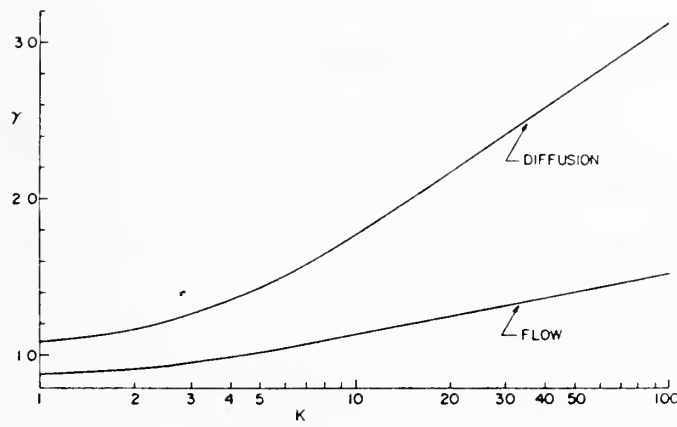


Figure 13. Factor  $\gamma$ , ( $\gamma_D$  or  $\gamma_F$ ), vs.  $K$  for a Gaussian beam  
(taken from ref. 170)



theoretical curve with the same K value. The general shape of the experimental curve provided information about the beam profile ( a Gaussian beam gives a sigmoidal curve; a uniform circular disc beam yields a linear curve), while the  $\tau_{1/2}$  of the curve could be substituted into eqn. 12 to get the  $1/e^2$  beam radius,  $w_0$ .

A thin, immobile layer of fluorophore was prepared as follows (adapted from ref. 200). Twenty  $\mu\text{l}$  of 0.3 mg/ml fluorescein-5-isothiocyanate (FITC, Molecular Probes) in ethanol were dissolved in 0.5 ml of a clear, colorless encapsulating resin (Sylgard 184; Dow-Corning). Two  $\mu\text{l}$  of the FITC-resin mixture were placed on a clean glass slide and covered with a cover slip, and pressure was applied to thin the sample as much as possible. The mixture was allowed to set at 60°C for 16 hrs. The final thickness of the set mixture, as measured by a micrometer, was 25 $\mu$ .

The FITC-resin slide was placed on the microscope stage of the FPR apparatus. A variable-speed infusion pump drive (B. Braun, Melsungen, W, Germany), to which a long, thin rod was attached in place of the syringe barrel, was used to translate the stage at constant velocity. The slowest translation speed was 0.23  $\mu/\text{sec}$  as calibrated by a vernier scale on the microscope stage and a stopwatch; this speed was used for the beam size calibration experiments. Prior to bleaching, the infusion pump was started and enough time allowed to elapse for all the slack to be taken out of the translation system. After focusing of the fluorescent spot, the prebleach fluorescence was measured and a brief bleaching



pulse (<0.5 sec) administered. As the translation system moved the bleached area out of the (stationary) beam at constant, known velocity, a flow recovery curve was generated. Eqn. 12 and fig. 13 were used to calculate  $w_0$  from the values of  $\tau_{1/2}$  and  $K$  obtained from the curve, viz.:

$$w_0 = (V_0 \tau_{1/2}) / \gamma_F. \quad (13)$$

### C. RESULTS: BEAM CALIBRATION

A representative example of a flow recovery curve generated by scanning the focused laser beam at 0.23  $\mu$ /sec out of a bleached spot in a layer of immobile fluorescein-isothiocyanate is given in fig. 14. The nature of transport (i.e. flow) is evident from the sigmoidal shape of the recovery curve. In addition, the experimental points are in good agreement with the theoretical flow recovery curve for a Gaussian beam, calculated for the same  $K$  value (170). A series of thirteen such measurements yielded an average  $1/e^2$  beam radius of  $1.2 \pm 0.3 \mu$ . The inference that diffusion and/or spontaneous recovery of fluorescence by previously bleached fluorophore were not contributing to the recovery process was confirmed by an experiment in which FITC-resin was bleached in the absence of translation. In this case, no recovery was observed over several minutes (fig. 14).



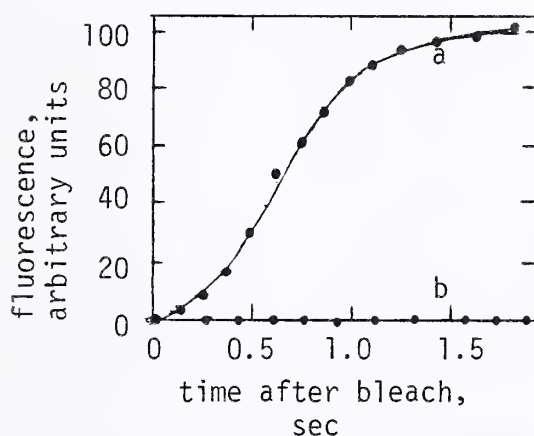


Figure 14. Flow Recovery Curve on Immobile Fluorophore Used for Beam Calibration.

$F(-)=100$ .  $K=10$ .

Smooth curve (a) is theoretical recovery curve for flow with a Gaussian beam.

See text for experimental details.

a. Experimental data in presence of translation of beam at  $0.23 \mu/\text{sec}$ .  $\tau_{1/2}=0.65 \text{ sec}$ .

b. Experimental data in absence of translation



## D. DISCUSSION

In this chapter the theory, instrumentation, and data analysis involved in performing a fluorescence photobleaching recovery (FPR) experiment are presented. A simple method for calibrating the size and profile of the laser beam used for bleaching and monitoring fluorescence recovery is also given. The results of the calibration experiment show conclusively that the beam has a Gaussian profile, and that the  $1/e^2$  beam radius is  $1.2 \pm 0.3 \mu$  in the plane of focus of the microscope objective. The irreversibility of photobleaching for the fluorophore fluorescein-isothiocyanate is also proven. These two conclusions, that the laser beam is Gaussian and that photobleaching is irreversible, are the two most important assumptions involved in the analysis of an FPR curve, and their confirmation is a necessary prerequisite to accurate data analysis.

The theoretically calculated  $1/e^2$  radius of the Gaussian laser beam ( $0.87 \mu$ ) is within experimental error of the experimentally measured radius ( $1.2 \pm 0.3 \mu$ ). I shall use the measured value of  $1.2 \mu$  in the calculation of lateral diffusion coefficients from experimental FPR curves (see chapter 4). Any systematic error which could be incorporated by choosing this or any other value for the beam radius would not affect the major conclusions of this thesis, which are based upon relative differences in FPR parameters between different preparations. In those cases where the absolute value of the diffusion coefficient is of significance (see chapter 6), a systematic overestimation of the diffusion coefficient by a factor of two (i.e. by  $(1.2/0.87)^2$ ) would not be great enough to substantially affect the conclusions.



### CHAPTER 3. EOSIN-ISOTHIOCYANATE LABELING OF BAND 3

#### A. MATERIALS AND METHODS

Human erythrocytes were the gift of Dr. A. Tauber. Eosin-5-isothiocyanate was purchased from Molecular Probes. Sodium dodecyl sulfate (SDS), acrylamide and N,N'-methylene-bis-acrylamide were obtained from Polysciences. Triton X-100 was purchased from New England Nuclear. Neuraminidase (grade IX) was from Sigma. Phenyl-methylsulfonylfluoride (PMSF) and 2-mercaptoethanol were purchased from Eastman. All other chemicals were reagent grade.

##### 1. Labeling of Human Erythrocytes with Eosin-isothiocyanate

The labeling procedure was modified from Cherry et al. (201-203). Human erythrocytes obtained from fresh human blood were washed three times in phosphate-buffered saline (10 mM sodium phosphate, 128 mM sodium chloride), pH 7.4 (PBS) at 4°C. Three mg of eosin-5-isothiocyanate (EITC) were dissolved in 6 ml of PBS at room temperature and added to 15 ml of packed, washed erythrocytes. This mixture was stirred gently at room temperature in the dark for three hours. The erythrocytes were then washed with four to five volumes of PBS three times and subsequently lysed in 750 ml of 5 mM sodium phosphate, pH 7.4, to which 30 nM PMSF had been added, for 30 min. Following lysis the ghosts were pelleted by centrifugation at 21,500 x g for 25 min and washed at least four times with forty volumes of 5 mM



sodium phosphate + 30 nM PMSF, pH 7.4. An orange precipitate appeared during the first two to three washes of the labeled ghosts; this was presumed to be EITC which had been noncovalently bound to the membrane and/or trapped inside the erythrocytes during the labeling. Washing was continued until a homogeneous orange-pink ghost pellet with a clear supernatant resulted. All operations except the labeling step were performed at 0-4°C in the dark. The labeled ghosts were stored up to a week in 5 mM sodium phosphate - 30 nM PMSF - 10 mM sodium azide at 4°C in the dark. Unlabeled ghosts were prepared from fresh erythrocytes by an identical procedure, omitting the three hour labeling step at room temperature.

For analytical purposes 150  $\mu$ l of packed labeled ghosts were dissolved in 1.5 ml 5 mM sodium phosphate + 1% SDS, pH 7.4. The amount of bound eosin was determined spectrophotometrically (204), assuming the maximum molar extinction coefficient of eosin-isothiocyanate to be  $8.3 \times 10^4 \text{ M}^{-1} \text{ cm}^{-1}$  (ref. 204; data not shown). The maximum extinction coefficient of this chromophore has been shown to change by <5% upon conjugation to protein (204). The absorption maximum for the solution occurred at 528 nm (Cary 14); the spectrum was identical in shape to that of published EITC spectra (204; data not shown). Protein was determined using the method of Lowry et al. (205).



## 2. Identification of Labeled Membrane Components

a. SDS-Polyacrylamide Gel Electrophoresis. SDS-polyacrylamide gel electrophoresis was performed using the discontinuous slab gel method of Laemmli (206). The resolving gel was prepared from a solution containing 8.5% acrylamide and 2.6% bis-acrylamide (with respect to acrylamide), the stacking gel from a solution containing 3% acrylamide. Dimensions of the resolving gel were 0.45 x 12 cm. One lane of the gel was 1 cm wide. Packed labeled or unlabeled ghosts were solubilized in a solution containing 10 mM Tris chloride, 1 mM EDTA, 3% SDS, 2% sucrose, and 2% 2-mercaptoethanol (final concentrations) at pH 7.4 and incubated for 2 min at 100°C. The solubilized ghosts containing 0.4 mg protein were then loaded onto the gels which were run for 3 hr at a current of 100 mA per gel. Duplicate samples were loaded in a symmetrical fashion about the center lane of the gel in order to facilitate comparison of Coomassie blue and PAS stained bands in the same preparation (see below).

When electrophoresis was complete, the various unstained gel lanes were scanned for eosin absorbance at 515 nm using a spectrodensitometer (Schoeffel Model SD3000). The absorbance from unlabeled ghosts could be subtracted directly from that of labeled ghosts in an adjacent lane by using the double-beam mode of the gel scanner. The gel was then divided in half with a scalpel to create two identical sets of sample lanes. One half was stained with Coomassie blue (14), and the absorbance scanned at 530 nm. The other half



was fixed in 10% acetic acid/25% 2-propanol for two days and stained using the periodic acid-Schiff base staining procedure (14); the absorbance was scanned at 560 nm.

#### b. Selective Extraction Procedures

1. Low Ionic Strength Extraction. One volume of packed labeled ghosts (approximately 5 mg protein/ml) was diluted with nine volumes of warm (37°C) 0.1 mM EDTA, pH 8, and incubated for 20 min at 37°C (ref. 14). The solution was then centrifuged at 35,000 rpm in a SW-41 rotor (Beckman) at 4°C for 30 min. The pellet was resuspended in 10 volumes of 5 mM sodium phosphate, pH 7.4 + 1% SDS. Eosin was determined spectrophotometrically. Protein was assayed by the Lowry method (205). All operations were performed in the dark.

2. Triton Extraction. One volume of packed labeled ghosts (approximately 5 mg protein/ml) was diluted with 5 volumes of a solution containing 0.5% Triton X-100 (vol/vol) in 56 mM sodium tetraborate, pH 8.0, and incubated for 20 min at 0°C (ref. 29). The solution was then centrifuged at 15,000 rpm in a SS-34 rotor (Sorvall) at 4°C for 30 min. The pellet was resuspended in 5 volumes of 56 mM sodium tetraborate, pH 8.0 + 1% SDS. Eosin and protein were determined as above. All operations were performed in the dark.

3. Chloroform/Methanol Extraction. One volume of packed labeled ghosts was diluted to approximately 2 mg protein/ml in a solution containing 10 mM Tris(hydromethyl)aminomethane, 0.1 mM EDTA, pH 7.4. Nine volumes of chloroform/methanol (2/1; vol/vol) were added



and the solution incubated with vigorous stirring at room temperature for 30 min (ref. 207). The mixture was then centrifuged at 1500 rpm for 10 min at 4°C and the aqueous layer aspirated off. This layer was recentrifuged at 100,000 x g in a 50-Ti rotor (Beckman) for 60 min at 4°C, in order to remove traces of the insoluble interphase layer remaining in the aspirated aqueous layer. All operations were performed in the dark. Eosin and protein were determined as above. Sialic acid was determined fluorimetrically by the method of Hammond and Papermaster (208), after sialidase treatment according to Tomita et al. (209).

## B. RESULTS

1. Eosin Labeling. Packed labeled ghosts generally contained 4-10 mg protein per ml and 6-15 µg eosin isothiocyanate per ml. The eosin/protein ratio was typically 1.1-1.7 µg eosin per mg total membrane protein.

2. SDS-Polyacrylamide Gel Electrophoresis. Densitometric scans of eosin absorbance, Coomassie blue stain, and PAS stain from gels run on labeled ghosts are given in fig. 15. To reduce background artifacts due to inhomogeneities in the gel, the eosin absorbance scan is a difference scan between adjacent lanes loaded with the same amount of labeled and unlabeled ghost protein, respectively. The same qualitative results were obtained using a single-beam scan of the labeled ghost lane, since the unlabeled ghost lane showed no detectable peaks of absorbance at 515 nm (data not shown).



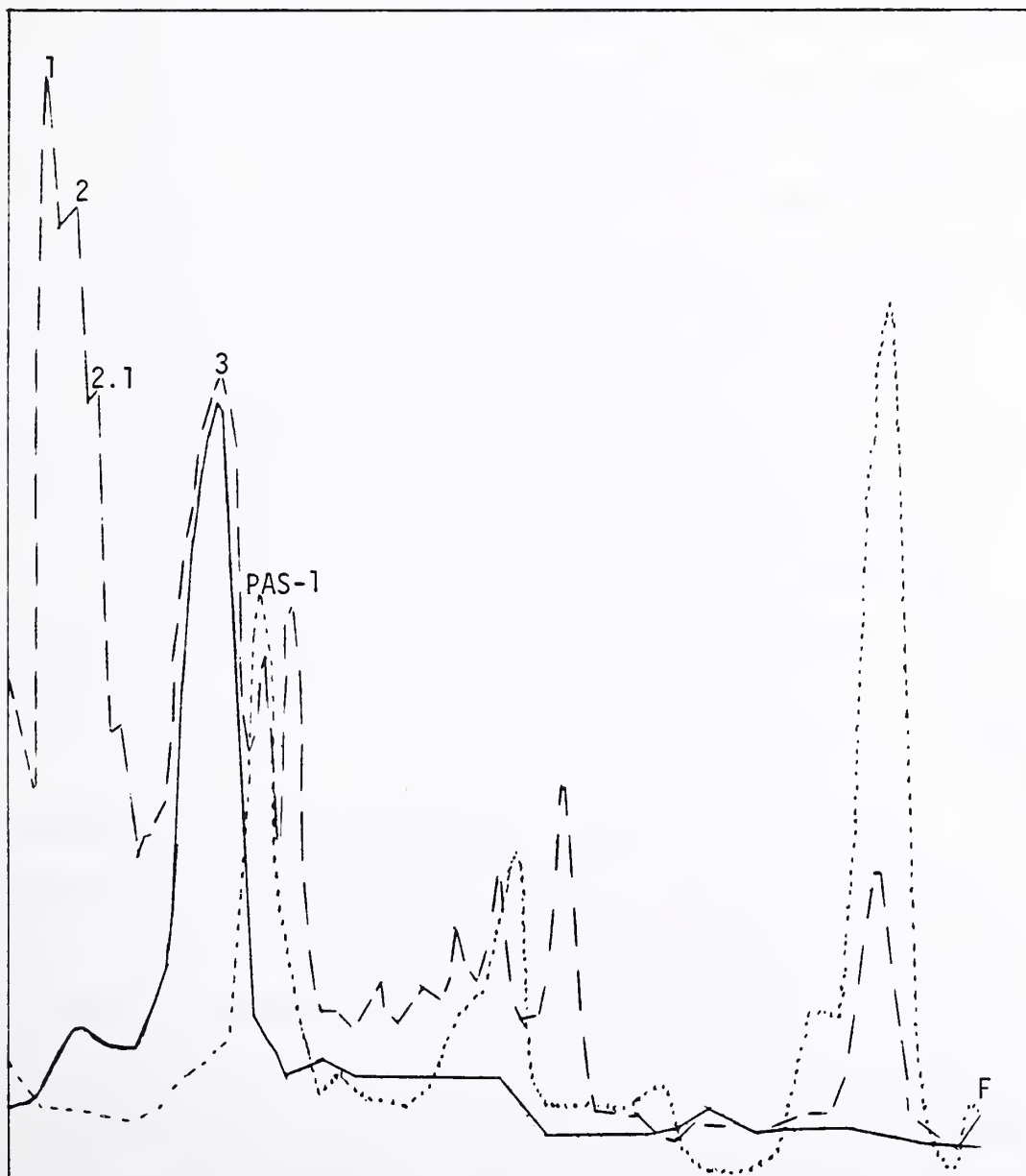


Figure 15. SDS-polyacrylamide gel electrophoresis of eosin-labeled ghost membranes.

--- : Coomassie blue stained  
 -----: PAS-Schiff base stained  
 ———: Eosin absorbance

Major proteins in high molecular-weight region of the gel are labeled for convenience. F, position of buffer front. See text for experimental details.



Most of the eosin absorbance is associated with band 3.

A small amount of absorbance is also detected in the region of bands 1 and 2 (spectrin). Only trace amounts, if any, are associated with other proteins stained by Coomassie blue. In the 8.5% gel system the peak of the glycophorin A band (PAS-1) is separated from band 3, although the trailing edge of PAS-1 overlaps the leading edge of band 3. The peak of eosin absorbance is clearly seen to run with band 3 and not PAS-1; a small amount of glycophorin labeling cannot be excluded from the results of this gel scan, however. Membrane proteins from labeled and unlabeled ghosts appeared identical on Coomassie blue and PAS staining, indicating that no major change in the proteins was caused by either eosin labeling or incubation of the intact erythrocytes at room temperature for 3 hrs (data not shown).

3. Selective Extraction Procedures. Selective extractions of membrane proteins from labeled ghosts were used to confirm the results of the SDS gel scans and to provide a quantitative estimate of the amounts of labeling on proteins other than band 3. The results of these extractions are given in table 4, in addition to literature values for the same extractions on similar preparations of EITC-labeled ghost membranes (202). Low ionic strength treatment of labeled ghosts released  $24 \pm 6\%$  of the total membrane protein but only  $8 \pm 2\%$  of the eosin label into the supernatant ( $N=3$ ). This treatment is reported to selectively solubilize nearly all of bands 1, 2, and 5 (refs. 14,202). Partial solubilization of



TABLE 4. SELECTIVE EXTRACTION EXPERIMENTS ON  
EOSIN-LABELED GHOST MEMBRANES<sup>a</sup>

<u>Extraction procedure</u>	<u>Supernatant</u>				<u>Pellet</u>			
	% eosin		% protein		% eosin		% protein	
	<u>norm</u> <sup>b</sup>	<u>raw</u>	<u>norm</u> <sup>b</sup>	<u>raw</u>	<u>norm</u> <sup>b</sup>	<u>raw</u>	<u>norm</u> <sup>b</sup>	<u>raw</u>
<u>Low ionic strength</u>								
experimental (n=3)	8±2	9±3	24±6	23±8	92±2	105±13	76±6	69±6
literature	7±3 <sup>C</sup>		25±7 <sup>C</sup>					74 <sup>d</sup>
<u>Triton X-100</u>								
experimental (n=1)	69	59	51	42	31	26	49	40
literature	60-80 <sup>C</sup>		40 <sup>C</sup>					45 <sup>e</sup>
	<u>Aqueous</u>			<u>Organic</u>				
	<u>% protein</u>	<u>% eosin</u>	<u>% NANA</u> <sup>f</sup>	<u>% eosin</u>	<u>% protein</u>			
<u>Chloroform/Methanol</u>								
experimental (n=1)	5	7	73	0	0			
literature	3.7 <sup>g</sup>	4 <sup>C</sup>	83 <sup>g</sup>	0 <sup>C</sup>	0 <sup>f</sup>			

<sup>a</sup>see text for detailed methods of extraction

<sup>b</sup>normalized to 100% total for supernatant + pellet

<sup>c</sup>ref. 201; not stated whether normalized or raw values

<sup>d</sup>ref. 14

<sup>e</sup>ref. 29

<sup>f</sup>sialic acid

<sup>g</sup>ref. 207



band 3 with Triton X-100 resulted in release of 69% of the bound eosin along with 51% of the membrane protein. This experiment was semiquantitative at best, since Triton extraction is only partially selective for band 3 (the major glycoproteins are released as well), and not all of the band 3 is released (29). Finally, chloroform/methanol extraction of labeled ghosts resulted in the appearance of 7% of the total eosin, 5% of the total protein, and 73% of the total sialic acid in the aqueous phase; the organic phase contained no detectable protein and no detectable eosin. This extraction is reported to selectively release nearly all of the PAS-staining glycoproteins into the aqueous phase (207), and all of the membrane lipids into the organic phase (201,202).

### C. DISCUSSION

In this chapter a procedure for selective labeling of band 3 with fluorophore in human erythrocyte membranes is presented. SDS-polyacrylamide gel electrophoresis and selective extraction experiments together demonstrate that at least 80% of the eosin-isothiocyanate label is present on band 3, with approximately 8% present on spectrin and 5-10% present on glycophorin. Membrane lipids do not appear to be labeled at all. These values accord well with the literature values for EITC labeling by an almost identical procedure (201-203).

The selective labeling demonstrated in this chapter and



elsewhere (201-203) is in accord with the finding that only glycophorin and band 3 among the major membrane proteins are present on the extracellular surface of the erythrocyte (3,13,74), although the small amount of spectrin labeling must be due to permeation of at least a small percentage of probe through the membrane. Selectivity of labeling is also consistent with the observation that eosin-isothiocyanate is a potent inhibitor of anion transport (112,201). Other inhibitors of anion transport such as DIDS bind selectively (>90%) to band 3, labeling glycophorin only to the extent of 7-10% (refs. 32,33). The stoichiometry of eosin binding (1.1-1.7  $\mu\text{g}$  per mg total membrane protein) corresponds to a molar ratio of eosin to band 3 of approximately 0.75 (assuming 100% binding of eosin to band 3, a molecular weight for band 3 of 90,000 daltons, and a ratio of band 3 to total membrane protein of 0.24), which is close to the theoretical limit as well as the experimental values found for anion transport inhibitors (32,33,38,110,111).



#### CHAPTER 4. FLUORESCENCE PHOTBLEACHING RECOVERY ON EOSIN-LABELED GHOSTS

Abundant indirect evidence exists implicating the erythrocyte cytoskeleton in restriction of integral membrane protein mobility (see chapter 1). In designing the experiments reported in this chapter, it was thought desirable to measure directly the lateral mobility of band 3 both in the presence and in the absence of cytoskeletal forces. The usual conditions for complete dissociation of the cytoskeleton from the membrane, however, lead to extensive vesiculation of erythrocyte ghosts (150). The resultant vesicles are comparable in size to the focused laser beam used in the FPR experiment; when subjected to a bleaching pulse, an entire vesicle will be bleached, leaving no unbleached fluorophore which is capable of lateral diffusion. For technical reasons, then, FPR cannot be used on such a system. It was hypothesized that the same experimental parameters important in complete dissociation of the cytoskeleton - i.e. low ionic strength, high temperature, and time - might also be involved in a rearrangement of cytoskeletal membrane proteins which would precede both complete cytoskeletal dissociation and ghost vesiculation. Such a rearrangement could involve a metastable state of cytoskeleton structure intermediate between tight binding to and complete dissociation from the membrane. The lateral mobility of band 3 might also be expected to change dramatically under such conditions. This chapter, then, examines



the effects of ionic strength, temperature and time on the lateral mobility of eosin-labeled band 3 in erythrocyte ghost membranes. All three parameters are found to affect greatly both the diffusion rate of the mobile band 3 and the fraction of total band 3 which is free to diffuse in the plane of the membrane.

## A. METHODS

### 1. Fluorescence Photobleaching Recovery System

The optics and electronics for the FPR system are described in chapter 2. Control of sample temperatures above room temperature was achieved with an air stream stage incubator (Nicholson Precision Instruments, Model C300) placed 4-6 inches from the microscope stage. A microprobe thermometer (YSI model 423 probe, model 42SC meter) was taped to the microscope slide to monitor the temperature at the sample. Once the system was equilibrated (10-15 min), temperature was controlled to  $\pm 1^{\circ}\text{C}$ . One experiment involved FPR measurements at  $10^{\circ}\text{C}$ . This temperature was achieved by blowing cold nitrogen gas (cooled by being passed through a coil of copper tubing submerged in a dry ice/acetone mixture) onto the microscope stage and monitoring the sample temperature as described above. Temperature was controlled by this method to  $\pm 2^{\circ}\text{C}$ .

### 2. Preparation of the Sample

Thirty  $\mu\text{l}$  of packed, eosin-labeled erythrocyte ghosts (4-10 mg protein/ml, 1.1-1.7  $\mu\text{g}$  eosin/mg protein) in 5 mM sodium phosphate,



10 mM  $\text{NaN}_3$ , 30 nM PMSF, pH 7.4 (see chapter 3) were diluted to 300  $\mu\text{l}$  with various concentrations of sodium phosphate buffer, pH 7.4. The diluted ghost suspension was degassed in a sealed, purged glove bag (Ventron, model X-27-17) by a stream of argon for 30 min (5.2 mM  $\text{NaPO}_4$  sample) or nitrogen for 3 hrs (all other samples) at room temperature in the dark. The nitrogen and argon were first bubbled through water to prevent excessive evaporation of the suspension.

Photoinduced oxidation of erythrocyte membrane proteins leading to extensive cross-linking has been shown in the presence of oxygen and fluorescein (210,211) or eosin (112), but not in the absence of oxygen (112,210,211). This finding implies that purging cell suspensions of oxygen prior to FPR experiments should eliminate the possibility of photosensitized cross-linking. These experiments are performed on macroscopic suspensions of ghosts using large doses of diffuse laser light, though, and their applicability to the microscopic situation of an FPR experiment is questionable. For example, the extent of cross-linking decreases with shorter exposure times to the same total irradiation dose of exciting light (211), suggesting that the bleaching pulses involved in FPR experiments (<1 sec duration) may induce only minimal cross-linking. Both irreversible dye bleaching (necessary for FPR measurements) and photosensitized oxidation (leading to production of singlet oxygen with subsequent cross-linking of membrane proteins) may proceed by so-called type II mechanisms



in which electronically excited dye triplet state interacts with molecular oxygen to produce singlet oxygen and either bleached (irreversibly oxidized) or ground-state dye (211). If this is the case, then removal of oxygen from the system should mean that a greater number of photons must be directed at the sample in order to get the same amount of fluorophore bleaching. This hypothesis was in fact borne out in the present study, and the successfulness of purging could be determined by the rapidity with which bleaching of fluorophore occurred at a given laser intensity (data not shown). It is likely, moreover, that photochemical bleaching of fluorophore can proceed by mechanisms which do not involve oxygen, while photoinduced cross-linking of membrane proteins almost certainly involves a diffusible oxygen intermediate. Purging the eosin-labeled ghosts of oxygen prior to FPR experiments was thus deemed the best method for eliminating adverse cross-linking effects mediated by excited state molecular oxygen.

One to two  $\mu\text{l}$  of the purged ghost suspension was placed on a microscope slide, covered with a 22 mm x 22 mm cover glass (No. 1 thickness), and sealed with epoxy (Devcon, "Five-Minute" Epoxy), all inside the glove bag. The ghost suspension spread spontaneously between the slide and cover glass, yielding a sample of average thickness 2-4 $\mu$  (calculated from the volume applied and the area occupied). This geometry oriented the ghosts parallel to the microscope slide and maintained them in a fixed position on the slide, a necessary prerequisite for measurements of diffusion by FPR. Defocusing



effects in bleaching and fluorescence measurements due to the small depth of field of the 100x objective were also almost entirely eliminated with a sample of this thinness (see ref. 172). Thus, it can be calculated that the focused laser beam irradiated both the top and bottom ghost membranes with a maximum difference in beam area of 14% between the two membranes, if the membranes were separated by  $2\mu$  (see ref. 172). This difference was well within the experimental error of the apparatus. The volume of the ghost suspension after purging was compared to the volume before purging, in order to determine the exact concentration of phosphate buffer in the sample which was sealed on the microscope slide.

In a control experiment, 300  $\mu$ l of human hemoglobin in distilled  $H_2O$  (prepared by lysis of intact erythrocytes and centrifugation to pellet the membranes, as described in chapter 3) were degassed with nitrogen for three hours and sealed on a microscope slide with epoxy, all in the glove bag. The absorbance spectrum (Cary 14) of the sample showed only deoxyhemoglobin immediately after degassing and sealing. No spectrophotometrically detectable oxyhemoglobin was regenerated on standing at room temperature for 24 hrs, confirming that the epoxy was impermeable to oxygen over a period of at least 24 hrs (data not shown).

### 3. Fluorescence Photobleaching Recovery Experiment

The degassed eosin-labeled ghost sample was placed on the



microscope stage of the FPR apparatus. Individual ghosts were located either by transmitted light or by incident-light fluorescence. The latter mode used the fully attenuated laser beam as the excitation source, with the diffuser plate placed in the beam in order to expand the area of the microscope field which was illuminated (see fig. 11). The cells appeared disc-like to cup-shaped and were uniformly fluorescent with a bright green perimeter; they were fairly homogeneous in size with diameter  $5-9\mu$ . A single cell was centered in the field so that the focused laser spot fell in the center of the cell. The field diaphragm (fig. 11) was adjusted to an area approximately ten times larger in the specimen plane than that of the ghost. The laser power output was adjusted so that a measuring light pulse would produce a convenient signal as measured by the photomultiplier tube. Typical settings were: laser power, 100 mW (attenuated by  $10^5$  by neutral density filters before the beam reached the sample); voltage to photomultiplier, 1100 V; electrometer,  $10-30 \times 10^{-9}$  amp full scale. The XY recorder was started in the time-base mode with a 0.25 sec filter and several values of the pre-bleach fluorescence from the laser-illuminated spot were measured. A brief ( $<1$  sec) intense bleaching pulse (approximately 1 mW) was delivered as described in chapter 2. Periodic measuring pulses (duration 1-2 sec) were delivered until a stable post-bleach fluorescence level was reached. Under certain circumstances the fluorescence recovery was seen to proceed with extreme rapidity ( $\tau_{1/2} < 5$  sec); in these cases, the beam stop was



left open for the entire recovery period and a smooth recovery curve was obtained. Sometimes a ghost was bleached two to four times in succession in the same spot, in order to compare diffusion coefficients and fractional recoveries of fluorescence when some of the (immobile) fluorophore in a given region of the cell was already bleached. At the conclusion of the experiment, a very long bleaching pulse was delivered (90-120 sec) in order to bleach all of the fluorophore in the illuminated area. The residual fluorescence value after this bleaching pulse (usually <5% of the fluorescence of an unbleached spot) was a measure of the background light level in the system when all the shutters and beam stops were removed. This value was taken to be the zero level in calculating the K parameter from the immediate pre- and post-bleach fluorescence values (eqn. 5).

In a control experiment a single cell was centered in the field and, with the diffuser plate in the beam and the field diaphragm wide open, the fluorescence produced on illumination of the entire cell was measured. The whole cell was then bleached by removing both neutral density filters from the beam but keeping the diffuser plate in the beam. No recovery of fluorescence was observed over a period of 15 min, indicating that spontaneous photochemical recovery of eosin fluorescence was not contributing to the recovery process in the normal FPR experiment, i.e. that bleaching was in fact an irreversible process (data not shown).



## B. RESULTS

The results of a series of fluorescence photobleaching recovery experiments on eosin-labeled erythrocyte ghosts are summarized in table 5. Incubation conditions ranged from 5.2 mM to 46 mM sodium phosphate buffer and from 21°C to 37°C temperature. Typical experimental recovery curves under the extremes of these incubation conditions are given in fig. 16 and compared to theoretical FPR curves for diffusion with a Gaussian beam (170). In general the fit is excellent, implying that lateral diffusion is the only process which is contributing significantly to fluorescence recovery. This notion was confirmed, albeit in a qualitative way, by the visual observation that the cell which had been bleached was immobile over the time course of the FPR experiment, retaining the same position in the microscope field at all times. The experimental data tended to be more scattered under conditions of high ionic strength and low temperature, where fractional recoveries of fluorescence were low (fig. 16c). This was mainly a signal-to-noise problem, since the percentage contribution of noise to the experimental data was greater with smaller changes in signal. The scatter was also reflected in the relatively large error in fractional recovery at 46 mM phosphate and 21°C (table 5). Nonetheless, even under these conditions the data fit a theoretical diffusion curve well.

1. Effect of Ionic Strength. Low temperature (21°C) and high ionic strength (46 mM phosphate) favored immobilization of band 3 ( $11 \pm 8\%$  fractional recovery) as well as slow diffusion of the mobile



TABLE 5. SUMMARY OF FPR EXPERIMENTS ON EOSIN-LABELED GHOST MEMBRANES

[P <sub>0</sub> ], mM <sup>a</sup>	21°C <sup>b</sup>			30°C <sup>c</sup>			37°C <sup>d</sup>		
	D × 10 <sup>11</sup> , cm <sup>2</sup> /sec	f(∞)	N	D	f(∞)	N	D	f(∞)	N
5.2	5.0 ± 2.2	0.72 ± 0.02	4	11 ± 1	0.69 ± 0.08	2	--- <sup>e</sup>	---	---
9.4	9.5 ± 2.3	0.51 ± 0.14	5				---	---	
13.3	6.7 ± 0.2	0.34 ± 0.05	3	14 ± 5	0.60 ± 0.12	4	65 ± 40	0.83 ± 0.06	3
18.8	8.7 ± 1.8	0.37 ± 0.09	3	7.9 ± 1.2	0.79 ± 0.05	3	58 ± 8	0.73 ± 0.11	2
21.4	8.2 ± 1.2	0.36 ± 0.09	6				29 ± 10	0.75 ± 0.11	7
26 <sup>f</sup>	7.0 ± 3.0	0.38 ± 0.09	4	7.0 ± 3.0	0.71 ± 0.10	2	14 ± 4	0.75 ± 0.13	2
46	4.3 ± 0.2	0.11 ± 0.08	2				4.6 ± 0.8	0.41 ± 0.12	3

<sup>a</sup> All samples also buffered in 1 mM NaN<sub>3</sub>, 30 nM PMSF<sup>b</sup> 4-5 hr incubation, except 5.2 mM P<sub>0</sub> which was 1-2 hr incubation<sup>c</sup> 0.5-1 hr incubation, except 5.2 mM P<sub>0</sub> which was 0.25-0.5 hr<sup>d</sup> 0.5-1 hr incubation      <sup>e</sup> 100% ghost vesiculation      <sup>f</sup> Approximate concentration

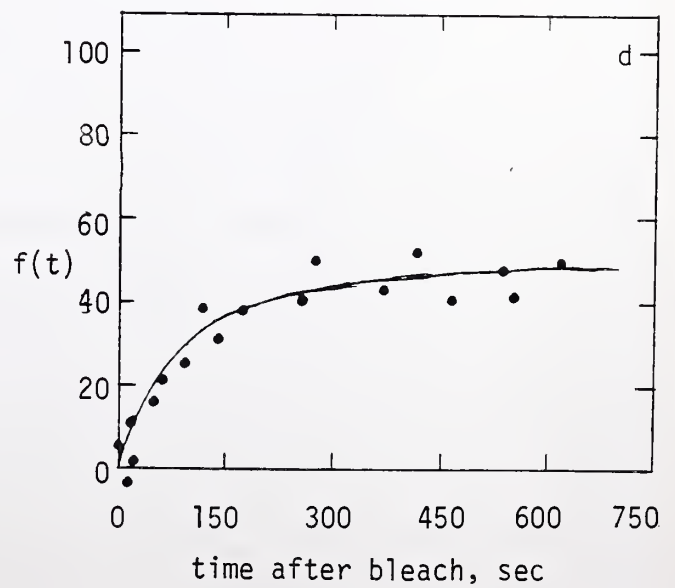
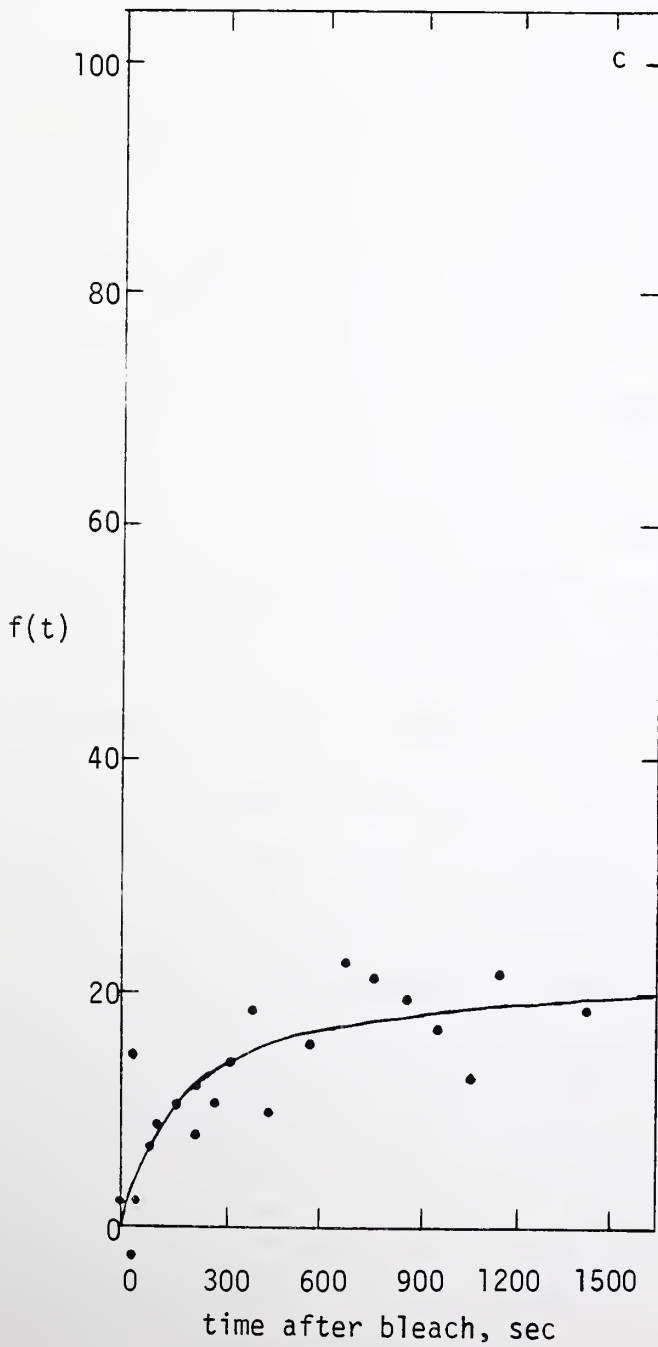
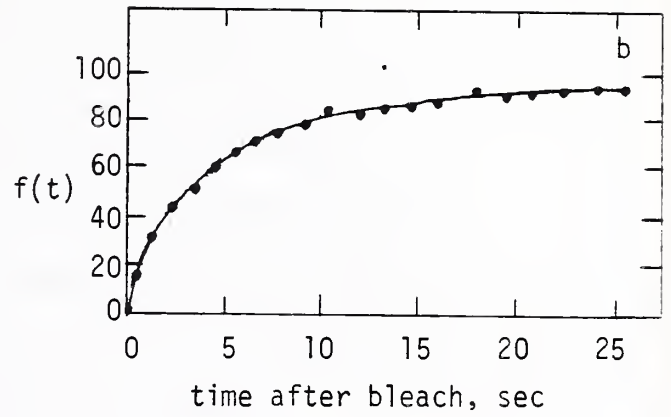
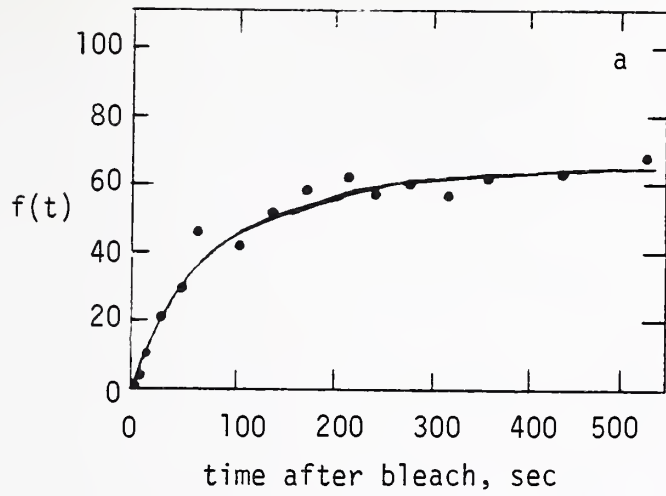




Figure 16. Experimental FPR curves under extreme conditions of  
[NaPO<sub>4</sub>] and temperature:

	<u>[NaPO<sub>4</sub>], mM</u>	<u>temp, °C</u>	<u>K</u>	<u><math>\frac{D \times 10^{11}}{\text{cm}^2/\text{sec}}</math></u>	<u><math>f(\infty)</math></u>
a	5	21	4.5	6.2	0.65
b	13	37	2.2	130.	0.94
c	46	21	1.8	2.1	0.20
d	46	37	1.6	4.4	0.50

Smooth curves are theoretical curves for diffusion, with a Gaussian beam.





fraction ( $D=4.3\pm0.2 \times 10^{-11} \text{ cm}^2/\text{sec}$ ) (table 5). Decreasing the ionic strength at the same temperature caused little if any change in diffusion coefficient ( $D=5-10 \times 10^{-11} \text{ cm}^2/\text{sec}$  at all phosphate concentrations) but a marked increase in fractional recovery ( $f(\infty)=72\pm2\%$  at 5 mM phosphate) (fig. 17). Experimental recovery curves at the extremes of ionic strength are given in fig. 18, showing the striking change in fractional recovery with ionic strength.

At 37°C much of the band 3 was mobile even at high ionic strength ( $41\pm12\%$  fractional recovery at 46 mM phosphate), although diffusion of the mobile fraction was still slow ( $D=4.6\pm0.8 \times 10^{-11} \text{ cm}^2/\text{sec}$ ). Decreasing ionic strength led first to a rapid increase in fractional recovery to  $75\pm13\%$ , followed by a sharp rise in diffusion coefficient to  $65\pm40 \times 10^{-11} \text{ cm}^2/\text{sec}$  (fig. 17). It should be noted that the sharp increase in diffusion coefficient occurred over an ionic strength range in which the fractional recovery was not changing at all. Measurement of lateral mobility at phosphate buffer concentrations less than 10 mM at 37°C was prevented by rapid (<15 min) and total vesiculation of ghost membranes. The 1-2 $\mu$  diameter vesicles produced were easily identified in the fluorescence microscope. In addition, cells containing endocytotic vesicles showed no fluorescence recovery after bleaching, since the vesicles which were bleached were approximately the same size as the bleaching laser beam. Experimental recovery curves at three different ionic strengths are given in fig. 19 for comparison.



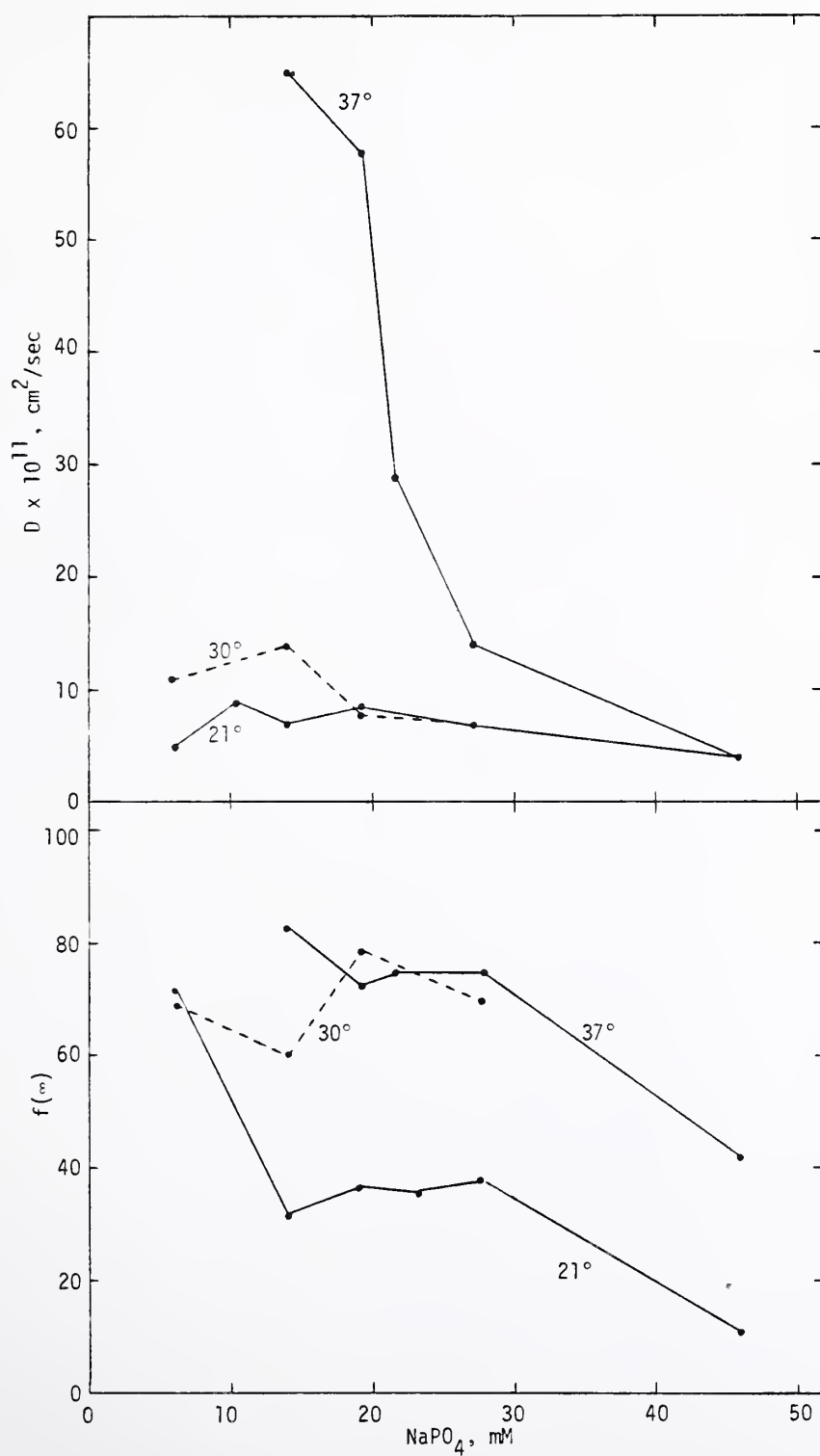


Figure 17. Diffusion Coefficients and Fractional Recoveries of Fluorescence Under Various Conditions of Ionic Strength and Temperature. See text for experimental details.





Figure 18. Smoothed experimental fluorescence recovery curves  
at 21°C. Curves were calculated from averages of  
diffusion coefficients and fractional recoveries of  
fluorescence at 21°C (see table 5).

- a.  $[PO_4] = 5 \text{ mM}$ .  $D = 5 \times 10^{-11} \text{ cm}^2/\text{sec}$ .  $f(\infty) = 0.72$
- b.  $[PO_4] = 46 \text{ mM}$ .  $D = 4.3 \times 10^{-11} \text{ cm}^2/\text{sec}$ .  $f(\infty) = 0.11$

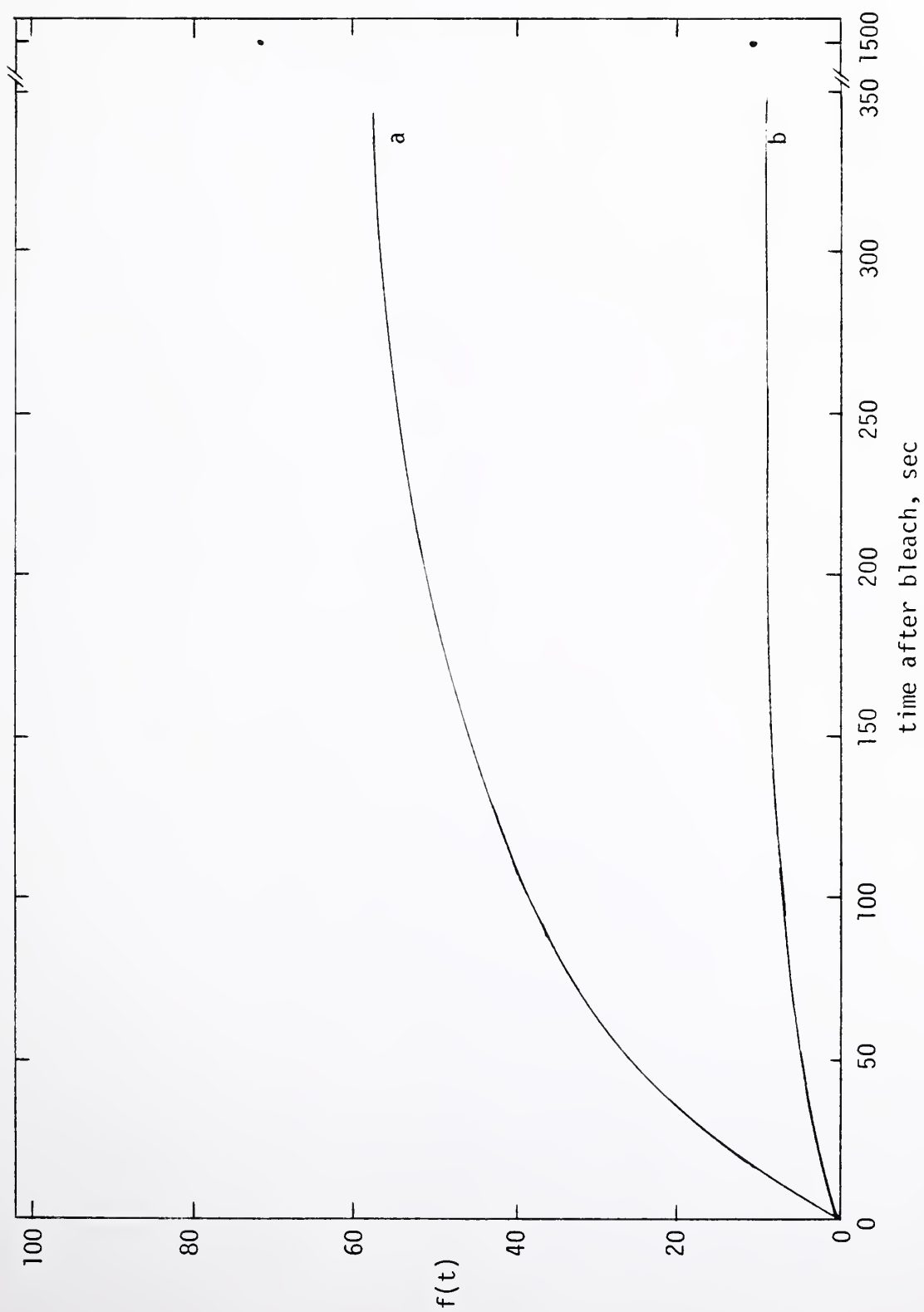


Figure 18.





Figure 19. Smoothed experimental fluorescence recovery curves  
at 37°C. Curves were calculated from averages of  
diffusion coefficients and fractional recoveries of  
fluorescence at 37°C (see table 5).

- a.  $[PO_4] = 13 \text{ mM}$ .  $D = 65 \times 10^{-11} \text{ cm}^2/\text{sec}$ .  $f(\infty) = 0.83$
- b.  $[PO_4] = 26 \text{ mM}$ .  $D = 14 \times 10^{-11} \text{ cm}^2/\text{sec}$ .  $f(\infty) = 0.75$
- c.  $[PO_4] = 46 \text{ mM}$ .  $D = 4.6 \times 10^{-11} \text{ cm}^2/\text{sec}$ .  $f(\infty) = 0.41$

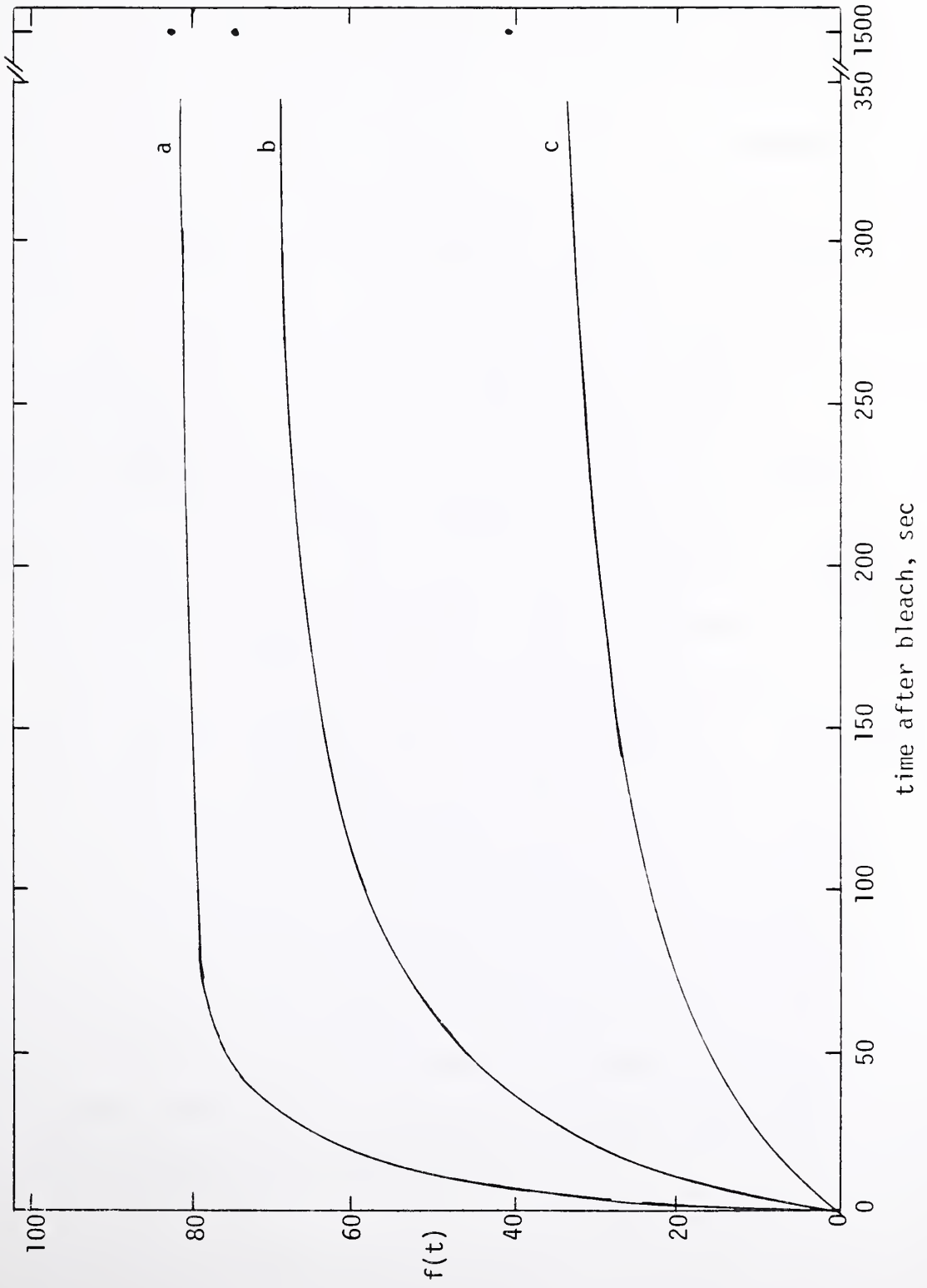


Figure 19.



2. Effect of Temperature. Increasing temperature led to increases in both diffusion coefficient and fractional recovery. These changes occurred over different ranges of ionic strength and temperature, however, and were thus dissociated from one another (fig. 20). At 46 mM phosphate, for example, increasing temperature from 21°C to 37°C caused a significant increase in the fractional recovery ( $11 \pm 8\%$  to  $41 \pm 12\%$ ) but no change in the (still slow) diffusion coefficient. Conversely, at 5 mM phosphate increasing temperature from 21°C to 30°C led to an increase in the diffusion coefficient ( $5 \pm 2$  to  $11 \pm 1 \times 10^{-11} \text{ cm}^2/\text{sec}$ ) but no change in the (already high) fractional recovery. At intermediate phosphate concentrations, increasing temperature resulted first in an increase in fractional recovery (from 30-40% to 60-80%), followed by a sharp rise in diffusion coefficient (fig. 20). In all cases the fractional recovery increased to 60-80% before the diffusion coefficient began to rise.

The reversibility of the two FPR parameters with changes in temperature provided further evidence of their dissociation (fig. 21). At ionic strengths of 13 mM and 21 mM phosphate, incubation of the ghosts at 37°C for 2.5 hr produced large increases in both diffusion coefficient and fractional recovery when compared to the initial values at 21°C. Cooling of the samples back to 21°C for two hours resulted in a return of the diffusion coefficients to the initial values. The fractional recoveries were only partially reversible with cooling, however, and did not return to initial values over a period of 24 hrs at 21°C (fig. 21a).





Figure 20. Diffusion coefficients and fractional recoveries of fluorescence vs. temperature at various ionic strengths.  
[PO<sub>4</sub>] (mM) is given for each curve in the figure.  
See text for experimental details.

Figure 20.

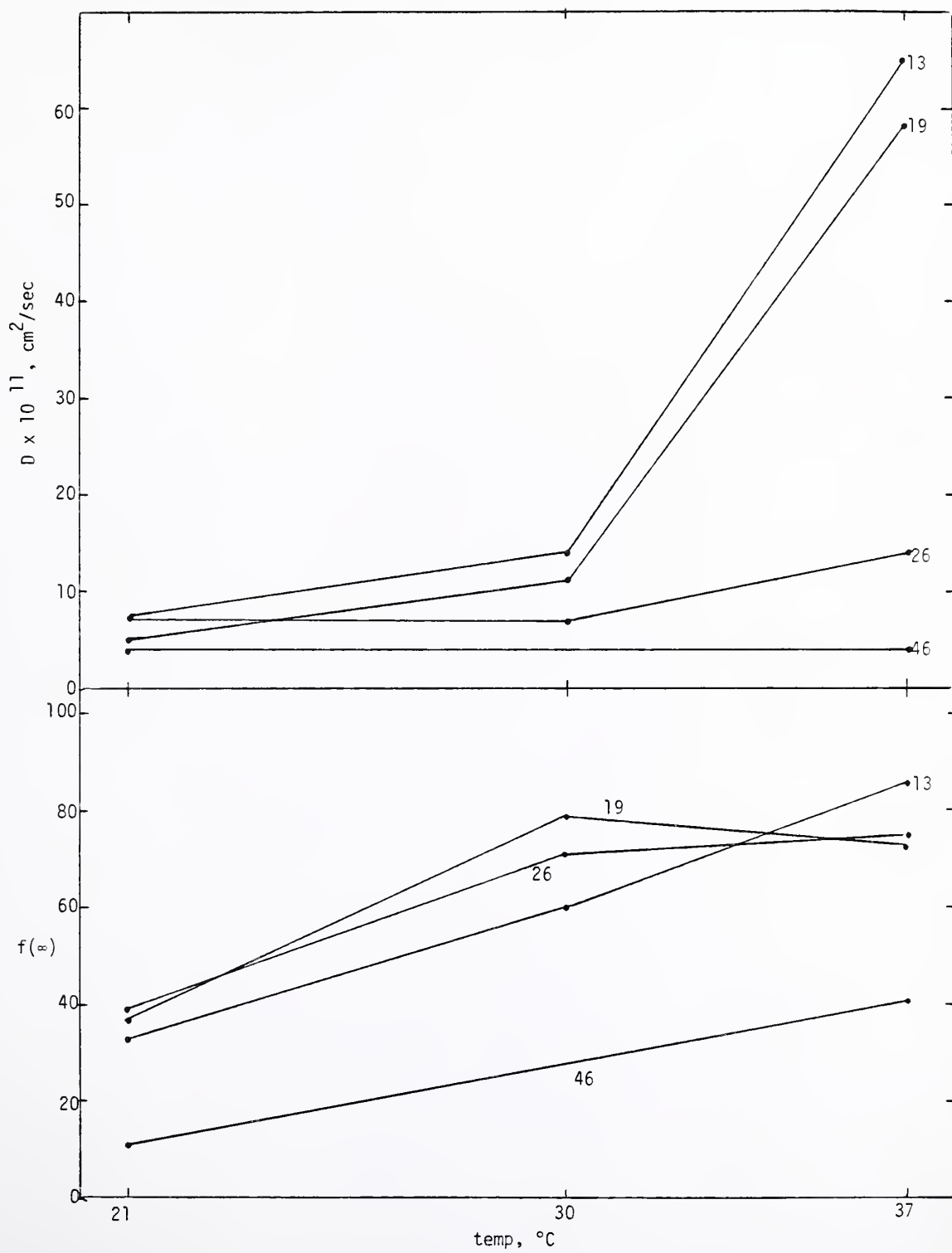






Figure 21. Reversibility of diffusion coefficients and fractional recoveries of fluorescence. Eosin-labeled ghost samples were incubated at 21°C for 4.5 hrs after which time FPR measurements were taken. The temperature was then increased to 37°C for 2.5 hrs and FPR experiments again performed. Finally the temperature was lowered back to 21°C for 2 hrs and FPR parameters were again measured.

- a. ghost sample prepared in 13 mM  $\text{NaPO}_4$
- b. ghost sample prepared in 21 mM  $\text{NaPO}_4$

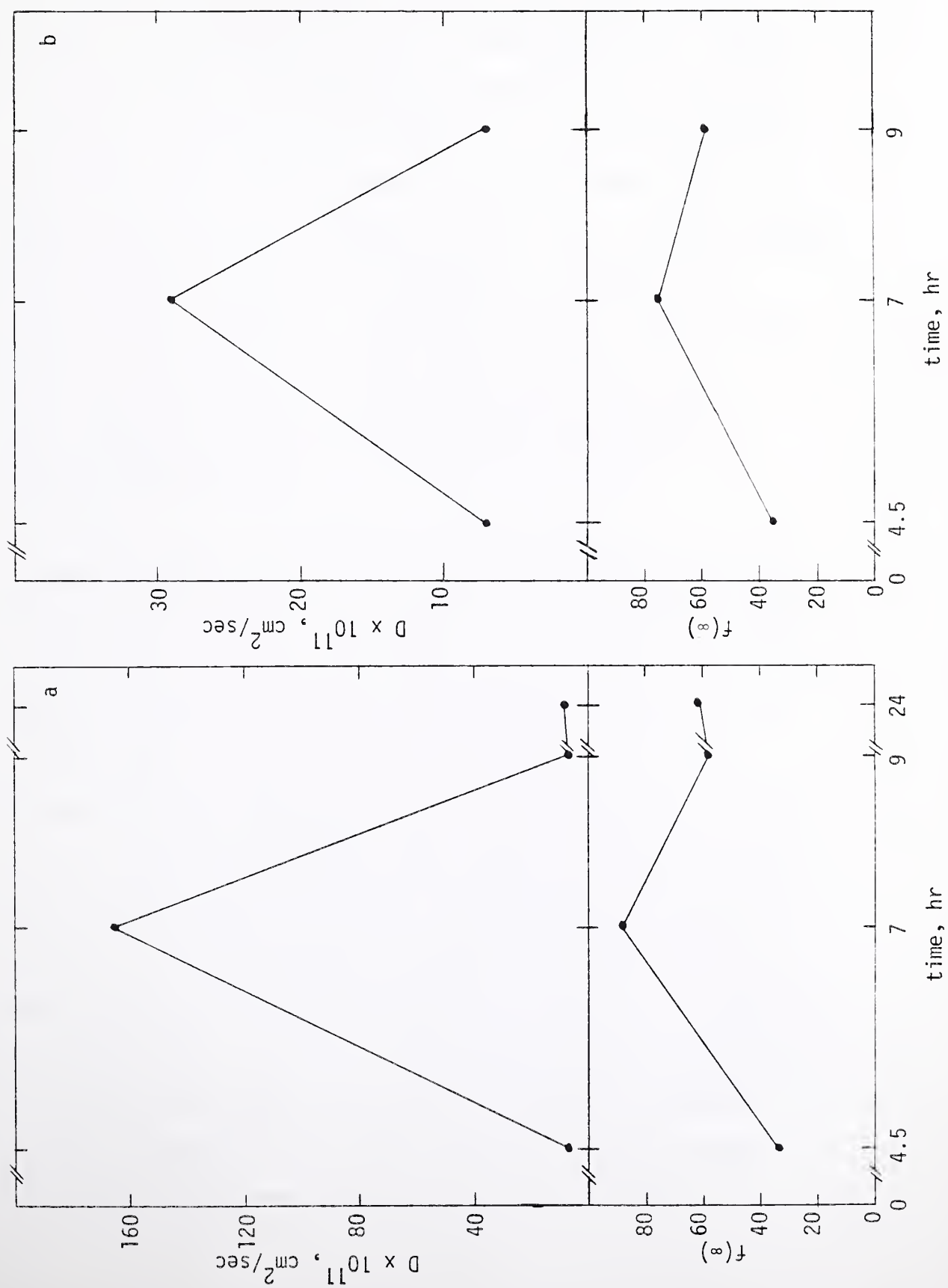


Figure 21.



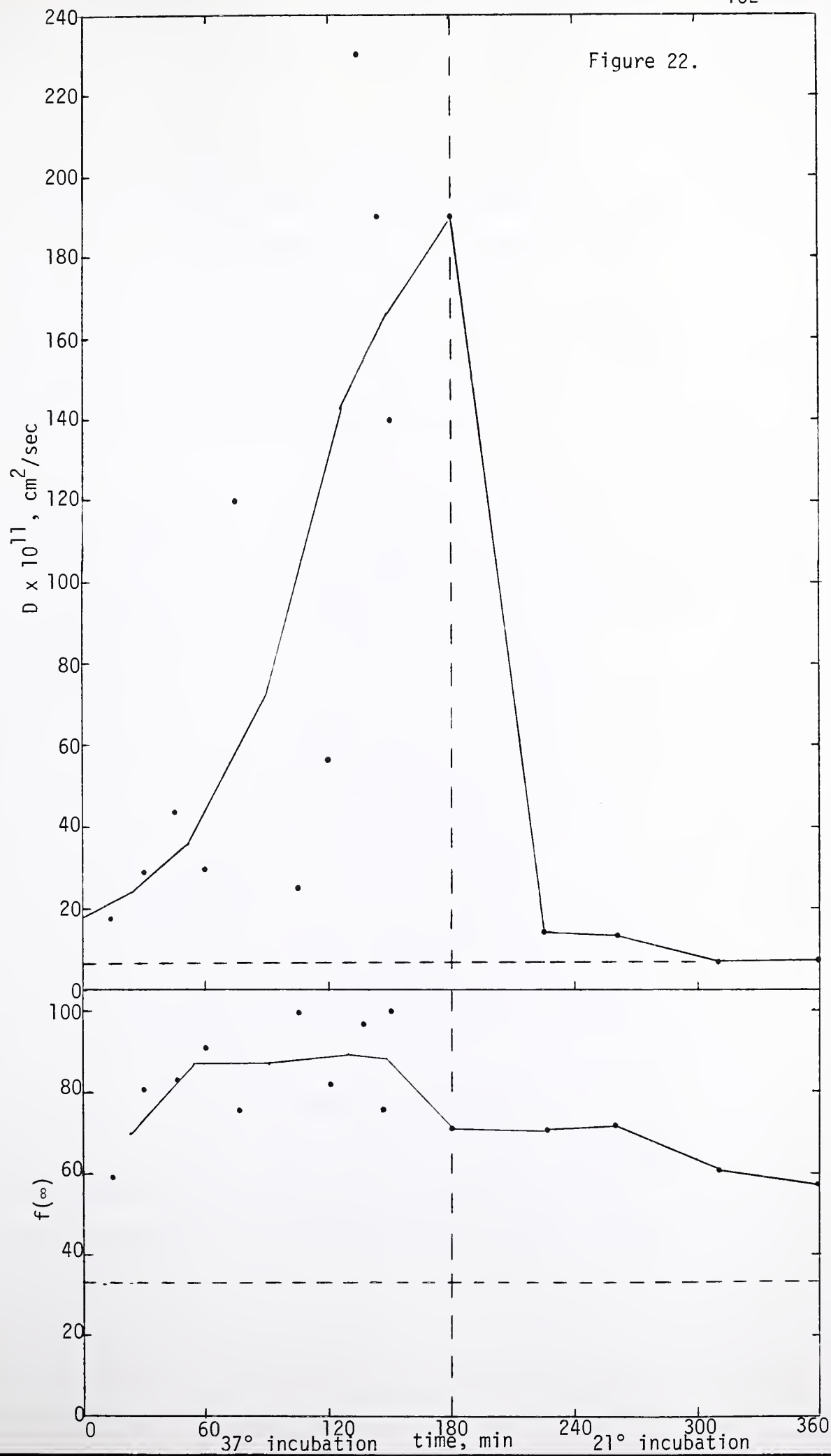
It was possible to inhibit completely the lateral mobility of band 3 in the membrane. A sample of labeled ghosts was prepared in the usual manner (see Methods) and incubated for 24 hrs at 4°C in the dark. The slide was then placed on the precooled microscope stage (10°C) and the FPR experiment performed at  $10 \pm 2^\circ\text{C}$ . No fluorescence recovery was detected in 30 min after bleaching. Warming of the sample to 21°C for 60 min resulted in a recovery curve whose parameters (diffusion coefficient, fractional recovery) were within experimental error of those from a sample at the same ionic strength and temperature which had not been incubated in the cold (data not shown).

3. Effect of Time. Under the proper conditions of ionic strength and temperature, the diffusion coefficient and fractional recovery of fluorescence were extremely sensitive to the time of incubation. Figure 22 presents the results of an experiment in which the FPR parameters were determined every 15 minutes for 3 hours after raising the temperature of the sample from 21°C to 37°C. A different cell was used for each point to avoid bleaching an area in a cell which had been bleached previously in the experiment. Within 50 minutes the fractional recovery increased to a maximum value of  $88 \pm 10\%$  and remained at that value for the duration of the experiment. On the other hand, the diffusion coefficient increased slowly for the first hour and much more rapidly over the following two hours, reaching a value of  $1.9 \pm 0.3 \times 10^{-9} \text{ cm}^2/\text{sec}$  at the end of three hours. This value (corresponding to  $\tau_{1/2} \approx 2 \text{ sec}$ ) approaches the





Figure 22. Diffusion coefficients and fractional recoveries of fluorescence vs. incubation time at 37°C, 13 mM NaPO<sub>4</sub>. Horizontal dotted lines represent initial values at 21°C, before increasing the temperature to 37°C. Smoothed curves are drawn through the experimental data by pairwise averaging of adjacent data points. Vertical dotted line represents reversal of temperature to 21°C. Temperature equilibration time was approximately 10-15 min.





fastest diffusion rate which can be measured with the FPR system as presently designed, and it is possible that even faster diffusion would have been observed with longer incubation times and an FPR system with faster response times. Reversal of the incubation temperature resulted in prompt and total reversibility of the diffusion coefficient but only slow and partial reversibility of the fractional recovery (fig. 22).

4. Rebleaching Experiments. Successive bleaches of the same fluorescently-labeled region on a cell membrane should theoretically result in increasingly greater fractional recoveries of fluorescence with each bleach (180,181). This is because the fractional recovery of fluorescence reflects the ratio of unbleached mobile to immobile fluorophore in the region prior to bleaching, and successive bleaches lead to progressively greater increases in this ratio. If the mobile fluorophore is only free to diffuse within discrete membrane domains significantly smaller than the size of the cell but comparable in size to the bleaching laser beam, however, a limiting fractional recovery which is considerably less than 100% would eventually be reached no matter how many bleaches are delivered (182).

To test this in the eosin-labeled band 3 system, successive rebleachings were performed under a variety of ionic strength and temperature conditions (table 6). In all cases the fractional recovery increased with each succeeding bleach, reaching a value



TABLE 6. REBLEACHING EXPERIMENTS ON EOSIN-LABELED  
GHOST MEMBRANES

$[PO_4]$ , mM <sup>a</sup>	temp, °C	bleach #	$K^b$	$D \times 10^{11}$ cm <sup>2</sup> /sec	$f(\infty)$
46	21	1	1.9	---	0.07
		2	1.9	4.4	0.50
	37	1	1.6	5.7	0.50
		2	2.6	5.8	0.60
		3	2.7	5.1	0.68
		4	4.5	16.	0.81
	21	1	1.9	9.6	0.32
		2	1.6	2.9	0.73
		3	1.8	2.3	0.94
21.4	37	1	2.1	22.	0.68
		2	2.0	9.6	1.06
	37	1	0.7	66.	0.64
		2	1.4	57	0.92
9.4	21	1	2.5	7.9	0.50
		2	2.9	8.5	0.73
5 <sup>c</sup>	21	1	2.4	7.9	0.45
		2	2.7	8.6	0.59
		3	1.5	7.2	0.66
		4	3.3	4.9	0.87
	21	1	2.3	5.4	0.44
		2	5.0	9.2	0.50
		3	3.4	6.2	0.67
		4	3.0	6.7	0.86

<sup>a</sup> +1 mM NaN<sub>3</sub>

<sup>b</sup> bleaching parameter

<sup>c</sup> +10 mM NaN<sub>3</sub>



of 80-100% after the third or fourth bleach. Unless the fractional recovery was very high on the first bleach (60-70%), it did not reach 80-100% after the second bleach because the bleaching of immobile fluorophore by two laser pulses with K parameters of 2-5 was still incomplete. Subsequent bleaches approached 100% recovery in all cases.

### C. DISCUSSION

This chapter presents the results of fluorescence photobleaching recovery experiments on eosin-labeled band 3 in erythrocyte ghost membranes under various conditions of ionic strength, temperature, and time. Experimental recovery curves were closely fit by theoretical curves for diffusion, proving that fluorescence recovery after photobleaching represented lateral diffusion in the plane of the membrane with negligible contribution from any systematic flow process. In general, low ionic strength and high temperature promoted rapid diffusion of band 3 and a high proportion of mobile to total band 3 molecules; high ionic strength and low temperature favored slow diffusion of band 3 and immobilization of band 3 molecules on the time scale of the experiment. It was repeatedly demonstrated, however, that the diffusion and the immobilization processes have different dependencies on ionic strength, temperature, and time. In all cases, increases in the diffusion coefficient occurred at lower ionic strength, higher temperature, or longer incubation times than comparable increases in fractional recovery.



An important consequence of this result is that large increases in the diffusion coefficient occurred only when the fractional recovery was already high, i.e. when nearly all the band 3 molecules were free to diffuse in the plane of the membrane. Furthermore, changes in the diffusion coefficient over almost two orders of magnitude were readily and completely reversible, while two- to three-fold changes in the fractional recovery were only slowly and partially reversible. Any model for erythrocyte membrane structure must take these observations into account; several such models are presented and discussed in chapter 6.

Several qualifications must be placed on the theoretical limits of the experimental data obtainable by the actual FPR experiment, due to both the finite size of the erythrocyte membrane and the finite length of time in which a single FPR curve is obtained. As noted in chapter 2, the  $1/e^2$  radius of the Gaussian laser beam used for bleaching is  $1.2\mu$ . The percentage of the total erythrocyte membrane surface (top and bottom) which is illuminated by the beam is approximately 6%, assuming a surface area for the membrane of  $150\mu^2$ . A bleaching pulse characterized by a K value of 2-5 therefore bleaches approximately 4-6% of the total fluorophore present on the membrane surface (see fig. 6), and the maximum possible fractional recovery of fluorescence is 94-96% rather than 100%. After correcting for the finite size of the cell, then, the maximum mobile fraction of fluorophore observed in these FPR experiments is  $(88/10)/95$ , or  $93\pm 10\%$ .



Unfortunately, the experimental error precludes a definitive statement as to whether all the band 3, or simply most of the band 3, is free to diffuse under these conditions. If it is assumed that eosin labeling of spectrin occurs to the extent of 8% (see chapter 3), and that most if not all of the spectrin is immobile on the membrane (see chapter 1), then the experimentally observed maximum mobile fraction of band 3 is probably  $100 \pm 10\%$ . If the ankyrin-linked band 3 (10-15% of total band 3) is ever free to diffuse in the plane of the membrane, then either band 3-ankyrin, ankyrin-spectrin, or some other spectrin-membrane bonds must be broken. The implications of this statement are discussed more fully in chapter 6.

The finite length of time for which fluorescence recovery after bleaching is monitored leads to an estimate of the maximum possible diffusion coefficient for the fraction of fluorophore which is immobile on the time scale of the experiment. Assuming an observation time of 20 minutes after bleaching and a bleaching parameter (K) of 2, and taking a 20% change in fluorescence to be the minimum significant difference observable, a maximum diffusion coefficient for the immobile fraction of  $1 \times 10^{-12} \text{ cm}^2/\text{sec}$  can be calculated (see fig. 9, eqn. 11). This number is forty times less than the minimum diffusion coefficient determined for the fraction of fluorophore which is mobile on the time scale of these experiments.

Under all conditions of ionic strength and temperature tested, successive bleachings on the same region of the ghost membrane resulted in 80-100% fractional recovery of fluorescence



after the third or fourth bleach. This is the result expected if mobile fluorophore is capable of diffusing over distances on the membrane much greater than the size of the laser beam (181). In particular, this result implies that bounded domains of protein or lipid were not responsible for the restricted lateral mobility of band 3 under various conditions of ionic strength and temperature in these FPR experiments. As noted above, a typical bleaching pulse leads to irreversible bleaching of approximately 5% of the total fluorophore on the membrane. Since the fractional recovery of fluorescence on repetitive bleaching is greater than 80%, the membrane area in which the fluorophore is freely diffusing can be no smaller than  $5\%/(100\%-80\%)$ , or at least 1/4 the area of the intact erythrocyte. Large domains of this size are highly unlikely.

The technical aspects of the experiments reported in this chapter are very reassuring in that the internal structure and consistency of the data excludes many potential artifacts from playing a major role in the results. The large dynamic range of values observed for both diffusion coefficients ( $4 \times 10^{-11}$  to  $2 \times 10^{-9}$  cm<sup>2</sup>/sec) and fractional recoveries (10% to 90%) under various conditions implies that all the values are meaningful, especially in comparison with one another. The demonstration of total reversibility in the diffusion coefficient and partial reversibility in the fractional recovery eliminates such a priori possibilities as a complete, irreversible breakdown in membrane structure as an explanation for large increases in these two



parameters. Finally, as noted above, relative differences between diffusion coefficients under various conditions are independent of the diameter of the laser beam used for bleaching, and a slightly smaller or larger value for the beam size would not affect these comparisons.



## CHAPTER 5. IONIC STRENGTH-DEPENDENT DISSOCIATION OF SPECTRIN FROM GHOST MEMBRANES

The lateral mobility of band 3 in the erythrocyte membrane is highly dependent on the same experimental parameters which favor complete dissociation of the cytoskeleton from the membrane (see chapter 4). In this chapter an attempt is made to elucidate the molecular basis for changes in the lateral mobility of band 3, by examining in detail the ionic strength dependence of dissociation of spectrin, the major cytoskeletal protein, from the ghost membrane. It can be inferred from the reversibility of changes in lateral mobility (complete reversibility in diffusion rate, partial reversibility in the fraction of molecules which are mobile) that such changes are not due to an irreversible alteration in membrane structure. The results presented in this chapter confirm this inference directly, by demonstrating that complete dissociation of spectrin occurs over a range of ionic strengths much lower than that over which dramatic changes in lateral mobility are seen.

### A. METHODS

The method used for analysis of spectrin dissociation was taken from Bennett and Branton (138). Four  $\mu$ l of packed, eosin-labeled erythrocyte ghosts (10.9 mg protein/ml; 1.1  $\mu$ g eosin/mg protein) in 5 mM sodium phosphate, 10 mM sodium azide, 30 nM PMSF, pH 7.4 were suspended in a 200  $\mu$ l volume containing 1 mM sodium



azide, 30 nM PMSF, and various concentrations of sodium phosphate, pH 7.4. After incubation for 60 min at 37°C, the samples were sonicated 15 times for 1 sec at 30 W (Ultrasonics model W-225R, microprobe tip), gently shaken, layered onto 200  $\mu$ l of 20% sucrose in 500  $\mu$ l microfuge tubes, and centrifuged (Eppendorf model 5412) at 4°C for 40 min at 15600 x g. The sonication and shaking steps were used to facilitate release into free solution of any solubilized protein molecules which had been entrapped within the ghosts. The resulting supernatants were carefully removed and discarded, and the orange-pink pellets dissolved in 50  $\mu$ l of 10 mM Tris chloride, 1 mM EDTA, 3% SDS, 2% sucrose, 2% 2-mercapto-ethanol, pH 7.4. The composition of the dissolved pellets was analyzed by discontinuous slab gel electrophoresis according to Laemmli (206). The stacking gel was 3% in acrylamide, the resolving gel 7.5% in acrylamide and 2.7% in bis-acrylamide (with respect to acrylamide). Dimensions of the gel were 0.15 x 12 cm. Following staining with Coomassie blue (14), the gel lanes were scanned at 550 nm (Schoeffel spectrodensitometer, model SD3000). The amount of spectrin (bands 1 and 2) remaining in the membrane pellets relative to band 3 (which was presumed inextractable without detergent) was estimated by the comparison of the heights of or the areas under the peaks corresponding to bands 1, 2, and 3. A control sample was maintained at 0°C in 16 mM sodium phosphate, pH 7.4 for 60 min and then subjected to the same analytical procedures as the experimental samples. The percent dissociation



of band 1 was calculated as  $\frac{(\text{height band 1/height band 3})_{\text{experimental}}}{(\text{height band 1/height band 3})_{\text{control}}}$ ;

the percent dissociation of band 2 was obtained from a similar equation.

The average dissociation of spectrin (bands 1+2) was calculated

either as  $\frac{[(\text{height band 1} + \text{height band 2})/\text{height band 3}]_{\text{experimental}}}{[(\text{height band 1} + \text{height band 2})/\text{height band 3}]_{\text{control}}}$ ;

or as  $\frac{(\text{area bands 1+2/area band 3})_{\text{experimental}}}{(\text{area bands 1+2/area band 3})_{\text{control}}}$ . These two methods of

calculation for the average dissociation of spectrin yielded the same results within experimental error ( $\pm 10\%$ ). Using an identical procedure, Bennett and Branton (138) have shown that less than 4% of the extracted spectrin is pelleted through 20% sucrose when centrifuged in the absence of membranes.

## B. RESULTS AND DISCUSSION

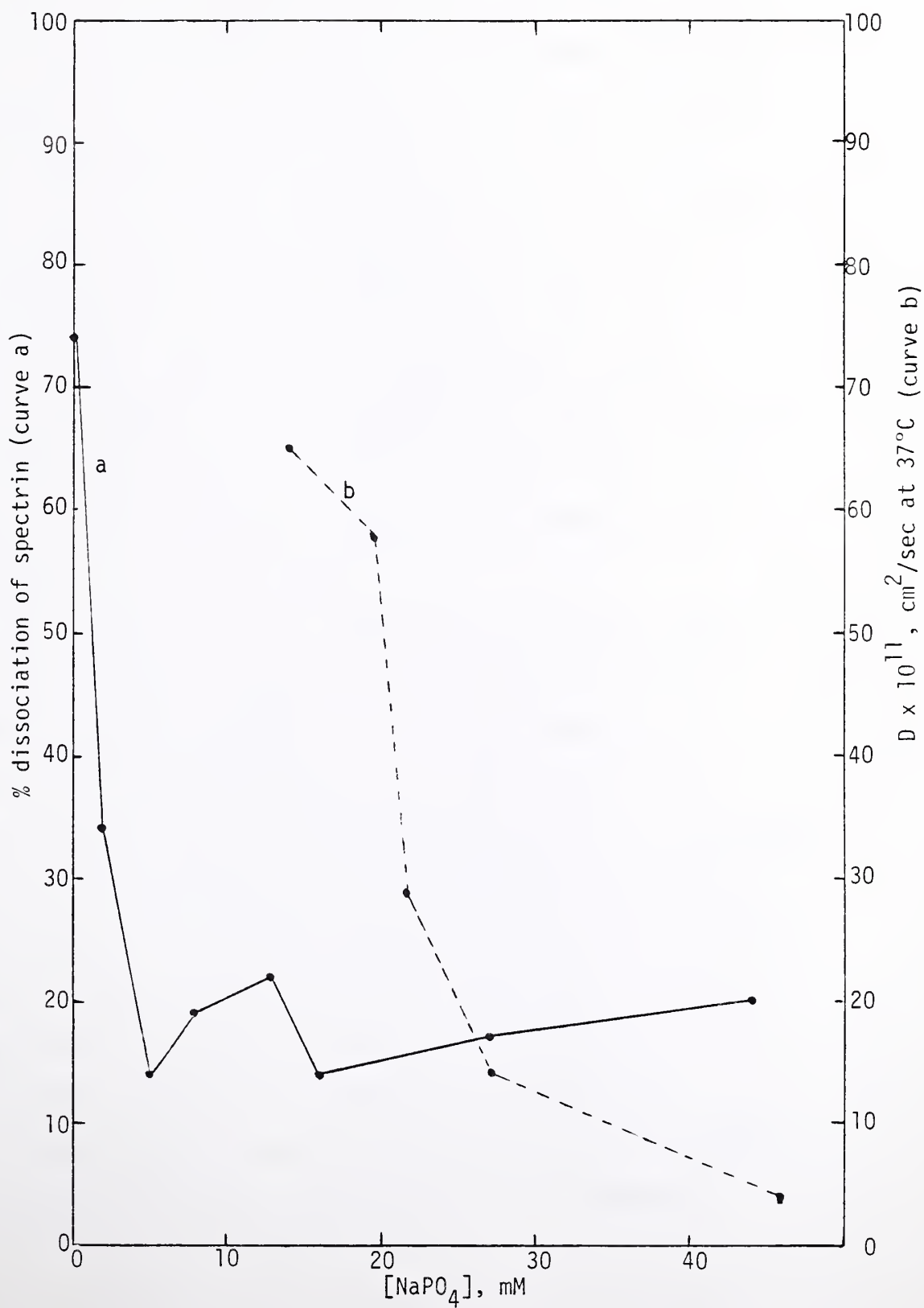
The ionic strength dependence of spectrin dissociation from eosin-labeled ghosts on incubation at 37°C for 60 minutes is presented in figure 23. At phosphate concentrations greater than 5 mM, approximately 15-20% of bands 1 and 2 were dissociated; this amount did not change with increasing ionic strength at least up to 44 mM phosphate. Below 5 mM phosphate there was an abrupt transition in the stability of the spectrin-membrane complex leading to 74% dissociation of spectrin (band 1:80%; band 2: 64%) at 0.1 mM phosphate. At 2 mM phosphate the degree of dissociation of band 1 (45%) was significantly greater than that of band 2 (18%);





Figure 23. Ionic Strength Dependent Dissociation of Spectrin.  
See text for experimental details. For comparison  
a curve of diffusion coefficient vs. ionic strength  
at 37°C is reproduced from fig. 17.

Figure 23.





at all other buffer concentrations the extents of dissociation of the two components of spectrin were not significantly different.

Figure 23 is in agreement with previous reports of spectrin elution from erythrocyte ghosts at low ionic strength (14,16,126, 138,150,212-215). Quantitative measurements of spectrin elution vs. KCl concentration (pH 7.6, incubation for 30 min at 37°C) showed a relationship very similar to that found in this chapter for spectrin dissociation vs. phosphate concentration. Thus,  $\approx 20\%$  dissociation at KCl concentrations greater than 10 mM was found, with a sharp increase in elution below 10 mM KCl leading to a maximum of 60-80% dissociation at 0 mM KCl (ref. 138). The buffer concentration at which 50% dissociation occurred was 5 mM KCl (ionic strength ( $\mu$ ) = 5 mM, ref. 138) compared with 2 mM  $\text{NaPO}_4$  ( $\mu \approx 5$  mM, this study).

Figure 23 also presents a comparison of the ionic strength dependence of spectrin dissociation with that of the diffusion coefficient for eosin-labeled band 3 in ghost membranes. In both cases, the ghosts were incubated for 60 minutes at 37°C, eliminating the effects of temperature and time from the comparison. It is readily apparent that changes in spectrin dissociation occurred only at very low ionic strengths whereas increases in the diffusion coefficient occurred at much higher phosphate concentrations. The elution of 20% of the total spectrin at high ionic strengths is an interesting observation in its own right, and may indicate heterogeneity of spectrin binding to the membrane (ref. 138: see chapter 6). This is especially



noteworthy because the 20% dissociation seen on incubation at 37°C did not occur in the control samples, which were incubated at 0°C. Nonetheless, this degree of spectrin dissociation was constant over the ionic strength range in which the lateral mobility of band 3 changed greatly, and complete spectrin dissociation alone cannot explain the increases in diffusion coefficient.

The relationship between spectrin elution and ghost membrane vesiculation is intriguing. As noted in chapter 4, photobleaching recovery experiments at 37°C at phosphate buffer concentrations less than 10 mM were prevented due to rapid and total membrane vesiculation. Extensive ghost membrane vesiculation was also seen at 37°C in 8 mM NaPO<sub>4</sub> buffer in another study (150). In this chapter, however, it was shown that significant (>20%) elution of spectrin from the ghost membrane did not occur until the buffer concentration was decreased below 5 mM phosphate. From these data, it would appear that membrane vesiculation occurs just before complete dissociation of spectrin, the major cytoskeletal protein. This is yet another indication that significant changes in membrane structure are possible without total removal of the cytoskeleton.



CHAPTER 6. DISCUSSION

The data reported in this dissertation describe a wide range of phenomena concerning the lateral mobility of band 3 in the human erythrocyte membrane. Within a fairly narrow range of temperatures (21°C-37°C) and ionic strengths (5-46 mM NaPO<sub>4</sub>, pH 7.4), conditions are described under which fifty-fold changes in diffusion coefficient ( $4\text{-}200 \times 10^{-11} \text{ cm}^2/\text{sec}$ ) and nearly maximal changes in the mobile fraction of band 3 (10%-90<sup>+</sup>%) occur. Clearly the lateral mobility of this integral membrane protein is regulated in some systematic way. In this discussion six possible models for intramembraneous forces capable of restricting translational diffusion of band 3 are presented. Careful consideration of the present data, as well as other observations from the literature, leads to a rejection of all but two of the models as likely options. Both of these involve an intimate association between the cytoplasmic portion of band 3 and the cytoskeleton of the erythrocyte membrane: one proposes a specific, low-affinity complex between band 3 and some immobile cytoskeletal component (most likely spectrin); the other postulates a nonspecific entanglement of band 3 in the cytoskeletal reticulum formed by spectrin, actin, and various other peripheral membrane proteins.



#### A. COMPARISONS WITH MEASUREMENTS OF TRANSLATIONAL AND ROTATIONAL DIFFUSION

Before considering specific models of erythrocyte membrane structure, it is relevant to compare the lateral mobility data obtained in this work with various measurements of translational and rotational diffusion for integral membrane proteins (including band 3) in the literature. Peters et al. (7) reported a maximum translational diffusion coefficient of  $3 \times 10^{-12} \text{ cm}^2/\text{sec}$  for fluorescein-isothiocyanate (FITC)-labeled erythrocyte membrane proteins in ghosts suspended in 7 mM  $\text{NaPO}_4$  buffer, pH 8.0 ( $\mu=25 \text{ mM}$ ) at 20-23°C. This value is in apparent disagreement with the results of the present study, in which a diffusion coefficient for band 3 in ghost membranes of  $9.5 \pm 2.3 \times 10^{-11} \text{ cm}^2/\text{sec}$  (with a fractional recovery of  $51 \pm 14\%$ ) in 9 mM  $\text{NaPO}_4$  buffer, pH 7.4 ( $\mu=23 \text{ mM}$ ) at 21°C was observed. In hindsight, however, there were several erroneous assumptions made in the paper of Peters et al. which led to an artificially low estimate of the diffusion coefficient of the integral membrane proteins. An SDS-polyacrylamide gel scan of FITC-labeled ghosts (see fig. 3b of ref. 7) shows approximately 40% of the label on band 3 or glycophorin, with about 10% on spectrin and about 50% either bound to lipid or noncovalently attached to the membrane in some way. The label on spectrin would presumably be immobile, while the lipid-bound or noncovalently bound fluorophore would probably exhibit extremely rapid



diffusion (see table 3). The authors took their first measurement of fluorescence recovery at 3 to 3.5 minutes after bleaching, however, by which time all the rapidly diffusing fluorophore could have recovered. It can also be calculated that, within this time period, about 40% of the maximum band 3-associated fluorescence recovery would have already occurred, given a lateral diffusion coefficient of  $9.5 \times 10^{-11} \text{ cm}^2/\text{sec}$  (see fig. 2 of ref. 7). Since the fractional recovery of band 3 fluorescence at this ionic strength is only about 50% (table 5), the expected overall recovery of fluorescence between 3 and 23 minutes after bleaching is  $40\% \times 60\% \times 50\%$ , or about 12%. In fact, Peters et al. estimated a fluorescence recovery during this time period of  $9 \pm 7\%$ , indicating actual agreement with the present study.

Fowler and Branton (8) used inactivated Sendai virus to fuse a 50/50 mixture of unlabeled and FITC-labeled erythrocytes (>70% of label on band 3 or PAS-1) in 310 mOsm phosphate-buffered saline, pH 7.6, at 0°, 23°, 30°, and 37°C. Minimum translational diffusion coefficients for the integral membrane proteins were determined from the rate of appearance of fused cell pairs with "uniform" distribution of fluorescence, based on a model for diffusion from one half of a spherical shell into the other (see table 2). Given the uncertainties concerning the (possibly temperature-dependent) effects of Sendai virus fusion, the unknown influence of immobile fluorophore on the scoring system used to determine the percentage of fused cells which are "uniformly



fluorescent" (see fig. 3 of ref. 8), and the fact that a spherical-shell model for diffusion will underestimate the actual diffusion coefficient in an hourglass-shaped system (see fig. 2b of ref. 8), the cell fusion results compare favorably with the FPR measurements at high ionic strength of this work. Thus, the diffusion coefficients at all temperatures agree to within a factor of 6-7; the photobleaching recovery values are greater than the cell fusion results in all cases, as expected.

The acetylcholine receptor (AChR) in developing rat myotube membrane (176) and rhodopsin in frog retinal rod outer segment disc membrane (169) are both integral membrane proteins whose lateral mobilities in the membrane have been carefully studied. The rhodamine- $\alpha$ -bungarotoxin-labeled AChR in the diffusely fluorescent region of myotube membrane has an apparent diffusion coefficient of  $5 \pm 2 \times 10^{-11} \text{ cm}^2/\text{sec}$  at  $22^\circ$  and  $16 \pm 3 \times 10^{-11} \text{ cm}^2/\text{sec}$  at  $37^\circ\text{C}$ , with fractional recoveries of 75% in both cases. In contrast, the AChR in the patchy, densely fluorescent region has a diffusion coefficient of  $< 10^{-12} \text{ cm}^2/\text{sec}$ , with fractional recovery  $\approx 0$ . The data for the diffuse region are similar to values for band 3 lateral mobility under conditions in which the fractional recovery of fluorescence is high but the diffusion coefficient is relatively low (cf. values at 5 mM phosphate,  $21^\circ\text{C}$ , and at 26 mM phosphate,  $37^\circ\text{C}$ ). The AChR is comparable in molecular weight to the band 3 dimer, and might be expected to have similar lateral mobility in the plane of the membrane. A diffusion coefficient of  $1-2 \times 10^{-10} \text{ cm}^2/\text{sec}$  at  $37^\circ\text{C}$  has been shown to represent a considerable degree



of restriction of band 3 diffusion, when compared to the maximum observed diffusion coefficient of  $1.9 \times 10^{-9} \text{ cm}^2/\text{sec}$  (fig. 22). It is not unreasonable to postulate, then, that the lateral mobility of the AChR in the diffuse region of the myotube membrane is also restricted by membrane-associated forces other than bilayer viscosity alone (see below), though obviously not to the same extent as AChR in the densely labeled patches.

In contrast to the relatively slow diffusion of the AChR, rhodopsin exhibits extremely rapid lateral diffusion in the plane of the membrane ( $D=3.5 \pm 1.5 \times 10^{-9} \text{ cm}^2/\text{sec}$ ,  $f(\infty) \approx 100\%$  at  $20^\circ\text{C}$ ). This diffusion rate is as fast as that of the lipid analogue diI in several natural membrane systems (see table 3), and is thought to represent unrestricted lateral mobility (i.e. mobility restricted only by the viscosity of the bilayer) for this integral membrane protein (2,169). The fastest lateral mobility of band 3 observed in the present study ( $1.9 \pm 0.3 \times 10^{-9} \text{ cm}^2/\text{sec}$ ,  $f(\infty) > 90\%$  at  $37^\circ\text{C}$ ) is within experimental error of the rhodopsin diffusion rate, although the band 3 measurement was made at a higher temperature. Given the smaller molecular weight of rhodopsin compared to the band 3 dimer and the extraordinarily large percentage of cholesterol in the erythrocyte membrane compared to the rod outer segment membrane, the agreement between the diffusion coefficients of rhodopsin at  $20^\circ\text{C}$  and band 3 at  $37^\circ\text{C}$  (under certain conditions) is striking. A diffusion coefficient of  $1.9 \times 10^{-9} \text{ cm}^2/\text{sec}$  for band 3 may thus be reflective of completely unrestricted lateral mobility (i.e.



governed only by bilayer viscosity) in the erythrocyte membrane.

It is instructive in this regard to estimate the viscosity of the erythrocyte membrane at 37°C, assuming that a translational diffusion coefficient of  $1.9 \times 10^{-9} \text{ cm}^2/\text{sec}$  represents unrestricted lateral mobility for band 3. There are two models for diffusion in a viscous medium which can be employed for such a calculation. The Einstein-Sutherland diffusion equation (cited in ref. 169) relates the translational diffusion coefficient  $D_T$  of a large spherical particle of radius  $r$  in an isotropic (three-dimensional) medium to the viscosity of the medium  $\eta$ :

$$\eta = (kT)/(6\pi D_T r), \quad (14)$$

where  $k$  is the Boltzmann constant and  $T$  is the absolute temperature. An approximate radius for the intramembranous portion of the band 3 dimer (mol. wt. approximately 100,000 daltons) of 40A is assumed, as this value is approximately twice the radius estimated by Poo and Cone (169) for the rhodopsin monomer (38,000 daltons) in the disc membrane and approximately half the diameter of the intramembranous particles in the erythrocyte membrane (which may be an overestimate). The resultant viscosity for a translational diffusion coefficient of  $1.9 \pm 0.3 \times 10^{-9} \text{ cm}^2/\text{sec}$  at 37°C is  $3 \pm 1P$ . This value compares favorably with previous estimates of erythrocyte membrane viscosity based on measurements of fluorescence polarization (216-218) and methanol diffusion (219), and with estimates of membrane viscosity in other systems (see table 7). The Saffman-Delbrück equation considers the translational diffusion of a cylinder of



TABLE 7. ESTIMATES OF MEMBRANE VISCOSITY

membrane	temp, °C	viscosity (poise)	method	label	ref.
erythrocyte ghosts	20	1.2	fl. pol. <sup>a</sup>	perylene	216
"	37	1.7	"	"	"
"	21	1-10	fl. pol.	retinol	217
"	20	5-7	fl. pol.	DPH <sup>b</sup>	218
"	37	2-4	"	"	"
"	20	1.7	methanol diffusion	methanol	219
"	21	25-100	rot. diff. band 3	EITC <sup>c</sup>	201
"	37	25-100	rot. diff. band 3	EITC	89
"	37	2-4 <sup>d</sup> 28-40 <sup>e</sup>	lat. diff. band 3	EITC	this study
frog disc	21	0.6-6.0 <sup>d</sup>	rot. diff. rhodopsin	retinal	221
amphibian disc	21	1-4 <sup>d</sup>	lat. diff. rhodopsin	retinal	221
mouse-human heterokaryon	37	8-10 <sup>d</sup>	lat. diff. surface antigens	fl. antibody	2,163

<sup>a</sup> fluorescence polarization

<sup>b</sup> 1,6-diphenyl-1,3,5-hexatriene

<sup>c</sup> eosin-5-isothiocyanate

<sup>d</sup> calculated according to eqn. 14

<sup>e</sup> calculated according to eqn. 15



radius  $a$  and height  $h$  through a two-dimensional viscous medium of viscosity  $\eta$  (i.e. the lipid bilayer) which is bounded on either side by a much less viscous medium of viscosity  $\eta'$  (i.e. the intracellular and extracellular aqueous fluid):

$$D_T = \frac{kT}{4\pi\eta h} \left( \ln \frac{\eta h}{\eta' a} - \gamma \right), \quad (15)$$

where  $\gamma$  is Euler's constant (0.5772). Again assuming the radius of the band 3 dimer to be 40Å, and taking values for the thickness of the hydrophobic membrane core of 40Å and for the aqueous phase viscosity of  $1 \times 10^{-2}$ P, the bilayer viscosity implied for  $D_T = 1.9 \pm 0.3 \times 10^{-9} \text{ cm}^2/\text{sec}$  at 37°C is  $34 \pm 6$ P. It should be noted that this estimate of viscosity is inversely proportional to the value chosen for the membrane thickness but relatively insensitive to small changes in particle radius, while the viscosity estimated from the Einstein-Sutherland relation is linearly related to particle radius but (of necessity) independent of membrane thickness.

The bilayer viscosity as estimated from the two-dimensional diffusion equation differs by an order of magnitude from that calculated assuming diffusion in an isotropic three-dimensional medium. It is in agreement, however, with the estimate of viscosity based on rotational diffusion of eosin-labeled band 3 in the ghost membrane (table 7). It is not at all clear that the bilayer viscosity sampled by small molecular probes such as diphenylhexatriene and methanol is the same effective viscosity governing the motion of large membrane proteins, nor is it obvious that a



three-dimensional diffusion equation has any quantitative bearing on a two-dimensional diffusion process. Furthermore, it is not unreasonable to imagine a considerably greater viscosity for the cholesterol-rich, sphingomyelin-rich erythrocyte membrane than for other biological membranes which do not contain as much cholesterol and sphingomyelin. The agreement between viscosity estimates based on models for both translational and rotational diffusion of band 3 in a two-dimensional viscous medium is striking, and suggests that the effective viscosity of the erythrocyte bilayer sampled by this integral membrane protein may be considerably higher than previously estimated.

Rotational diffusion of eosin-labeled band 3 has been studied by observing the decay of flash-induced absorption anisotropy of the eosin probe (89,201-203,222). A single rotational correlation time of about 0.5 msec at both 21°C (201-203) and 37°C (89) in 5 mM NaPO<sub>4</sub> buffer, pH 7.4 was originally estimated; this value corresponds to a rotational diffusion coefficient about the membrane normal ( $D_R$ ) of 500-2000 sec<sup>-1</sup>. More recently, two components of the decay of flash-induced anisotropy have been reported (222), but their relationship to any physical model (such as rapidly and slowly rotating forms of band 3) cannot be unambiguously stated. In particular it is difficult from this data to implicate any particular membrane-associated process in restriction of the rotational mobility of band 3, since the physical meaning of the anisotropy decay components is highly uncertain. In the rapid



diffusion limit, however, a comparison between the translational and rotational diffusion coefficients is instructive. At 37°C a considerable contribution to the overall anisotropy decay is made by the fast component, which has a rotational correlation time of about 0.15 msec (ref. 222). Let us assume that this represents the smallest possible correlation time for band 3 rotation at 37°C. The theoretical relationship between translational and rotational diffusion coefficients for protein embedded in a lipid bilayer (220) can then be used to estimate the translational diffusion coefficient which should be supported by the lipid viscosity at 37°C:

$$\frac{D_T}{D_R} = a^2 \left( \ln \frac{\eta h}{\eta' a} - \gamma \right). \quad (16)$$

For a bilayer viscosity of 30P (see above), a maximum translational diffusion coefficient of  $1.8-7.2 \times 10^{-9} \text{ cm}^2/\text{sec}$  would be expected. The agreement between the predicted value and the value obtained in the present study ( $1.9 \pm 0.3 \times 10^{-9} \text{ cm}^2/\text{sec}$ ) is striking, suggesting that in the rapid (or unrestricted) mobility limit at least, rotation and translation of band 3 are governed by identical forces. It should be noted that rotational diffusion of band 3 has only been measured at low ionic strength, where the fraction of band 3 which is free to diffuse laterally is >70% (table 5). Measurements of rotational mobility under high ionic strength, low temperature conditions would be very instructive in deciding whether the membrane-associated process which causes translational immobilization



of band 3 (i.e. low fractional recovery) also induces rotational immobilization of band 3.

## B. MODELS OF ERYTHROCYTE MEMBRANE STRUCTURE

From the data presented in this dissertation, it appears that there are at least two separate processes restricting the lateral mobility of band 3 in the human erythrocyte membrane. One process regulates the fraction of band 3 which is free to diffuse in the plane of the membrane; the other controls the rate at which the mobile fraction of band 3 diffuses. Both processes are dependent on ionic strength and temperature, in that high ionic strength (46 mM phosphate) and low temperature (21°C) favor immobilization (10% mobile) and slow diffusion ( $D = 4 \times 10^{-11} \text{ cm}^2/\text{sec}$ ) of band 3, while low ionic strength (13 mM phosphate) and high temperature (37°C) favor mobilization (>90% mobile) and fast diffusion ( $D = 2 \times 10^{-9} \text{ cm}^2/\text{sec}$ ) of band 3. Detailed analysis of the ionic strength and temperature dependencies of these two experimental parameters reveals, however, that they are clearly dissociated and therefore must result from at least two different membrane-associated processes. Thus, increases in the fraction of mobile band 3 to near maximal levels (>75%) always precede (i.e. occur at higher ionic strength and lower temperature than) large increases in the diffusion coefficient. Similarly, on prolonged incubation of ghosts at constant ionic strength (13 mM  $\text{NaPO}_4$ , pH 7.4)



and temperature (37°C), the mobile fraction increases within one hour to 90<sup>+</sup>% while the diffusion rate of the mobile fraction increases only slowly for the first hour and much more rapidly over the following two hours. Further evidence of the dissociation of the processes responsible for regulating immobilization and diffusion is the difference in reversibility of these two parameters: changes in the diffusion rate of band 3 with temperature are promptly and totally reversible whereas increases in the mobile fraction of band 3 are only slowly and partially reversible.

There are at least six theoretical membrane-associated processes capable of regulating the lateral mobility of band 3 to some degree. In increasing order of likelihood, these include: 1) electrostatic repulsion between putative band 3-glycophorin complexes; 2) lipid domain formation on the membrane; 3) planar aggregation of band 3 dimers; 4) lipid viscosity; 5) specific complex formation between band 3 and some immobile cytoskeletal component; and 6) nonspecific entanglement of the cytoplasmic portion of band 3 in the cytoskeletal network.

An association between band 3 and glycophorin in the intramembranous particles revealed on freeze-fracture of the erythrocyte membrane has been postulated for some time (see chapter 1). Such a complex might render band 3 mobility susceptible to ionic strength changes, since the electrostatic repulsion between such particles (due to the very large amount of negatively-charged sialic acid present on each glycophorin monomer) would become accentuated at low ionic strength. One would not expect the



lateral mobility of the putative band 3-glycophorin complex to be especially temperature-sensitive, however, if electrostatic repulsion were the major factor governing restriction of mobility. In addition, electrostatic effects would be expected to become manifest instantaneously upon changes of ionic strength or other conditions; the characteristic slow rise in diffusion coefficient on prolonged incubation at 37°C (fig. 22) thus argues strongly against this mechanism.

The likelihood of domain formation in the erythrocyte membrane is low on several accounts, including the results of the present study. X-ray diffraction studies indicate that there is negligible liquid-crystalline phase lipid present in the erythrocyte membrane above 0°C (ref. 223). Similarly, differential scanning calorimetry could not detect a phase transition below 40°C (ref. 224). Both of these studies are consistent with the high cholesterol content and heterogeneous lipid composition of the membrane. In the present study the presence of domains smaller in area than about 1/4 of the total membrane surface was explicitly ruled out over a wide range of ionic strengths and temperatures, since rebleaching laser pulses delivered to the same area of eosin-labeled ghost membrane consistently resulted in 80-100% fractional recovery of fluorescence after the third or fourth bleach. Had bounded domains comparable in size to the focused laser spot been present, fractional recoveries on rebleaching would never have reached these high levels (see chapter 4).



Self-aggregation of band 3 dimers has been postulated as the physical explanation for the temperature dependence of the two components of rotational diffusion of eosin-labeled band 3 (ref. 222). Large aggregates are highly unlikely, since cross-linking and solubilization studies show mainly dimers of band 3 (with some trimers and tetramers, but no higher aggregates), and no temperature-dependent aggregation of band 3-associated intramembranous particles in the erythrocyte membrane has ever been seen. The increased trypsin susceptibility of band 3 at low ionic strength (54) may imply a conformational change in band 3 structure with ionic strength; there is no a priori reason to suppose, however, that such a change would necessarily be associated with aggregation of band 3 dimers. Nigg and Cherry (222) invoke microaggregates of 5-10 band 3 dimers as sufficient to explain the temperature dependence of the data on rotational diffusion. Assuming a dependence of translational diffusion coefficient on particle size of  $D \propto 1/r$ , where  $r$  is the radius of the particle, however, an aggregation of at least 2500 band 3 dimers would be necessary to explain a 50-fold change in diffusion coefficient. Even this is probably an underestimate, since  $D$  may actually have a  $\log(1/r)$  rather than a  $1/r$  dependence on particle size (cf. eqn. 15 vs. eqn. 14). Clearly the large changes in diffusion coefficient seen in the present study under various conditions of ionic strength and temperature cannot be explained on the basis of planar aggregation.



There is little evidence for or against lipid viscosity as a major mediator of large changes in the lateral mobility of band 3. Obviously lipid viscosity plays a crucial role in setting a "baseline" level of lateral mobility for integral membrane proteins (see eqns. 14,15), but there are two pieces of circumstantial evidence against this factor as a regulator of changes in lateral mobility in the erythrocyte membrane. Preliminary data indicate that the lateral diffusion coefficient of the lipid probe diI in erythrocyte ghosts changes only two-fold from 0°C to 40°C (ref. 191), implying that the membrane viscosity also changes little over this wide range of temperatures. In the present study we have shown temperature effects on the diffusion coefficient to be highly time-dependent (fig. 22), with a lag of more than 60 minutes between warming up to temperature and achieving of the maximum rate of diffusion at that temperature. Viscosity effects should become manifest almost instantaneously on warming up to a given temperature. It is unlikely, therefore, that large changes in lipid viscosity are responsible for major alterations in the lateral mobility of band 3.

There is a great deal of experimental evidence to support the contention that band 3 interacts intimately with the cytoskeleton of the erythrocyte membrane. Indeed, it would be surprising on steric grounds alone if such associations did not occur, since the anastomosing cytoskeletal reticulum covers approximately 1/3 of the inner membrane surface (115) and a considerable portion



of the band 3 molecule is entirely intracellular. Much of this data is summarized in chapter 1, and will not be repeated here. Of particular interest are the observations that: 1) cross-linking between band 1 of spectrin and band 3 at pH 7.4 is ionic strength dependent (occurring in isotonic KCl but not in 10 mM KCl) (123); 2) antibodies directed against the cytoplasmic portion of band 3 inhibit spectrin binding to inside-out vesicles (6); and 3) approximately 10-15% of the total band 3 is tightly linked to ankyrin, a cytoskeletal protein (146). None of these findings, however, is conclusive proof that the major portion of band 3 forms a specific complex with the cytoskeleton in a manner which could restrict lateral mobility. Although up to 40% of band 3 remains with the cytoskeleton upon Triton X-100 extraction of erythrocyte ghosts in isotonic buffer (118), band 3 cannot be solubilized with the major cytoskeletal proteins (spectrin, actin) in low ionic strength medium and it does not serve as a high-affinity binding site ( $K_D < 10^{-7} \text{M}$ ) for spectrin on the inner membrane surface (138).

It is claimed that the rotational diffusion of band 3 has the same characteristics (rate, temperature dependence, etc.) in spectrin-depleted membrane vesicles as in native ghost membranes, and that this evidence excludes the spectrin-actin network from any possible role in restriction of rotational diffusion (201,222). These experiments were performed in low ionic strength buffer (5 mM  $\text{NaPO}_4$ ), however, under which conditions



we find the (laterally) mobile fraction of band 3 to be high (>70%). Unless the cytoskeleton is free to diffuse on the membrane (which is unlikely but not impossible), one would expect specific band 3-cytoskeleton bonds to immobilize totally the band 3 involved. Such interactions, then, would surely decrease the fraction of band 3 which is mobile but would probably not affect the diffusion coefficient of the mobile fraction. Since the rotational diffusion measurements were gathered in a manner which is insensitive to changes in the (laterally) mobile fraction of band 3, they can tell us nothing about any process responsible for changing the percentage of total band 3 which is mobile. If specific band 3-cytoskeleton complexes were the physical explanation behind a decreased fractional recovery of fluorescence at low temperature and/or high ionic strength, then any change in rotational diffusion due to such complex formation would not have been seen by Cherry et al., even in intact ghosts. Thus, although specific interactions between the major portion of band 3 and the cytoskeleton have never been conclusively demonstrated, they have not been ruled out either. In particular, a low-affinity ( $K_D \approx 10^{-5}$ - $10^{-6}$ M) complex between band 3 and spectrin would not be inconsistent with any available data. If such a complex were to form at high ionic strength and/or low temperature, then it could easily lead to total immobilization of the band 3 involved and hence a decreased fractional recovery of fluorescence in FPR experiments. Furthermore, if the postulated complex had specific steric requirements for formation such that,



once disrupted, it would be difficult to reform, increases in the fractional recovery governed by this process might be only slowly and partially reversible, as seen in these experiments.

While formation of a stable, long-lived complex between band 3 and some immobile cytoskeletal element could explain changes in fractional recovery under various conditions, it could not explain variations in the diffusion coefficient of the mobile fraction of band 3. A satisfactory explanation for the large, reversible changes observed in diffusion coefficient in this study must involve more dynamic membrane forces affecting the long-range environment in which the individual band 3 molecules are diffusing. As noted above, lipid viscosity, domain formation, planar aggregation, and electrostatic repulsion are unlikely candidates for this dynamic membrane force. Nonspecific entanglement of the cytoplasmic portion of band 3 in the cytoskeletal reticulum in a manner which is dependent on ionic strength, temperature, and time seems to be the most probable explanation for our data on diffusion coefficients. As we have seen, interactions between various cytoskeletal elements are exquisitely sensitive to the same parameters which affect lateral mobility strongly. Thus, the elution of spectrin from ghost membranes as well as the binding back of spectrin to inside-out vesicles, the vesiculation of ghost membranes, the spectrin dimer-tetramer equilibrium, and the susceptibility of membrane proteins to cross-linking and aggregation are all dependent on ionic strength and temperature.



It is not difficult to imagine a metastable state of cytoskeleton structure intermediate between tight binding to and complete dissociation from the membrane which would allow rapid lateral diffusion of band 3. Indeed, heterogeneity of spectrin binding to the membrane in the form of high-affinity interactions with ankyrin as well as low-affinity interactions with other membrane proteins or membrane lipid has been postulated by at least one author (138). The stabilities of the lipid-free cytoskeleton formed on Triton extraction of ghosts and of the pure spectrin-actin-band 4.1 shell produced after hypertonic treatment of the intact cytoskeletal reticulum (118) are further indications that, under some conditions at least, the cytoskeleton may be attached to the membrane by very tenuous forces without involving actual membrane fragmentation. To be consistent with our data on the reversibility of the diffusion coefficient of band 3, the postulated metastable state must be in rapid equilibrium (minutes to hours) with the tightly bound form of the cytoskeleton; this is again not unreasonable given the high affinity of at least one interaction between spectrin and the membrane.

In summary, then, the model for erythrocyte membrane structure most consistent with the data presented in this dissertation is as follows. Under conditions of high ionic strength and low temperature, nearly all of the band 3 is totally immobilized on the membrane, either through specific, low-affinity complexes between the band 3 molecules and some immobile cytoskeletal component(s) (most likely



spectrin in addition to ankyrin), or through severe restriction within very small domains (molecular size) by entrapment in a tightly bound cytoskeletal net. As the ionic strength is decreased and the temperature increased, two sequential processes occur which progressively lift the restrictions on band 3 lateral mobility. The first process, which is only partially reversible, allows a greater and greater proportion of band 3 molecules to diffuse over large distances (at least  $4\mu$ ; see table 6) on the membrane. This process probably involves either the breaking of low-affinity bonds between the cytoskeleton and band 3 (if such are actually formed), or the disruption of low-affinity bonds between spectrin and other membrane elements such as lipid. While the first membrane-associated process is sufficient for increases in the percentage of the total band 3 which is mobile on the membrane surface, it does not allow that mobile fraction to diffuse much faster. For this a second, separate process is required, which is more difficult to set in motion than the first process but which is rapidly and totally reversible on a change of conditions back to the original. The second process almost certainly involves disruption of some spectrin-membrane bonds, as it occurs to an appreciable degree only under conditions which approach (but do not include; see fig. 23) complete spectrin dissociation from the membrane and vesiculation of ghost membranes. Disruption of these bonds would lead to a very loose but metastable state of cytoskeleton structure which would allow unrestricted lateral mobility of band 3 in the plane of the membrane. It is impossible to say from these



FPR data whether the spectrin-membrane bonds which are broken are of the high-affinity (i.e. spectrin-ankyrin) type or the low-affinity variety. For this distinction to be made with any degree of certainty, it would be necessary to know whether all (i.e. 100%) or merely most (i.e. the 85-90% which is not ankyrin-linked) of band 3 is ever free to diffuse in the membrane; as discussed in chapter 4, the experimental uncertainty in the measurement of fractional recovery is too great to allow a definitive statement on this issue.

### C. CONCLUDING REMARKS

This thesis describes a series of phenomena concerning the restriction of lateral mobility of band 3 in the human erythrocyte membrane and the effects of changes in ionic strength, temperature, and incubation time on that restriction. Possible molecular bases for these phenomena are discussed, but further experimental work is needed to elucidate further the mechanisms underlying the control of lateral mobility. Such work would include studies of glycophorin and even spectrin mobility on the membrane, using specifically labeled endogenous proteins or labeled exogenous protein fragments. Studies concerning the effects of inhibitors of cytoskeletal binding such as spectrin, actin, or ankyrin fragments on lateral mobility would also be informative. Finally, correlation between integral protein mobility and specifically labeled lipid mobility would provide further insight into the relationship between the "fast diffusion limit" observed in this



study and unrestricted protein mobility on the membrane (i.e. controlled by lipid viscosity alone).

It is highly likely that changes in cytoskeletal structure are responsible for part or all of the changes in lateral mobility observed in the present study. If this is the case, then a detailed analysis of changes in lateral mobility should help answer the as yet unresolved questions relating to molecular interactions both within the cytoskeleton and between the cytoskeleton and various other membrane components. Such interactions are important in maintaining red cell shape and flexibility, and may be governed by dynamic equilibria regulating the state of phosphorylation of membrane elements such as spectrin and band 3. The study of these interactions is important not only for its clinical relevance to various diseases of erythrocyte membrane structure (e.g. hereditary spherocytosis), but also for its basic implications concerning the structure and function of cytoskeleton-containing membrane systems more complex than the erythrocyte.



# REFERENCES

1. Singer, S.J. and G.L. Nicolson. The Fluid Mosaic Model of the Structure of Cell Membranes. Science 175:720-731 (1972).
2. Edidin, M. Rotational and Translational Diffusion in Membranes. Ann. Rev. Biophys. Bioeng. 3:179-201 (1974).
3. Bretscher, M.S. Membrane Structure: Some General Principles. Science 181:622-629 (1973).
4. Nicolson, G.L. Transmembrane Control of the Receptors on Normal and Tumor Cells. Biochim. Biophys. Acta 457:57-108 (1976).
5. Edelman, G.M. Surface Modulation in Cell Recognition and Cell Growth. Science 192:218-226 (1976).
6. Marchesi, V.T. Functional Proteins of the Human Red Blood Cell Membrane. Semin. Hematol. 16:3-20 (1979).
7. Peters, R., J. Peters, K.H. Tews, and W. Bahr. A Microfluorimetric Study of Translational Diffusion in Erythrocyte Membranes. Biochim. Biophys. Acta 367:282-294 (1974).
8. Fowler, V. and D. Branton. Lateral Mobility of Human Erythrocyte Integral Membrane Proteins. Nature 268:23-26 (1977).
9. Marchesi, V.T., H. Furthmayr, and M. Tomita. The Red Cell Membrane. Ann. Rev. Biochem. 45:667-698 (1976).
10. Guidotti, G. Membrane Proteins. Ann. Rev. Biochem. 41:731-752 (1972).
11. Wallach, D.F.H. The Dispositions of Proteins in the Plasma Membranes of Animal Cells: Analytical Approaches Using Controlled Peptidolysis and Protein Labels. Biochim. Biophys. Acta 265:61-83 (1972).
12. Juliano, R.L. The Proteins of the Erythrocyte Membrane. Biochim. Biophys. Acta 300:341-378 (1973).
13. Steck, T.L. The Organization of Proteins in the Human Red Blood Cell Membrane. J. Cell Biol. 62:1-19 (1974).
14. Fairbanks, G., T.L. Steck, and D.F.H. Wallach. Electrophoretic Analysis of the Major Polypeptides of the Human Erythrocyte Membrane. Biochem. 10:2606-2617 (1971).



15. Bennett, V. and P.J. Stenbuck. Identification and Partial Purification of Ankyrin, the High Affinity Membrane Attachment Site for Human Erythrocyte Spectrin. J. Biol. Chem. 254:2533-2541 (1979).
16. Tilney, L.G. and P. Detmers. Actin in Erythrocyte Ghosts and Its Association with Spectrin. J. Cell Biol. 66:508-520 (1975).
17. Cabantchik, Z.I., P.A. Knauf, and A. Rothstein. The Anion Transport System of the Red Blood Cell: The Role of Membrane Protein Evaluated by the Use of "Probes." Biochim. Biophys. Acta 515:239-302 (1978).
18. Rothstein, A. The Functional Roles of Band 3 Protein of the Red Blood Cell. in, Molecular Specialization and Symmetry in Membrane Function (A.K. Solomon and M. Karnovsky, eds.) Cambridge, Mass: Harvard Univ. Press (1978) pp. 128-159.
19. Juliano, R.L. and A. Rothstein. Properties of an Erythrocyte Membrane Lipoprotein Fraction. Biochim. Biophys. Acta 249:227-235 (1971).
20. Steck, T.L. and G. Dawson. Topographical Distribution of Complex Carbohydrates in the Erythrocyte Membrane. J. Biol. Chem. 249:2135-2142 (1974).
21. Drickamer, L.K. Orientation of the Band 3 Polypeptide from Human Erythrocyte Membranes: Identification of NH<sub>2</sub>-Terminal Sequence and Site of Carbohydrate Attachment. J. Biol. Chem. 253:7242-7248 (1978).
22. Furthmayr, H., I. Kahane, and V.T. Marchesi. Isolation of the Major Intrinsic Transmembrane Protein of the Human Erythrocyte. J. Membrane Biol. 26:173-187 (1976).
23. Adair, W.L. and S. Kornfeld. Isolation of Receptors for Wheat Germ Agglutinin and the Ricinus communis Lectins from Human Erythrocytes Using Affinity Chromatography. J. Biol. Chem. 249:4676-4704 (1974).
24. Findlay, A. The Receptor Proteins for Concanavalin A and Lens culinaris Phyto-hemagglutinin in the Membrane of the Human Erythrocyte. J. Biol. Chem. 249:4378-4403 (1974).
25. Tanner, M.J.A. and D.H. Boxer. Separation and Some Properties of the Major Proteins of the Human Erythrocyte Membrane. Biochem. J. 129:333-347 (1972).



26. Yu. J. and T.L. Steck. Isolation and Characterization of Band 3, the Predominant Polypeptide of the Human Erythrocyte Membrane. J. Biol. Chem. 250:9170-9175 (1975).
27. Ross, A.H. and H.M. McConnell. Reconstitution of Band 3, the Erythrocyte Anion Exchange Protein. Biochem. Biophys. Res. Commun. 74:1318-1325 (1977).
28. Ho, M.K. and G. Guidotti. A Membrane Protein from Human Erythrocytes Involved in Anion Exchange. J. Biol. Chem. 250:675-683 (1975).
29. Yu, J., A. Fischman, and T.L. Steck. Selective Solubilization of Proteins and Phospholipids from Red Blood Cell Membranes by Nonionic Detergents. J. Supramol. Struct. 1:233-248 (1973).
30. Clarke, S. The Size and Detergent Binding of Membrane Proteins. J. Biol. Chem. 250:5459-5469 (1975).
31. Cabantchik, Z.I. and A. Rothstein. The Nature of the Membrane Sites Controlling Anion Permeability of Human Red Blood Cells as Determined by Studies with Disulfonic Stilbene Derivatives. J. Membrane Biol. 10:311-330 (1972).
32. Cabantchik, Z.I., and A. Rothstein. Membrane Proteins Related to Anion Permeability of Human Red Blood Cells. I. Localization of Disulfonic Stilbene Binding Sites in Proteins Involved in Permeation. J. Membrane Biol. 15:207-226 (1974).
33. Cabantchik, Z.I. and A. Rothstein. Membrane Proteins Related to Anion Permeability of Human Red Blood Cells. II. Effects of Proteolytic Enzymes on Disulfonic Stilbene Sites of Surface Proteins. J. Membrane Biol. 15:227-248 (1974).
34. Rothstein, A., Z.I. Cabantchik, M. Balshin, and R. Juliano. Enhancement of Anion Permeability in Lecithin Vesicles by Hydrophobic Proteins Extracted from Red Blood Cell Membranes. Biochem. Biophys. Res. Commun. 64:144-150 (1975).
35. Zaki, L., H. Fasol, B. Schulmann, and H. Passow. Chemical Modification of Membrane Proteins in relation to Inhibition of Anion Exchange in Human Red Blood Cells. J. Cell. Physiol. 86:471-494 (1975).
36. Rothstein, A., Z.I. Cabantchik, and P.A. Knauf. Mechanism of Anion Transport in Red Blood Cells: Role of Membrane Proteins. Fed. Proc. 35:3-10 (1976).
37. Passow, H., H. Fasold, S. Lepke, M. Pring, and B. Schuhmann. Chemical and Enzymatic Modification of Membrane Proteins and Anion Transport in Human Red Blood Cells. in, Membrane Toxicity (M. Miller and A.E. Shamoo, eds). New York:Plenum Press (1977), pp. 353-379.



38. Lepke, S., H. Fasold, M. Pring, and H. Passow. A study of the Relationship between Inhibition of Anion Exchange and Binding to the Red Blood Cell Membrane of 4,4'-diisothiocyanostilbene-2,2'-disulfonic acid (DIDS) and its Dihydro Derivative ( $H_2$ DIDS). J. Membrane Biol. 29:147-177 (1976).
39. Avruch, J. and G. Fairbanks. Demonstration of a Phosphopeptide Intermediate in the  $Mg^{++}$ -dependent  $Na^+$ -and  $K^+$ -stimulated Adenosine Triphosphatase Reaction of the Erythrocyte Membrane. Proc. Natl. Acad. Sci. USA 69:1216-1220 (1972).
40. Knauf, P.A., F. Proverbio, and J. Hoffman. Chemical Characterization and Pronase Susceptibility of the Na:K Pump-associated Phosphoprotein of Human Red Blood Cells. J. Gen. Physiol. 63:305-323 (1974).
41. Brown, P.A., M.B. Feinstein, and R.I. Sha'afi. Membrane Proteins Related to Water Transport in Human Erythrocytes. Nature 254:523-535 (1975).
42. Bellhorn, M.B., O.O. Blumenfeld, and P.M. Gallop. Acetylcholinesterase of the Human Erythrocyte Membrane Labeled with Tritiated Diisopropylfluorophosphate. Biochem. Biophys. Res. Commun. 39:267-273 (1970).
43. Sachs, J.R., P.A. Knauf, and P.B. Dunham. Transport through Red Cell Membranes. in, The Red Blood Cell, 2nd edition, vol. 2 (D.M. Surgenor, ed.) New York: Academic Press (1974), pp. 613-705.
44. Taverna, R.D. and R.G. Langdon. D-glucosyl-isothiocyanate: An Affinity Label for the Glucose Transport Proteins of the Human Erythrocyte Membrane. Biochem. Biophys. Res. Commun. 54:593-599 (1973).
45. Lin, S. and J.A. Spudich. Binding of Cytochalasin B to a Red Cell Membrane Protein. Biochem. Biophys. Res. Commun. 61:1471-1476 (1974).
46. Kahlenberg, A. Partial Purification of a Membrane Protein from Human Erythrocytes involved in Glucose Transport. J. Biol. Chem. 251:1582-1590 (1976).
47. Batt, E.R., R.E. Abbott, and D. Schachter. An Exofacial Component of Glucose Transport Mechanism of Human Erythrocyte. Fed. Proc. 5:606a (1976).
48. Goldin, S. and V. Rhoden. Reconstitution and "Transport Specificity Fractionation" of the Human Erythrocyte Glucose Transport System. J. Biol. Chem. 253:2575-2583 (1978).
49. Kasahara, M. and P.C. Hinkle. Reconstitution and Purification of the D-glucose Transporter from Human Erythrocytes. J. Biol. Chem. 252:7384-7390 (1977).



50. Anselstetter, V. and J.H.Horstmann. Two-dimensional Polyacrylamide Gel Electrophoresis of the Proteins and Glycoproteins of the Human Erythrocyte Membrane. Eur. J. Biochem. 56:259-269 (1975).
51. Conrad, M.J. and J.T. Penniston. The Resolution of Erythrocyte Membrane Proteins by Two-dimensional Electrophoresis. J. Biol. Chem. 251:253-255 (1976).
52. Drickamer, L.K. Fragmentation of the 95,000-Dalton Transmembrane Polypeptide in Human Erythrocyte Membranes: Arrangement of the Fragments in the Lipid Bilayer. J. Biol. Chem. 251: 5115-5123 (1976).
53. Markowitz, S.D. personal communication.
54. Jenkins, R.E. and M.J.A. Tanner. The Structure of the Major Protein of the Human Erythrocyte Membrane: Characterization of the Intact Protein and Major Fragments. Biochem. J. 161: 139-147 (1977).
55. Steck, T.L., G.Fairbanks, and D.F.H. Wallach. Disposition of the Major Proteins in the Isolated Erythrocyte Membrane: Proteolytic Dissection. Biochem. 10:2617-2624 (1971).
56. Bretscher, M.S. A Major Protein Which Spans the Human Erythrocyte Membrane. J. Mol. Biol. 59:351-357 (1971).
57. Bretscher, M.S. Human Erythrocyte Membranes: Specific Labelling of Surface Proteins. J. Mol. Biol. 58:775-781 (1971).
58. Arrotti, J.J. and J.E. Garvin. Selective Labelling of Human Erythrocyte Membrane Components with Tritiated Trinitrobenzenesulfonic Acid and Picryl Chloride. Biochem. Biophys. Res. Commun. 49:205-211 (1972).
59. Staros, J.W. and F.M. Richards. Photochemical Labelling of the Surface Proteins of Human Erythrocytes. Biochem. 13: 2720-2726 (1974).
60. Berg, H.C. Sulfanilic acid diazonium salt: a Label for the Outside of the Human Erythrocyte Membrane. Biochim. Biophys. Acta 183:65-78 (1969).
61. Whiteley, H.M. and H.C. Berg. Amidation of the Outer and Inner Surfaces of the Human Erythrocyte Membrane. J. Mol. Biol. 87: 541-561 (1974).



62. Cabantchik, Z.I., M. Balshin, W. Breuer, H. Markus, and A. Rothstein. A Comparison of Intact Human Red Blood Cells and Resealed and Leaky Ghosts with respect to their Interactions with Surface Labelling Agents and Proteolytic Enzymes. Biochim. Biophys. Acta 382:621-633 (1975).
63. Cabantchik, Z.I., M. Balshin, W. Breuer, and A. Rothstein. Pyridoxal Phosphate: an Anionic Probe for Protein Amino Groups Exposed on the Outer and Inner Surfaces of Intact Human Red Blood Cells. J. Biol. Chem. 250:5130-5136 (1975).
64. Bender, W.W., H. Garen, and H.C. Berg. Proteins of the Human Erythrocyte Membrane as Modified by Pronase. J. Mol. Biol. 58: 783-797 (1971).
65. Jenkins, R.E. and M.J.A. Tanner. The Major Human Erythrocyte Membrane Protein: Evidence for an S-Shaped Structure which Traverses the Membrane Twice and has Duplicated Sets of Sites. Biochem. J. 147:393-399 (1975).
66. Phillips, D.R. and M. Morrison. Exterior Proteins on the Human Erythrocyte Membrane. Biochem. Biophys. Res. Commun. 45: 1103-1108 (1971).
67. Steck, T.L., B. Ramos, and E. Strapazon. Proteolytic Dissection of Band 3, the Predominant Transmembrane Polypeptide of the Human Erythrocyte Membrane. Biochem. 15:1154-1161 (1976).
68. Triplett, R.B. and K.L. Carraway. Proteolytic Digestion of Erythrocytes, Resealed Ghosts and Isolated Membranes. Biochem. 11:2897-2903 (1972).
69. Reichstein, E. and R. Blostein. Asymmetric Iodination of the Human Erythrocyte Membrane. Biochem. Biophys. Res. Commun. 54:494-500 (1973).
70. Reichstein, E. and R. Blostein. Arrangement of Human Erythrocyte Membrane Proteins. J. Biol. Chem. 250: 6256-6263 (1975).
71. Boxer, D.H., R.E. Jenkins, and M.J.A. Tanner. The Organization of the Major Protein of the Human Erythrocyte Membrane. Biochem. J. 137:531-534 (1974).
72. Hubbard, A.L. and Z.A. Cohn. The Enzymatic Iodination of the Red Cell Membrane. J. Cell. Biol. 55:390-415 (1972).
73. Mueller, T.J. and M. Morrison. The Transmembrane Proteins in the Plasma Membrane of Normal Human Erythrocytes. J. Biol. Chem. 249:7568-7573 (1974).



74. Shin, B.C. and K.L. Carraway. Lactoperoxidase Labelling of Erythrocyte Membranes from the Inside and Outside. Biochim. Biophys. Acta 345:141-153 (1974).
75. Drickamer, L.K. Fragmentation of the Band 3 Polypeptide from Human Erythrocyte Membranes. J. Biol. Chem. 252:6909-6917 (1977).
76. Abbott, R.E. and D. Schachter. Impermeant Maleimides: Oriented Probes of Erythrocyte Membrane Proteins. J. Biol. Chem. 251: 7176-7183 (1976).
77. Rao, A. Disposition of the Band 3 Polypeptide in the Human Erythrocyte Membrane: the Reactive Sulfhydryl Groups. J. Biol. Chem. 254:3503-3511 (1979).
78. Jenkins, R.E. and M.J.A. Tanner. Ionic-Strength-Dependent Changes in the Structure of the Major Protein of the Human Erythrocyte Membrane. Biochem. J. 161:131-138 (1977).
79. Rao, A. and R.A.F. Reithmeir. Reactive Sulfhydryl Groups of the Band 3 Polypeptide from Human Erythrocyte Membranes: Location in the Primary Structure. J. Biol. Chem. 254: 6144-6150 (1979).
80. Steck, T.L., J.J. Koriarz, M.K. Singh, G. Reddy, and H. Kohler. Preparation and Analysis of Seven Major, Topographically Defined Fragments of Band 3, the Predominant Transmembrane Polypeptide of Human Erythrocyte Membranes. Biochem. 17: 1216-1222 (1978).
81. Fukuda, M., Y. Eshdat, G. Tarone, and V.T. Marchesi. Isolation and Characterization of Peptides Derived from the Cytoplasmic Segment of Band 3, the Predominant Intrinsic Membrane Protein of the Human Erythrocyte. J. Biol. Chem. 253:2419-2428 (1978).
82. Grinstein, S., S. Ship, and A. Rothstein. Anion Transport in Relation to Proteolytic Dissection of Band 3 Protein. Biochim. Biophys. Acta 507:294-304 (1978).
83. Knauf, P.A., W. Breuer, L. McCulloch, and A. Rothstein. N-(4-Azido-2-Nitrophenyl)-2-Aminoethylsulfonate (NAP-Taurine) as a Photoaffinity Probe for Identifying Membrane Components Containing the Modifier Site of the Human Red Blood Cell Anion Exchange System. J. Gen. Physiol. 72:631-649 (1978).
84. Yu, J. and T.L. Steck. Associations of Band 3, the Predominant Polypeptide of the Human Erythrocyte Membrane. J. Biol. Chem. 250:9176-9184 (1975).



85. Steck, T.L. Cross-linking the Major Proteins of the Isolated Erythrocyte Membrane. J. Mol. Biol. 66:295-305 (1972).
86. Wang, K. and F.M. Richards. An Approach to Nearest Neighbor Analysis of Membrane Proteins. J. Biol. Chem. 249: 8005-8018 (1974).
87. Wang, K. and F.M. Richards. Reaction of dimethyl-3,3'-dithio-bispropionimide with Intact Human Erythrocytes. J. Biol. Chem. 250:6622-6626 (1975).
88. Kiehm, D.J. and T.H. Ji. Photochemical Cross-Linking of Cell Membranes. J. Biol. Chem. 252:8524-8531 (1977).
89. Nigg, E. and R.J. Cherry. Dimeric Association of Band 3 in the Erythrocyte Membrane Demonstrated by Protein Diffusion Measurements. Nature 277:493-494 (1979).
90. Reithmeier, R.A.F. and A. Rao. Reactive Sulfhydryl Groups of the Band 3 Polypeptide from Human Erythrocyte Membranes. J. Biol. Chem. 254:6151-6155 (1979).
91. Tillack, T.W. and V.T. Marchesi. Demonstration of the Outer Surface of Freeze-etched Red Blood Cell Membranes. J. Cell Biol. 45:649-653 (1970).
92. Pinto da Silva, P. and D. Branton. Membrane Splitting in Freeze-etching: Covalently Bound Ferritin as a Membrane Marker. J. Cell Biol. 45:598-605 (1970).
93. Branton, D. Freeze-etching Studies of Membrane Structure. Phil. Trans. Roy. Soc. Lond. B 261:133-138 (1971).
94. Pinto da Silva, P., S.D. Douglas, and D. Branton. Location of A Antigen Sites on Human Erythrocyte Ghosts. Nature 232: 194-195 (1971).
95. Marchesi, V.T., T.W. Tillack, R.L. Jackson, J.P. Segrest, and R.E. Scott. Chemical Characterization and Surface Orientation of the Major Glycoprotein of the Human Erythrocyte Membrane. Proc. Natl. Acad. Sci. USA 69:1445-1449 (1972).
96. Tillack, T.W. R.E. Scott, and V.T. Marchesi. The Structure of Erythrocyte Membranes Studied by Freeze-etching. J. Exp. Med. 135:1209-1227 (1972).
97. Pinto da Silva, P., P.S. Moss and H.H. Fudenberg. Anionic Sites on the Membrane Intercalated Particles of Human Erythrocyte Ghost Membranes: Freeze-Etch Localization. Exp. Cell Res. 81: 127-138 (1973).
98. Pinto da Silva, P. and G.L. Nicolson. Freeze-Etch Localization of Concanavalin A Receptors to the Membrane Intercalated Particles of Human Erythrocyte Ghost Membranes. Biochim. Biophys. Acta 363: 311-319 (1974).



99. Wolosin, J.M., H. Ginsburg, and Z.I. Cabantchik. Functional Characterization of Anion Transport System Isolated from Human Erythrocyte Membranes. J. Biol. Chem. 252:2419-2427 (1977).
100. Yu, J. and D. Branton. Reconstitution of Intramembrane Particles in Recombinants of Erythrocyte Protein Band 3 and Lipid: Effects of Spectrin-Actin Association. Proc. Natl. Acad. Sci. USA 73:3891-3895 (1976).
101. Bachi, T., K. Whiting, M.J.A. Tanner, M.N. Metaxas, and D.J. Anstee. Freeze-fracture Electron Microscopy of Human Erythrocytes Lacking the Major Membrane Sialoglycoprotein. Biochim. Biophys. Acta 464:635-639 (1977).
102. Grant, C.W.M. and H.M. McConnell. Glycophorin in Lipid Bilayers. Proc. Natl. Acad. Sci. USA 71:4653-4657 (1974).
103. Phillips, D.R. and M. Morrison. Changes in Accessibility of Plasma Membrane Protein as the Result of Tryptic Hydrolysis. Nature New Biol. 242:213-215 (1973).
104. Ji, T.H. The Application of Chemical Crosslinking for Studies on Cell Membranes and the Identification of Surface Receptors. Biochim. Biophys. Acta 559:39-69 (1979).
105. Kant, J.A. and T.L. Steck. Specificity in the Association of Glyceraldehyde-3-Phosphate Dehydrogenase with Isolated Human Erythrocyte Membranes. J. Biol. Chem. 248:8457-8464 (1973).
106. Strapazon, E. and T.L. Steck. Binding of Rabbit Muscle Aldolase to Band 3, the Predominant Polypeptide of the Human Erythrocyte Membrane. Biochem. 15:1421-1424 (1976).
107. Strapazon, E. and T.L. Steck. Interaction of Aldolase and the Membrane of Human Erythrocytes. Biochem. 16:2966-2971 (1977).
108. Fossel, E.T. and A.K. Solomon. Membrane-mediated Link between Ion Transport and Metabolism in Human Red Cells. Biochim. Biophys. Acta 464:82-92 (1977).
109. Gunn, R.B. Transport of Anions Across Red Cell Membranes. in, Transport Across Biological Membranes (G. Giebisch, D.C. Tosteson, and H. Ussing, eds), in press.
110. Halestrap, A.P. Transport of Pyruvate and Lactate into Human Erythrocytes. Biochem. J. 156:193-207 (1976).
111. Ship, S., Y. Shami, and A. Rothstein. Synthesis of Tritiated 4,4'-diisothiocyano-2,2'-stilbene disulfonic acid ( $[^3\text{H}]\text{DI DS}$ ) and its Covalent Reaction with Sites Related to Anion Transport in Human Red Blood Cells. J. Memb. Biol. 33:311-324 (1977).



112. Nigg, E., M. Kessler, and R.J. Cherry. Labeling of Human Erythrocyte Membranes with Eosin Probes used for Protein Diffusion Measurements. Biochim. Biophys. Acta 550: 328-340 (1979).
113. Cabantchik, Z.I., P.A. Knauf, T. Ostwald, H. Markus, L. Davidson, W. Breuer, and A. Rothstein. The Interaction of an Anionic Photoreactive Probe with the Anion Transport System of the Human Red Blood Cell. Biochim. Biophys. Acta 455:526-537 (1976).
114. Sheetz, M.P., D.Sawyer, and S. Jacowski. The ATP-dependent Red Cell Membrane Shape Change. in, The Red Cell (G. Brewer, ed.) New York: Liss (1978) pp. 431-450.
115. Lux, S.E. Spectrin-Actin Membrane Skeleton of Normal and Abnormal Red Blood Cells. Semin. Hematol. 16:21-51 (1979).
116. Lux, S.E. Dissecting the Red Cell Membrane Skeleton. Nature 281:426-429 (1979).
117. Lux, S.E., K.M. John, and M.J. Karnovsky. Irreversible Deformation of the Spectrin-Actin Lattice in Irreversibly Sickled Cells. J. Clin. Invest. 58:955-963 (1976).
118. Sheetz, M.P. Integral Membrane Protein Interaction with Triton Cytoskeletons of Erythrocytes. Biochim. Biophys. Acta 557:122-134 (1979).
119. Sheetz, M.P. DNase I-Dependent Dissociation of Erythrocyte Cytoskeletons. J. Cell Biol. 81:266-270 (1979).
120. Nicolson, G.L., V.T. Marchesi, and S.J. Singer. The Localization of Spectrin on the Inner Surface of Human Red Blood Cell Membranes by Ferritin-Conjugated Antibodies. J. Cell Biol. 51:265-272 (1971).
121. Hainfeld, J.F. and T.L. Steck. The Sub-Membrane Reticulum of the Human Erythrocyte: A Scanning Electron Microscope Study. J. Supramol. Struct. 6:301-311 (1977).
122. Kirkpatrick, F.H. Spectrin: Current Understanding of its Physical, Biochemical, and Functional Properties. Life Sci. 19:1-18 (1976).
123. Palek, J. and S.-C. Liu. Dependence of Spectrin Organization in Red Blood Cell Membranes on Cell Metabolism: Implications for Control of Red Cell Shape, Deformability, and Surface Area. Semin. Hematol. 16:75-93 (1979).



124. Anderson, J.M. Structural Studies on Human Spectrin: Comparison of Subunits and Fragmentation of Native Spectrin. J. Biol. Chem. 254:939-944 (1979).
125. Schechter, N.M., M. Sharp, J.A. Reynolds, and C. Tanford. Erythrocyte Spectrin: Purification in Deoxycholate and Preliminary Characterization. Biochem. 15:1897-1904 (1976).
126. Gratzer, W.B. and G.H. Beaven. Properties of the High-Molecular-Weight Protein (Spectrin) from Human-Erythrocyte Membranes. Eur. J. Biochem. 58:403-409 (1975).
127. Ralston, G.B. Physico-Chemical Characterization of the Spectrin Tetramer from Bovine Erythrocyte Membranes. Biochim. Biophys. Acta 455:163-172 (1976).
128. Ralston, G.B., J. Dunbar, and M. White. The Temperature-Dependent Dissociation of Spectrin. Biochim. Biophys. Acta 491:345-348 (1977).
129. Kam, Z., R. Josephs, H. Eisenberg, and W.B. Gratzer. Structural Study of Spectrin from Human Erythrocyte Membranes. Biochem. 16:5568-5572 (1977).
130. Ungewickell, E., and W.B. Gratzer. Self-Association of Human Spectrin. Eur. J. Biochem. 88:379-385 (1978).
131. Shotton, D.M., B.E. Burke, and D. Branton. The Molecular Structure of Human Erythrocyte Spectrin. J. Mol. Biol. 131:303-329 (1979).
132. Ungewickell, E., P.M. Bennett, R. Calvert, V. Ohanian, and W. B. Gratzer. In vitro Formation of a Complex between Cytoskeletal Proteins of the Human Erythrocyte. Nature 280:811-814 (1979).
133. Brenner, S.L. and E.D. Korn. Spectrin-Actin Interaction. J. Biol. Chem. 254:8620-8627 (1979).
134. Fowler, V. and D.L. Taylor. Actin-Binding Proteins from Human Erythrocyte Membranes. J. Cell Biol. 79:222a (1978).
135. Tyler, J.M., W.R. Hargreaves, and D. Branton. Purification of Two Spectrin-Binding Proteins. Proc. Natl. Acad. Sci. USA 76: 5192-5196 (1979).
136. Cohen, C.M. and D. Branton. The Role of Spectrin in Erythrocyte Membrane-stimulated Actin Polymerization. Nature 279:163-165 (1979).



137. Dunbar, J.C. and G.B. Ralston. The Incorporation of  $^{32}\text{P}$  into Spectrin Aggregates Following Incubation of Erythrocytes in  $^{32}\text{P}$ -Labelled Inorganic Phosphate. Biochim. Biophys. Acta 510:283-291 (1978).
138. Bennett, V. and D. Branton. Selective Association of Spectrin with the Cytoplasmic Surface of Human Erythrocyte Plasma Membranes. J. Biol. Chem. 253:2753-2763 (1977).
139. Bennett, V. Purification of an Active Proteolytic Fragment of the Membrane Attachment Site for Human Erythrocyte Spectrin. J. Biol. Chem. 253:2292-2299 (1978).
140. Yu, J. and S.R. Goodman. Syndeins: The Spectrin-Binding Protein(s) of the Human Erythrocyte Membrane. Proc. Natl. Acad. Sci. USA 76: 2340-2344 (1979).
141. Luna, E.J., G.H. Kidd, and D. Branton. Identification by Peptide Analysis of the Spectrin-Binding Protein in Human Erythrocytes. J. Biol. Chem. 254:2526-2532 (1979).
142. Mombers, C., P.W.M. Van Dijck, and L.L.M. Van Deenen. The Interaction of Spectrin-Actin and Synthetic Phospholipids. Biochim. Biophys. Acta 470:152-160 (1977).
143. Haest, C.W.M., G. Plasa, D. Kamp, and B. Deuticke. Spectrin as a Stabilizer of the Phospholipid Asymmetry in the Human Erythrocyte Membrane. Biochim. Biophys. Acta 509:21-32 (1978).
144. Marinetti, G.V. and R.C. Crain. Topology of Amino-phospholipids in the Red Cell Membrane, in Normal and Abnormal Red Cell Membranes. (S.E. Lux, V.T. Marchesi, and C.F. Fox, eds.) Liss: New York, in press.
145. Cohen, C.M., P.L. Jackson, and D. Branton. Actin-membrane Interactions Association of G-Actin with the Red Cell Membrane. in Normal and Abnormal Red Cell Membranes (S.E. Lux, V.T. Marchesi, and C.F. Fox, eds.) Liss: New York, in press.
146. Bennett, V. and P.J. Steinbuck. The Membrane Attachment Protein for Spectrin is Associated with Band 3 in Human Erythrocyte Membranes. Nature 280:468-473 (1979).
147. Lux, S.E., K.M. John, and B. Pease. Functional Heterogeneity of Spectrin: Effect on Interactions with Actin. Fed. Proc. 37:1507 (1978).
148. Sheetz, M.P. and D. Sawyer. Triton Shells of Intact Erythrocytes. in Normal and Abnormal Red Cell Membranes (S.E. Lux, V.T. Marchesi, and C.F. Fox, eds.) Liss: New York, in press.



149. Pinto da Silva, P. Translational Mobility of the Membrane Intercalated Particles of Human Erythrocyte Ghosts. J. Cell Biol. 53:777-787 (1972).
150. Elgsaeter, A. and D. Branton. Intramembrane Particle Aggregation in Erythrocyte Ghosts. I. The Effects of Protein Removal. J. Cell Biol. 63:1018-1030 (1974).
151. Nicolson, G.L. Anionic Sites of Human Erythrocyte Membranes. I. Effects of Trypsin, Phospholipase C, and pH on the Topography of Bound Positively Charged Colloidal Particles. J. Cell Biol. 57:373-387 (1973).
152. Speth, V., D.F.H. Wallach, E. Weidekamm, and H. Knufermann. Micromorphologic Consequences Following Perturbation of Erythrocyte Membranes by Trypsin, Phospholipase A, Lysolecithin, Sodium Dodecyl Sulfate, and Saponin. Biochim. Biophys. Acta 255: 386-394 (1972).
153. Nicolson, G.L. and R.G. Painter. Anionic Sites of Human Erythrocyte Membranes. II. Antispectrin-Induced Transmembrane Aggregation of the Binding Sites for Positively Charged Colloidal Particles. J. Cell Biol. 59:395-406 (1973).
154. Elgsaeter, A., D.M. Shotton, and D. Branton. Intramembrane Particle Aggregation in Erythrocyte Ghosts. II. The Influence of Spectrin Aggregation. Biochim. Biophys. Acta 426:101-122 (1976).
155. Shotton, D., K. Thompson, L. Wofsy, and D. Branton. Appearance and Distribution of Surface Proteins of the Human Erythrocyte Membrane. J. Cell Biol. 76:512-531 (1978).
156. Ji, T.H. and G.L. Nicolson. Lectin Binding and Perturbation of the Outer Surface of the Cell Membrane Induces a Transmembrane Organizational Alteration at the Inner Surface. Proc. Natl. Acad. Sci. USA 71:2212-2216 (1974).
157. Huang, C.-K. and F.M. Richards. Reaction of a Lipid-soluble Unsymmetrical, Cleavable, Cross-linking Reagent with Muscle Aldolase and Erythrocyte Membrane Proteins. J. Biol. Chem. 252:5514-5521 (1977).
158. Liu, S.-C., G. Fairbanks, and J. Palek. Spontaneous, Reversible Protein Cross-linking in the Human Erythrocyte Membrane. Biochem. 16:4066-4074 (1977).
159. Bhakdi, S., H. Knufermann, and D.F.H. Wallach. Separation of EDTA-Extractable Erythrocyte Membrane Proteins by Isoelectric Focusing linked to Electrophoresis in Sodium Dodecyl Sulfate. Biochim. Biophys. Acta 345:448-457 (1974).



160. Cherry, R.J. Protein Mobility in Membranes. FEBS Lett. 55:1-7 (1975).
161. Edidin, M., and D. Fambrough. Fluidity of the Surface of Cultured Muscle Fibers. J. Cell Biol. 57:27-37 (1973).
162. Poo, M.-M., J.W. Lam, N. Orida, and A.W. Chao. Electrophoresis and Diffusion in the Plane of the Cell Membrane. Biophys. J. 26:1-21 (1979).
163. Frye, L.D. and M. Edidin. The Rapid Intermixing of Cell Surface Antigens After Formation of Mouse-Human Heterokaryons. J. Cell Sci. 7:319-335 (1970).
164. Edidin, M., and T. Wei. Diffusion Rates of Cell Surface Antigens of Mouse-Human Heterokaryons. I. Analysis of the Population. J. Cell Biol. 75:475-482 (1977).
165. Petit, V.A. and M. Edidin. Lateral Phase Separation of Lipids in Plasma Membranes: Effect of Temperature on the Mobility of Membrane Antigens. Science 184:1183-1185 (1974).
166. Linden, C.D., K.L. Wright, H.M. McConnell, and C.F. Fox. Lateral Phase Separations in Membrane Lipids and the Mechanism of Sugar Transport in Escherichia coli. Proc. Natl. Acad. Sci. USA 70:2271-2275 (1973).
167. Edidin, M. and T. Wei. Diffusion Rates of Cell-Surface Antigens of Mouse-Human Heterokaryons. II. Effect of Membrane Potential on Lateral Diffusion. J. Cell Biol. 75:483-489 (1977).
168. Fowler, V. and V. Bennett. Association of Spectrin with its Membrane Attachment Site Restricts Lateral Mobility of Human Erythrocyte Integral Membrane Proteins. J. Supramol. Struct. 8:215-221 (1978).
169. Poo, M.-M. and R.A. Cone. Lateral Diffusion of Rhodopsin in the Photoreceptor Membrane. Nature 247:438-441 (1974).
170. Axelrod, D., D.E. Koppel, J. Schlessinger, E. Elson, and W. Webb. Mobility Measurement by Analysis of Fluorescence Photobleaching Recovery Kinetics. Biophys. J. 16:1055-1069 (1976).
171. Koppel, D.E., D. Axelrod, J. Schlessinger, E. Elson, and W. Webb. Dynamics of Fluorescence Marker Concentration as a Probe of Mobility. Biophys. J. 16:1315-1329 (1976).
172. Jacobson, K., Z. Derzko, E.-S. Wu, Y. Hou, and G. Poste. Measurement of the Lateral Mobility of Cell Surface Components in Single, Living Cells by Fluorescence Recovery After Photobleaching. J. Supramol. Struct. 5:565-576 (1976).



173. Wu, E.-S., K. Jacobson, and D. Papahadjopoulos. Lateral Diffusion in Phospholipid Multibilayers Measured by Fluorescence Recovery After Photobleaching. Biochem. 16:3936-3941 (1977).
174. Edidin, M., Y. Zagyansky, and T.J. Lardner. Measurement of Membrane Protein Lateral Diffusion in Single Cells. Science 191:466-468(1976).
175. Smith, B.A. and H.M. McConnell. Determination of Molecular Motion in Membranes Using Periodic Pattern Photobleaching. Proc. Natl. Acad. Sci. USA 75:2759-2763 (1978).
176. Axelrod, D., P. Ravdin, D.E. Koppel, J. Schlessinger, W. Webb, E. Elson, and T. R. Podleski. Lateral Motion of Fluorescently Labeled Acetylcholine Receptors in Membranes of Developing Muscle Fibers. Proc. Natl. Acad. Sci. USA 73:4594-4598 (1976).
177. Liebman, P.A. and G. Entine. Lateral Diffusion of Visual Pigment in Photoreceptor Disk Membranes. Science 185:457-459 (1974).
178. Zagyansky, Y. and M. Edidin. Lateral Diffusion of Concanavalin A Receptors in the Plasma Membrane of Mouse Fibroblasts. Biochim. Biophys. Acta 433:209-214 (1976).
179. Jacobson, K., E. Wu, and G. Poste. Measurement of the Translational Mobility of Concanavalin A in Glycerol-Saline Solutions and on the Cell Surface by Fluorescence Recovery After Photobleaching. Biochim. Biophys. Acta 433:215-222 (1976).
180. Schlessinger, J., D.E. Koppel, D. Axelrod, K. Jacobson, W. Webb, and E. Elson. Lateral Transport on Cell Membranes: Mobility of Concanavalin A Receptors on Myoblasts. Proc. Natl. Acad. Sci. USA 73:2409-2413 (1976).
181. Schlessinger, J., D. Axelrod, D.E. Koppel, W. Webb, and E. Elson. Lateral Transport of a Lipid Probe and Labeled Proteins on a Cell Membrane. Science 195:307-309 (1977).
182. Zagyansky, Y.A. and S. Jard. Does Lectin-Receptor Complex Formation Produce Zones of Restricted Mobility within the Membrane? Nature 280:591-593 (1979).
183. Zagyansky, Y.A., P. Benda, and J.C. Bisconte. Restricted Lateral Diffusion of Concanavalin A Receptors of Different Malignant Cells of the Nervous System. FEBS Lett. 77:206-208 (1977).
184. Axelrod, D., A. Wight, W. Webb, and A. Horwitz. Influence of Membrane Lipids on Acetylcholine Receptor and Lipid Probe Diffusion in Cultured Myotube Membrane. Biochem. 17:3604-3609 (1978).



185. Axelrod, D., P.M. Ravdin, and T.R. Podleski. Control of Acetylcholine Receptor Mobility and Distribution in Cultured Muscle Membranes. Biochim. Biophys. Acta 511:23-38 (1978).
186. Schlessinger, J., L.S. Barak, G.G. Hammes, K.M. Yamada, I. Postan, W. Webb, and E. Elson. Mobility and Distribution of a Cell Surface Glycoprotein and its Interaction with Other Membrane Components. Proc. Natl. Acad. Sci. USA 74:2909-2913 (1977).
187. Johnson, M. and M. Edidin. Lateral Diffusion in Plasma Membrane of Mouse Egg is Restricted after Fertilization. Nature 272:448-450 (1978).
188. Schlessinger, J., W.W. Webb, E.L. Elson, and H. Metzger. Lateral Motion and Valence of Fc Receptors on Rat Peritoneal Mast Cells. Nature 264:550-552 (1976).
189. Schlessinger, J., E.L. Elson, W.W. Webb, I. Yahara, U. Rutishauser, and G.M. Edelman. Receptor Diffusion on Cell Surfaces Modulated by Locally Bound Concanavalin A. Proc. Natl. Acad. Sci. USA 74:1110-1114 (1977).
190. Dragsten, P., J. Schlessinger, P. Henkart, J.N. Weinstein, and R. Blumenthal. Lateral Diffusion of Membrane Antigens and a Lipid Probe in Lymphocytes. Biophys. J. 25:294a (1979).
191. Thompson, N.L. and D. Axelrod. Reduced Lateral Mobility of a Fluorescent Lipid Probe in Cholesterol-Depleted Erythrocyte Membrane. Biophys. J. 25:65a (1979).
192. Smith, L.M., B.A. Smith, and H.M. McConnell. Lateral Diffusion of M-13 Coat Protein in Model Membranes. Biochem. 18:2256-2259 (1979).
193. Scandella, C.J., P. Devaux, and H.M. McConnell. Rapid Lateral Diffusion of Phospholipids in Rabbit Sarcoplasmic Reticulum. Proc. Natl. Acad. Sci. USA 69:2056-2060 (1972).
194. Stier, A. and E. Sackmann. Spin Labels as Enzyme Substrates: Heterogeneous Lipid Distribution in Liver Microsomal Membranes. Biochim. Biophys. Acta 311:400-408 (1973).
195. Davis, D.G. Phosphorus Nuclear Magnetic Resonance in Egg Yolk Lecithin: Field-Dependent Line Widths and Phosphate Group Mobility. Biochem. Biophys. Res. Commun. 49:1492-1497 (1972).
196. Davis, D.G. and G. Inesi. Phosphorus and Proton Nuclear Magnetic Resonance Studies in Sarcoplasmic Reticulum Membranes and Lipids. Biochim. Biophys. Acta 282:180-186 (1972).



197. Lee, A.G., N.J.M. Birdsall, and J.C. Metcalfe. Measurement of Fast Lateral Diffusion of Lipids in Vesicles and in Biological Membranes by <sup>1</sup>H Nuclear Magnetic Resonance. Biochem. 12:1650-1659 (1973).
198. Kogelnik, H. and T. Li. Laser Beams and Resonators. Appl. Optics 9:1550-1567 (1966).
199. Dickson, L.D. Characteristics of a Propagating Gaussian Beam. Appl. Optics 9:1854-1861 (1970).
200. Axelrod, D. Carbocyanine Dye Orientation in Red Cell Membrane Studied by Microscopic Fluorescence Polarization. Biophys. J. 26:557-573 (1979).
201. Cherry, R.J., A. Burkli, M. Busslinger, and G. Schneider. Rotational Diffusion of Band 3 Proteins in the Human Erythrocyte Membrane. Nature 263:389-393 (1976).
202. Cherry, R.J., A. Burkli, M. Busslinger, and G. Schneider. Rotational Diffusion of Proteins in Membranes. in Biochemistry of Membrane Transport, FEBS Symp. 42 (G. Semenza and E. Carafoli, eds.) Berlin: Springer-Verlag (1977), pp. 86-95.
203. Cherry, R.J. Measurement of Protein Rotational Diffusion in Membranes by Flash Photolysis. Meth. Enzymol. 54:47-61 (1978).
204. Cherry, R.J., A. Cogoli, M. Opplinger, G. Schneider, and G. Semenza. A Spectroscopic Technique for Measuring Slow Rotational Diffusion of Macromolecules. I: Preparation and Properties of a Triplet Probe. Biochem. 15:3653-3656 (1976).
205. Lowry, O.H., N.J. Rosebrough, A.L. Farr, and R.J. Randall. Protein Measurement with the Folin Phenol Reagent. J. Biol. Chem. 193:265-275 (1951).
206. Laemmli, U.K. Cleavage of Structural Proteins During the Assembly of the Head of Bacteriophage T4. Nature 227:680-685 (1970).
207. Hamaguchi, H., and H. Cleve. Solubilization and Comparative Analysis of Mammalian Erythrocyte Membrane Glycoproteins. Biochem. Biophys. Res. Commun. 47:459-464 (1972).
208. Hammond, K.S. and D.S. Papermaster. Fluorometric Assay of Sialic Acid in the Picomole Range: A Modification of the Thiobarbituric Acid Assay. Anal. Biochem. 74:292-297 (1976).
209. Tomita, M., H. Furthmayr, and V.T. Marchesi. Primary Structure of Human Erythrocyte Glycophorin A: Isolation and Characterization of Peptides and Complete Amino Acid Sequence. Biochem. 17:4756-4770 (1978).



210. Lepock, J.R., J.E. Thompson, J. Kruuv, and D.F.H. Wallach. Photoinduced Crosslinking of Membrane Proteins by Fluorescein Isothiocyanate. Biochem. Biophys. Res. Commun. 85:344-350 (1978).
211. Sheetz, M.P. and D.E. Koppel. Membrane Damage Caused by Irradiation of Fluorescent Concanavalin A. Proc. Natl. Acad. Sci. USA 76:3314-3317 (1979).
212. Marchesi, V.T. and E. Steers, Jr. Selective Solubilization of a Protein Component of the Red Cell Membrane. Science 159:203-204 (1968).
213. Furthmayr, H. and R. Timpl. Immunochemical Studies on Structural Proteins of the Red Cell Membrane. Eur. J. Biochem. 15:301-310 (1970).
214. Clarke, M. Isolation and Characterization of a Water-Soluble Protein from Bovine Erythrocyte Membranes. Biochem. Biophys. Res. Commun. 45:1063-1070 (1971).
215. Marchesi, S.L., E. Steers, V.T. Marchesi, and T.W. Tillack. Physical and Chemical Properties of a Protein Isolated from Red Cell Membranes. Biochem. 9:50-57 (1970).
216. Rudy, B. and C. Gitler. Microviscosity of the Cell Membrane. Biochim. Biophys. Acta 288:231-236 (1972).
217. Radda, G.K. and D.S. Smith. Retinol: A Fluorescent Probe for Membrane Lipids. FEBS Lett. 9:287-289 (1970).
218. Aloni, B., B. Shinitzky, and A. Livne. Dynamics of Erythrocyte Lipids in Intact Cells, in Ghost Membranes and in Liposomes. Biochim. Biophys. Acta 348:438-441 (1974).
219. Solomon, A.K. Apparent Viscosity of Human Red Cell Membranes. Biochim. Biophys. Acta 373:145-149 (1974).
220. Saffman, P.G. and M. Delbruck. Brownian Motion in Biological Membranes. Proc. Natl. Acad. Sci. USA 72:3111-3113 (1975).
221. Cone, R.A. Rotational Diffusion of Rhodopsin in the Visual Receptor Membrane. Nature (New Biol.) 236:39-43 (1972).
222. Nigg, E.A. and R.J. Cherry. Influence of Temperature and Cholesterol on the Rotational Diffusion of Band 3 in the Human Erythrocyte Membrane. Biochem. 18:3457-3465 (1979).
223. Gottlieb, M.H. and E.D. Eanes. On Phase Transitions in Erythrocyte Membranes and Extracted Membrane Lipids. Biochim. Biophys. Acta 373:519-522 (1974).
224. Ladbroke, B.D. and D. Chapman. Thermal Analysis of Lipids, Proteins, and Biological Membranes. Chem. Phys. Lipids 3:304-367 (1969).









WELLS BINDERY, INC.

NOV 1979

WALTHAM, MASS. 02154

YALE MEDICAL LIBRARY

Manuscript Theses

Unpublished theses submitted for the Master's and Doctor's degrees and deposited in the Yale Medical Library are to be used only with due regard to the rights of the authors. Bibliographical references may be noted, but passages must not be copied without permission of the authors, and without proper credit being given in subsequent written or published work.

This thesis by \_\_\_\_\_ has been  
used by the following persons, whose signatures attest their acceptance of the  
above restrictions.

---

NAME AND ADDRESS

DATE

